ABSOLUTE TOTAL CROSS SECTION MEASUREMENTS FOR THE SCATTERING OF LOW ENERGY ELECTRONS BY RUBIDIUM, CESIUM AND POTASSIUM

by

Paul Joseph Visconti

A dissertation submitted to the Graduate Faculty in Physics in partial fulfillment of the requirements for the degree of Doctor of Philosophy, the City University of New York.

1970

This manuscript has been read and accepted for the Graduate Faculty in Physics in satisfaction of the dissertation requirement for the degree of Doctor of Philosophy.

11/30/70
date

Chairman of Examining Committee

11/30/70
date

Executive Officer

Benjamin Bederson

Rudolf Ehrlich

Daniel Greenberger

Alvin Halpern

Supervisory Committee

The City University of New York

ACKNOWLEDGEMENTS

I wish to express my sincere gratitude to my adviser, Professor Kenneth Rubin, whose ideas and originated techniques formed the basis of this work and whose encouragement and aid were invaluable throughout the course of the experiment.

I am very grateful to Dr. James Slevin for many valuable discussions and for his assistance during several difficult periods.

I am also grateful to Mr. Bill Robeson who assisted with the data taking during the latter part of the experiment.

I wish to acknowledge the assistance and cooperation of Professor Benjamin Bederson, of New York University, who supplied us with detailed shop drawings of the components of the electron gun.

I also wish to express my thanks to Professor Marvin Mittleman who by his papers and by lecture notes

derived from his course illuminated much of the theory to me.

Finally, I wish to thank Mr. Gerald Canella, Mr. Patrick Lynch and Mr. Joseph Lane for their work in the construction of the experimental system. Mr. Canella is deserving of special thanks for the skill and enthusiasm which he brought to the project.

ABSTRACT

With the exception of potassium, no experimental absolute total cross sections for low energy ($1ev \leq E \leq 100ev$) electron-alkali collisions have been published since the work of Brode more than forty years ago. Thus up to the present time Brode's values have been the accepted numbers. However, recent measurements on potassium by Collins as well as several theoretical calculations involving all of the alkalies have yielded cross section values which are in firm disagreement with Brode. Therefore it was considered worthwhile to undertake a series of very accurate absolute measurements of low energy electron-alkali total cross sections.

Using the atom beam recoil method, we have measured absolute total cross sections for the scattering of electrons by cesium, rubidium and potassium over the electron energy range .3ev - 9ev. We have also investigated how the measured cross sections vary with the resolution of our apparatus.

For all three alkalies our results strongly

disagree with Brode but are in fair to excellent agreement with recent calculations. Also our potassium sections compare very favorably with those obtained by Collins.

TABLE OF CONTENTS

LIST OF FIGURES

I. INTRODUCTION

(A) Within the last ten years, there has been much theoretical interest in the scattering of low energy (100 ev) electrons from heavy atoms and this has made apparent a scarcity of modern experimental data in this area. In particular, low energy electron-alkali collisions have lately been studied by a variety of theoretical methods and approximations with results differing from each other both quantitatively and qualitatively.[1-9] For electrons on potassium, the only recent absolute measurements of total cross sections were performed at New York University by Collins et al.[10] For rubidium and cesium, there has been no new absolute experimental total cross sections since those obtained by Brode[11] more than forty years ago. His results, however, differ significantly from those predicted by several different modern calculations.[4,5,6,8,9] Further, the potassium data of Collins et al is in strong disagreement with Brode's both in magnitude (about half of Brode's value) and in variation with electron energy. Perel et al[12] have made measurements on lithium and sodium and normalized these to potassium at each electron energy through the use of a double oven method. Absolute magnitudes were then obtained

by normalization to Brode's potassium values. The resulting total cross sections lie about a factor of two above the theoretical calculations presented in references 4,5 and 9. But, as indicated by Bederson,[13] renormalization of the Perel values to the Collins potassium values brings Perel's lithium cross sections into much better agreement with theory.

Brode performed his measurements using a modified Ramsauer type apparatus[14], and it is possible that his results may be incorrect for the following reasons:

(1) electron energy selection and collisions with the vapor under study were not, in Brode's system, performed in separate chambers. Therefore the filament of his electron gun was continuously exposed to an atmosphere of hot alkali vapor. Such exposure could result in a significant lowering of the emitter's work function. Because of this, an implicit assumption by Brode that his electron velocity distribution remained constant for different vapor densities may be incorrect.

(2) Uncertainties, indicated by Brode himself[11], in the determination of the true vapor density of the element under study.

The method which we have employed to measure total cross sections is known as the atom beam recoil technique[12,15] and is subject to neither of the above problems. In this method an electron beam orthogonally crossfires an atom beam, and the total scattering is observed by measuring the decrease in atom beam intensity in the forward direction. This decrease is due to the momentum transferred during the scattering process. In crossed beam experiments, the electron source is not exposed to the alkali vapor. However, in all such experiments in which observations are made on the scattered electrons, it is extremely difficult to make absolute density measurements. With the recoil method, it is not necessary to know the absolute value of the atom density since the determination of the cross section depends only on the ratio of the scattered atom current to the unscattered atom beam and both quantities are measured with the same detector.

We have obtained absolute total cross sections for electrons, in the energy range .3ev - 9ev, incident upon rubidium, cesium and potassium. In addition, we have investigated the variation of these cross sections with the resolution of our experimental system.

(B) The study of electron collisions with the alkalies- lithium, sodium, potassium, rubidium, cesium - is of practical importance because the alkalies possess low ionization potentials (from 3.9ev to 5.4ev). This property leads to high ionization probablities for the alkalies and places them in the role of electron donors. The alkalies, therefore, are very interesting as components of stellar atmospheres and other plasmas. Of particular note are low energy electron collisions with cesium because of the importance of cesium seeding as a means of producing a gas of sufficient electrical conductivity for use in the proposed magnetohydrodynamic techniques for direct conversion of heat to electricity. Knowledge of the low energy electron scattering cross section is an important design requirement.

II. THEORY

(A) Introduction

In considering the scattering of electrons by atoms, complications arise which make the problem much more difficult than that of scattering by a static force field:

(1) the equation of motion for the system of incoming electron and target atom is a many body problem. As such it will not be subject to exact solution, which is in principle possible for the central static field scattering problem.

(2) inelastic processes may take place if the incident energy is high enough to cause a transition of the target atom to any of its excited states.

In treating low energy electron atom scattering, there are two additional major effects which further complicate calculations. These effects are the possibilities of exchange between the incident electron and the atomic electrons, and the distortion of the atom by the electric field of the incident charged particle.

Exchange effects may be taken into account by explicit anti-symmetrization of the total wavefunction for

the composite system. Regarding atom distortion, there is a sequence of inter-related effects as the electron approaches from a distance and draws near to the atom. For very large separations, the system consists of a point charge and a neutral atom. There exists between them an attractive $1/r^4$ polarization potential due to the electric di-pole moment induced in the atom by the electric field of the point charge. The strength of this potential is characterized by the polarizability "α" of the atom. Basically, the polarizability is defined as the mean displacement of atomic charge per unit external electric field. It is clear that α is related to the structure of the atom, being more pronounced for atoms of loose electronic structure. For highly polarizable atoms then, the Born approximation, which neglects deformation of the atom by the incident electron, is definitely not applicable.

As its separation from the atom decreases, the electron is accelerated by the polarization potential and can achieve a velocity of similar magnitude to the orbital electrons. This leads to velocity dependent interactions. Finally, upon penetrating the atom, correlation effects between the scattering electron and the atomic electrons become

important since the atomic configuration must adjust for the close proximity of this additional electron.

In general, most theoretical efforts have considered only the first of these effects. What is done then is to assume that the velocity of the incident electron remains much less than the velocities of the atomic electrons so that the entire electronic configuration of the atom instantaneously readjusts for each position of the incident electron. From the resulting distortion, usually only the dipole polarization part is retained. This constitutes the adiabatic approximation. This approximation works best for a very low energy electron (i.e. its velocity is $\ll$ that of the orbital electrons) at a large distance from the atom. All the electron experiences is the long range $1/r^4$ attractive potential. This potential, however, has the effect of increasing the electron's velocity towards the atom. The next term in the perturbation expansion describing the distortion of the atom is of the form $\hat{r}.\nabla/r^5$. This amounts to a velocity dependent correction on the adiabatic approximation. As the incident electron's velocity continues to increase, the magnitude of this velocity dependent correction, also known as a dynamic polarizability, will begin to be

important. In fact, at some radial distance from the atom, the dynamic polarizability will be comparable to the static polarization potential thus destroying the adiabatic approximation. (e.g. such a distance calculated for hydrogen was found to be 2.5 bohr radii.) Because this distance is energy dependent, increasing rapidly with the energy of the incident electron, the adiabatic approximation is simply not a good approximation at most energies, breaking down more rapidly for more polarizable atoms.

In the method of polarized orbitals (p.o.) devised by Temkin and Lamkin[16], the composite system trial wavefunction includes a function which represents the distortion of the atomic wavefunction when the atom is perturbed by the presence of an electron fixed at a point external to the atom. This is likely to be a reasonable procedure when the velocity of the incident electron is much less than that of the atomic electron. Since the approximation is meaningless for the incident electron being within the atom, the trial wavefunction is discontinuous, containing a step function which cancels that portion of the wavefunction arising from distortion due to an external charge if the incident electron passes within the atom. Because of this

discontinuity, the integro-differential equations of the polarized orbital approximation are not variationally based. Mittleman and Peacher[17] have attempted to improve the p.o. method by removing the discontinuity in the trial wave-function and then obtaining a variationally based set of integro-differential equations. They concluded that their apparently improved version has enough dependence upon arbitrary parameters associated with the short range cutoff of the long range polarization potential to eliminate both it and the original p.o. method from being a predictive theory at this point.

(B) Special Characteristics of the Alkalies

In considering low energy electron scattering with the alkalies, because of two unusual properties of these atoms, certain simplifications arise in the theoretical treatment of the scattering problem. The electron configuration in the ground state of an alkali atom consists of one or several filled shells outside of which is found one S-electron. The filled shells are very stable but the valence electron is weakly bound. Consequently all discrete atomic states of the alkali metals can be attributed to this electron alone. And it is not a bad approximation to

consider that the valence electron moves in the spherically symmetric stationary effective field of the nucleus and the inner electrons. Because of the valence electron's weak binding, its state changes easily under the action of an external field and therefore the alkali metals are characterized by a high polarizability.* Thus the long range polarization potential $\frac{-\alpha}{r^4}$ plays a major role in determining the low energy electron-alkali atom collision cross section. The strength of these polarized interactions lead to very large effective cross sections, of the order of several hundred square angstroms, in the 1-10 ev incident energy range.

Since almost all of the deformation of an alkali atom can be attributed to deformation of the state of the valence electron, the effect of an incident electron upon electrons of the filled shells need not be considered so that the problem of the collision of an electron with an alkali amounts essentially to a consideration of the motion of the incident and valence electrons in the stationary

---

*The polarizability of the alkali atom is somewhat less than the polarizability of the outer electron, since in the polarized state this electron polarizes the core electrons in the opposite direction.

field of the nucleus and inner electrons - basically, a two electron problem.

The Hamiltonian describing this is given by:

$$H = -\frac{\hbar^2}{2m}(\nabla_1^2 + \nabla_2^2) + V_c(r_1) + V_c(r_2) - \frac{Ze^2}{r_1} - \frac{Ze^2}{r_2} + \frac{e^2}{|\vec{r}_1 - \vec{r}_2|}$$

where $V_c(r)$ is the potential created by the electrons of the filled shells (CORE). This form neglects both magnetic and relativistic interactions, the importance of which are discussed in reference 4.

(C) Close Coupling Approximation (c.c.)

The most general method of seeking a solution to the Schrodinger equation describing the incident electron-target atom system is to express the composite system wavefunction as an expansion over the complete set of eigenfunctions of the atom's stationary states with the expansion coefficients describing the motion of the impinging electron. The possibility of exchange is included through explicit antisymmetrization of this wavefunction. For an electron incident upon a hydrogen atom in its ground state, the total system wavefunction is then described by:

$$\Psi^{\pm}(\vec{r}_1, \vec{r}_2) = (1 \pm P_{12})\left[\sum_{n=1}^{\infty} + \int\right] \phi_n(\vec{r}_1) F_n^{\pm}(\vec{r}_2)$$

where: the summation is over the discrete spectrum of hydrogen,

the integration is over the atom's continuum states,

P_{12} is an operator which exchanges the coordinates* of the incident and atomic electrons,

the functions $\phi_m(\vec{x}_i)$ are the eigenfunctions of the unperturbed hydrogen atom,

the functions $F_m^{\pm}(\vec{x}_j)$, to be determined, describe the motion of the bombarding electron and satisfy the boundary condition:

$$F_m^{\pm}(\vec{x}_j) \underset{r_j \to \infty}{=} e^{i\vec{k}_m \cdot \vec{x}_j}\delta_{m1} + \frac{e^{ik_m r_j}}{r_j} f_m^{\pm}(\hat{x}_j)$$

with the + and - signs referring to the spins of both electrons being respectively antiparallel and parallel.

The expression for $\Psi^{\pm}(\vec{x}_1, \vec{x}_2)$ contains an infinite number of terms, and therefore its substitution into the Schrodinger equation will require the solution of an infinite set of differential equations. This is clearly impossible to handle and various methods of approximation have been proposed. Among these the most important, at low incident electron energies, is the close coupling approximation.

---

*Both the spatial and spin coordinates of the incident and atomic electrons are taken to be included in the designations $F_m^{\pm}(\vec{x}_j)$ and $\phi_m(\vec{x}_i)$.

The basic assumption of this method which was first considered by Massey and Mohr[18] is that the infinite expansion for the composite system wavefunction can be truncated to a sum over only a few of the atom states, namely:

$$\Psi_{cc}^{\pm}(\vec{r}_1,\vec{r}_2) = \sum_{n=0}^{N} \left[\phi_n(\vec{r}_2) F_n^{\pm}(\vec{r}_1) \pm \phi_n(\vec{r}_1) F_n^{\pm}(\vec{r}_2) \right]. \quad (1)$$

According to Burke, Ormonde and Whittaker[19], the close coupling expansion can lead to very reliable results due to the effect of the explicit antisymmetrization. Since the inner regions of the functions $F_n(\vec{r}_i)$ are arbitrary, they can take up part of the atomic distortion induced by the electron-electron interaction. In fact, the exchange term in the expansion may be regarded as representing part of the continuum explicitly omitted from the summation. Thus the exchange term as well as satisfying the Pauli principle allows for distortion of the atom.

The expression for the wavefunction Ψ_{cc} upon substitution into the Kohn variational principle yields N coupled integro-differential equations of the form:

$$(\nabla^2 + k_n^2) F_n^{\pm}(\vec{r}) = \sum_{m=0}^{N} \left(U_{nm} F_m^{\pm}(\vec{r}) \pm \int K_{nm}(\vec{r},\vec{r}') F_m^{\pm}(\vec{r}')\, d\vec{r}' \right)$$

$$(n = 0, \ldots, N) \quad (2)$$

where: $k_n^2 \equiv \frac{2m}{\hbar^2}(E - E_n + E_0)$

E = the energy of the incident electron
E_0 = the ground state energy of the atom
E_n^o = the energy of the atom's nth excited state

$$U_{nm} \equiv \frac{2me^2}{\hbar^2}\int \phi_n^*(\vec{x}')\left[\frac{1}{|\vec{x}-\vec{x}'|} - \frac{1}{r}\right]\phi_m(\vec{x}')\,d\vec{x}'$$

and $K_{nm}(\vec{x},\vec{x}')$ are non-local interaction kernels arising from exchange.

With partial wave analysis, equations 2 are reduced to radial equations which then can be solved numerically by computer to yield an approximation for the cross section matrix coupling the N eigenstates included in the expansion 1.

It is characteristic of the close coupling approximation that explicit allowance is made for every mutual coupling or transition. Such self-consistency automatically provides the unitary property of the S-matrix.

There are several difficulties with the close coupling method. These include the fundamental problem of choosing sufficiently accurate atomic wavefunctions especially in the case of heavy atoms and uncertainties about the convergence of the eigenfunction expansion with increasing N. However, the main source of difficulty with the close

coupling approximation is gauging its accuracy when the complexity of the computational problem is such that only a few excited states can be included in the expansion 1.

In the case of the alkalies, this problem is lessened considerably because of the following property. The alkali atom ground state (an S orbital of large radius) is separated in energy by a small amount (the maximum separation is 2.1 ev for sodium) from the first excited state (a P orbital). As a result, practically all the polarizability of the alkalies arises from interaction between these orbitals. Because of this strong coupling between the ground and first excited states, a close coupling calculation, for electron energies below threshold, which included just these two states will be a very good approximation. At electron energies $\geq$ the first excitation threshold, the total cross section is the sum of the elastic and inelastic cross sections. The elastic cross section is still well-accounted for just by inclusion of the ground and first excited states. However, as discussed by Burke et al[19], in computing inelastic cross sections, the close coupling expansion should include every channel that is energetically open. From the computational point of view, this becomes

increasingly difficult as the energy of the incident electron increases. Thus far only some inconclusive studies have been made of the convergence of the eigenfunction expansion as more and more atom states are included.

To summarize, the close coupling method appears to be extremely well-suited to the calculation of low energy elastic electron alkali total cross sections. With regard to inelastic total cross sections, the method will also be applicable as long as the electron energies are such that only a few excited atom states need be included in the expansion. For higher electron energies, there is uncertainty, and therefore reliable experimental data with which the predictions of the close coupling method may be compared is very important.

(D) Existing Conditions

As mentioned in Section I, there have been a number of recent calculations on the scattering of low energy electrons by alkali atoms. Only two of these, however, have been close coupling calculations with exchange - on lithium by Burke and Taylor[9] and on lithium, sodium, potassium and cesium by Karule[4] and Karule and Peterkop[5]. The remaining theoretical efforts have, for the most part,

focussed on the adiabatic and polarized orbital approximations.

With regard to electron-cesium and electron-potassium scattering, the most extensive calculations thus far are those of Karule (electron energies from zero to the first inelastic threshold) and Karule and Peterkop (electron energies from the first inelastic threshold to 5ev). For both energy ranges, the close coupling approximation with just the ground and first excited states included was applied*. Semiempirical atomic wavefunctions found by the method of Gaspar[20] were adopted for both potassium and cesium. Up to nine angular momentum states were included in the partial wave analysis: $0 \leq L \leq 8$, where L represents the total angular momentum of the composite system. In the case of potassium at $L \geq 4$ and in the case of cesium at $L \geq 5$, exchange was ignored. In order to evaluate the effect of the choice of different atomic wavefunctions, similar calculations were made on Cs using

---

*The fact that some of the inelastic cross sections calculated by Karule and Peterkop were obtained with only the first excited state included in the c.c. expansion when other excited states were energetically possible implies an error in these calculations beyond that resulting from the atomic wavefunction used.

atomic functions derived from the potentials** of Stone[21]. It was found that this change in the wavefunction increased the magnitude of the cross section by 27.5% at zero energy and decreased it by 13% at 1 ev. However, the general shape of the plot of the dependence of the partial cross-section on electron energy did not change. The magnitudes of the potassium and cesium cross-sections obtained by both Karule and Karule and Peterkop were approximately half as large as the experimental values of Brode.

For electron-Rubidium collisions at low energies, there apparently has been only one calculation. This was made by Balling[8] in 1969 over the electron energy range 0.03-13.7ev. This calculation, which only obtained elastic X-sections, did not use the c.c. method but rather consisted of a polarized orbitals approximation with Hartree-Fock-Slater*** wavefunctions. These atomic functions yielded excessively high electric dipole polarizabilities as compared to the experimental values of Chamberlain and Zorn[22].

**This potential was so constructed that the difference between theoretical and experimental values of the energy levels and oscillator strengths were minimal. The cesium eigenfunctions thus calculated ignored spin-orbital interactions.

***The HFS wavefunctions were calculated employing the Slater approximation. In this approximation, exchange integrals in the Hartree-Fock equations are replaced by an average exchange potential.

Balling obtained elastic total cross sections using both the calculated polarizabilities and a modified version based upon the experimental values. His results differed with each other by about 30% in magnitude and also varied qualitatively. Both sets of cross sections values however were approximately smaller by a factor of two as compared with the measurements of Brode.

III. EXPERIMENTAL SYSTEM

A. General Physical Description

Figure 1 is a block diagram of the vacuum and its components. The apparatus essentially consists of three sections or main chambers: the oven chamber, the scattering or interaction chamber and the detection chamber. With the exception of the oven chamber, which is constructed of aluminum, the system has been assembled from interchangeable and varied thick-walled pyrex glass units. Employing viton o-ring seals, the chambers can be outgassed by baking them with heating tapes.

The three chambers are each primarily exhausted by a water cooled oil diffusion pump; the oven chamber by a 1000 liter per second 4" diameter Dresser pump and both the detector and scattering chambers by 600 liter persecond 4" Edwards' pumps. These are in turn evacuated by a Welch duoseal mechanical pump. This pump also serves to rough out from atmospheric pressure any part or all of the apparatus. Three Bayard-Alpert ionization guages as well as three thermocouple gauges are mounted on the system in order that the pressure in any segment can be spot checked or monitored continuously.

Each chamber is protected by a freon-cooled baffle from diffusion pump-oil migration. In addition, both the oven and interaction chambers have liquid nitrogen traps above the baffles. The trap below the oven chamber is necessary to prevent large amounts of alkali vapor from descending into the diffusion pump since this vapor reacts in a chemically destructive fashion with the silicone-base pump oil. The second liquid nitrogen trap is used to stop any oil vapor which manages to get beyond the freon baffle from entering the scattering chamber. The presence of oil vapor can seriously affect the performance of the electron gun through the formation of surface layers or films that can acquire electric charge. These deposits may also form on the surface of the cathode significantly decreasing its emission and altering the electron energy distribution. Consequently, this liquid nitrogen trap is continuously maintained full. The trap below the source chamber, however, is only kept filled while the oven is hot. During all data runs, the pressure within each of the chambers was less than $5(10)^{-7}$ torr.

All three of the system's major components - the oven, the electron gun and the atom detector - are attached

to mounts which are connected to stainless steel rotary shaft vacuum feedthroughs. These permit both up and down and rotational motion. In the case of the electron gun, through the employment of a sliding o-ring seal, motion transverse to the atom beam is also possible.

A flexible coupling or bellows between the interaction and detection chambers permits horizontal motion of the detection chamber. A fine thread lead screw driven by a variable speed motor then furnishes a precise and continuous movement of the atom detector transverse to the atom beam. Through the use of a dial gauge and a linear potentiometer, this motion can be calibrated and electronically recorded.

Figure 2 is a schematic of the total cross section system indicating the overall size of the system and the separation between various components.

B. System Alignment

With one or more micrometers mounted on each of the main chambers, the positions of the oven, electron gun and detector can be precisely varied. Alignment of the system was achieved in several steps. First, with the electron gun not present, the oven and atom detector

positions were varied until the measured atom beam was a maximum. The electron gun was then inserted. Initially, the correct height for the gun was approximately established using a transit. Then, in small steps, the gun was moved transversely to the atom beam direction - after each transverse step, being rotated both clockwise and counterclockwise. This process was continued until the atom beam signal reappeared, and then fine adjustments on all the degrees of freedom of the electron gun were made until a maximum signal was noted. Due to additional collimation being imposed upon the atom beam by slits on the mount of the electron gun, the detected atom beam was reduced in magnitude.

C. Atom Beam Source

The atom beam is generated by heating a slug of alkali metal within a roughly cubical oven until the vapor pressure of the alkali is sufficient to produce an easily detectable signal (10^6 - 10^7 atoms per second striking the atom detector). The oven has been machined from regular monel, a high strength, high melting point (1300° - 1350°C) metal composed mainly of nickel (63-67%) and copper. In addition to offering excellent corrosion resistance to the

alkalies and to many acids, monel also posseses a high thermal conductivity. To prevent any significant heat loss, the oven was supported on three needle standoffs set in a micalex plate. The oven temperature was determined by measuring the potential difference across the junction of an attached ironconstantan thermocouple. Two such thermocouples were employed: one at the front of the oven near the orifice and the other at the rear close to the well containing the alkali slug. This was to check that no significant temperature gradient existed along the oven's length (found to be $< 5^{\circ}C$ at $200^{\circ}C$). Knife edge slits (set at .006" apart) mounted on the aperture and a series of collimating slits beyond served to define the emitted atoms into a narrow rectangular beam.

D. Electron Gun

The electron gun employed has been constructed according to a design which is described in great detail in reference 23, and, therefore, the following discussion on the details of the electron gun has been abbreviated.

Figures 3-7 are drawings of the various gun parts giving dimensions and tolerances. As indicated on these diagrams, almost all of the metallic parts of the gun are

machined from molybdenum. Molybdenum has been chosen because it possesses a very low thermal coefficient of expansion and has both a low vapor pressure and exceptionally good mechanical properties at elevated operating temperatures. The insulators, acquired from Sheffield Precision Ceramics company, are made of the ceramic "alumina" (Al_2O_3: 99% pure). Alumina is chemically inert and has a very high electrical resistivity: at 300°C, 10^{12} ohms. Consequently, very little or no leakage current has been noted during operation of the gun.

The filament and the cathode are parts of a Raytheon 4D32 tube. The filament, which is made of tungsten wire, is used to indirectly heat the cathode. The indirect heating is essential in order to maintain a constant potential over the emitting surface. A potential gradient could lead to an excessive energy spread among the emitted electrons. The cathode, an oxide-coated type, consists of a flat nickel tube which is sprayed with a mixture of barium and strontium carbonates. Upon heating in vacuum, the carbonates are reduced to the oxide, with a substancial lowering of the work function resulting in copious electron emission. Since it is necessary that the cathode maintain good emis-

sion properties over a long lifetime, then the following requirements are imposed:

1. Contamination from all the other components of the gun must be eliminated so that these objects when heated do not give off substances that may damage the cathode. Consequently, stringent cleaning procedures were applied to the various gun parts, e.g.: all molybdenum parts were electropolished, rinsed in deionized water and then passed through a degreasing process. Also the gun was assembled in a clean working area while using special vinyl gloves.

2. The cathode must be carefully activated. This is accomplished by gradually increasing current to the filament in steps of .1 ampere while always maintaining the pressure below $5(10)^{-6}$ torr. This process usually takes about two days. If the temperature of the cathode is raised too rapidly, there is risk of blistering, flaking or evaporating the coating. Furthermore, since there is likely to be significant out-gassing of the cathode during its activation, it is important that there be no potentials applied to any of the electrodes in the gun at this time. This is to prevent ionization of outgassed molecules by accelrated electrons and ensuing bombardment and destruction of the

cathode by these ions. For the same reason, throughout the cathode's lifetime the pressure in the gun chamber should be maintained below $5(10)^{-6}$ torr.

The components of the gun have been machined so that they can be sequentially stacked on four accurately located ceramic rods (see Figure 8). Besides the advantages of great ease of assembly and versatility of internal design, this stacking ensures that the components are rigidly fixed closely parallel to each other. Electrical contacts to the gun were made by spot welding .040" diameter nickel wire to the filament leads and .013" diameter nickel wire to tabs on the other electrodes.

The essential requirements for the electron gun were as follows:

1. the production of a stable parallel beam of electrons.
2. the electron energy spread about the central energy should be less than 350 millivolts.
3. the electron beam should be intense enough so that the signal resulting from electron atom collisions is sufficient to yield a tractable signal to noise ratio.

The electrons are confined through the action of an external magnetic field. This field is generated by a

cast alnico C-shaped permanent magnet mounted so that the electron gun is centered in the gap space of the magnet. The field strength across this gap is 1200 gauss. Also the electrons are collimated heightwise through the employment of three or more masks deployed through the gun before the equipotential region.

Two somewhat different internal designs have been used for the electron gun. The first design, illustrated schematically in Figure 9, will be designated the four grid gun. In the four grid gun, the third and fourth grids, separated by .050" but maintained at the same electric potential, establish an equipotential region. The height of the electron beam through the region is collimated to .150". The second design, illustrated schematically in Figure 10, will be designated the three grid gun. In place of a fourth grid, it employes two molybdenum blocks that form a .250" long by .067" high channel. In the three grid gun, the equipotential region is established by the third grid and the two molybdenum blocks, all tied together electrically. The height of the electron beam through this region is collimated to .057", and the amount of current striking the region's walls is less than 4% of the total electron current

through the region thus indicating the effectiveness of the magnetic field and the masks.

Through the use of moveable knife edge slits on the gun mount and a calibrated motion travelling microscope, the atom beam is directed through the desired portion of the equipotential region. The gun also serves to additionally collimate the atom beam so that its dimensions in the equipotential region are:

(a) 4-grid gun: height .100", width .008".

(b) 3-grid gun: height .067", width .008".

In using the four grid design, a serious problem arises, namely: ensuring that in stacking the various components of the gun, the fourth grid is very accurately aligned with the third grid. If this is not the case, there will be a large number of electron collisions with the fourth grid's mesh, and many electrons will be reflected back into the equipotential region. This effect can result in a large error in the measured cross sections. To minimize electron collisions with the fourth grid, the grid alignment was checked under a microscope during the assembly of the gun. In the three grid gun, because the equipotential region offers no impediment to the existing electrons, the

above problem is not present. An advantage offered by the four grid design, however, is the ability to pass much larger (twice as much) electron currents and greater atom fluxes through the interaction region resulting in much higher signal levels. In both design guns, the grids are separated from each other by a distance approximately equal to five times the spacing between the grid mesh wires in order to prevent any significant inter-electrode field penetration.

The cathode was heated to a high enough temperature so that its operation was space-charge limited. The space charge cloud formed in front of the cathode is useful in that it tends to mask any small variation in work function over the cathode's surface. The control grid, G_1, run positively, draws electrons from the space charge cloud. Together with the second grid, it serves to control the amount of electron current and to some extent the velocity distribution of the electrons in the equipotential region.

Some typical operating voltages for the electrodes of both gun design were:

Cathode	Ground Potential
G_1(control grid)	+1.5 volts
G_2(focussing grid)	+3 volts
G_3(equipotential grid)	+4 volts
G_4(equipotential grid)	+4 volts
or Channel formed by molybdenum blocks	+4 volts
slit anode, anode } collector	+30 volts relative to the equipotential region

All these voltages were obtained using well-regulated modular Kepco power supplies (PBX) run in the constant voltage mode. Employing an NJE model SVC power supply in the constant current mode, the filament current was held steady at 3.5 amperes, and consequently the temperature of the cathode remained constant. At the above settings, the total amount of current passing through the interaction region was about 250 microamperes for the four grid gun and about 110 microamperes for the three grid gun. This electron current was determined both through the use of a precision microammeter and by measuring the amplified voltage drop across a known resistor in the plate circuit.

With the liquid nitrogen trap below the gun chamber continuously maintained full, the cathode's emission

remained steady and its lifetime exceeded five months.

E. Detection System

The beam atoms are detected through surface ionization with a .010" wide by .004" thick platinum wire (highest purity obtainable, better than 99.99%). The positive ions boiled off the hot wire are accelerated by a negative potential of 2000 volts into the first dynode of an ITT FW-141 electron multiplier. The gain of the multiplier is of the order of 10^5. An electrometer (Keithley Model 601) measures the multiplier output.

The number of atoms scattered per second is determined in the following manner. The platinum wire detector is maintained on the axis of the unscattered atom beam. In a collision an atom will experience momentum transfer and thus there will be a smaller number of atoms reaching the detector with the electron beam present than without it (a scattering-out process). Because the number density of particles in the atom beam is considerably less than the molecules of residual or recombined gas (at a chamber pressure of $6(10)^{-7}$ torr, the number density of residual gas molecules is about $2(10)^{10}$ per c.c.), to distinguish atom collisions with electrons from those with this back-

ground gas, the electron beam is modulated. Specifically, a reference signal from a lock-in amplifier (Princeton Applied Research Model HR-8) drives a circuit which causes the electron gun control grid to swing between its positive operating voltage and cutoff at the frequency of the reference signal (20hz). This ac modulation of the electron beam is impressed upon the atom beam during its passage through the interaction region. As a result the signal from the atom detector has a small amplitude (of the order of 1/1000th of the full signal) 20hz square wave component. This ac portion, known as the scattering-out signal, is amplified by a narrow-band amplifier tuned to the modulation frequency and is measured by a phase-sensitive detector. Figure 11 is a block diagram of the detection system.

If the detector is displaced far enough off the axis in the direction of the electron beam, then scattered atoms that had recoiled enough to miss the detector when situated on axis will now be picked up. The resulting ac signal is 180° out of phase with the scattering-out signal and is usually called the differential scattering-in signal.

IV. DATA ACQUISITION SYSTEM

Because of the variation in the atom beam due to vacuum fluctuations and shot noise, it was necessary to accumulate data for long periods of time in order to obtain good statistics. To accomplish this, an automatic data acquisition system was set up.

Employing an input scanner, a voltage to frequency converter and a preset counter (respectively Hewlett-Packard models 2901A, 2212A and 5214L), nine separate voltages were automatically sequentially digitalized and integrated. Contact closures available at the output of the scanner allowed any or all of the various monitored signals to pass through voltage dividers, time delays to be imposed before digitalizing and variations in the preset number of counts so that more than one integration time could be employed during a run. With the addition of an output coupler (Hewlett-Packard model 2547A) and an IBM 526 keypunch, the results of a single data run were recorded as nine 5-digit numbers on an IBM card. Each data run, of approximate duration five minutes, included an eighty second integration of the scattering out signal and ten second integrations of both the atom beam and electron

beam signals. By taking between five and ten runs at each electron energy, quite good statistics could be obtained. A standard cell was used to calibrate the digital system. Figure 12 is a block diagram of the data acquisition system.

V. EXPRESSION FOR THE TOTAL CROSS SECTION

In the case of a rectangular beam of electrons orthogonally cross-firing a rectangular atom beam, the total cross section Q for the scattering of an electron by an atom is directly obtained from a simple relation containing experimentally measured quantities and a geometrical factor. This relation is derived as follows:

Since the average velocity in the electron beam is much greater (a factor of 1000 or more) than the average atom velocity, we can consider the electron beam to be crossing a region within which there is a density of atoms N_a. Then the probability dP that an electron, in moving a distance dz into this region, will be scattered by an atom is given by:

$$dP = N_a \, dz \, Q$$

where Q is the effective target area for scattering presented to an electron per atom or more briefly the total collision cross section.

In reality, there is a flux of atoms propagating in the y-direction through this region (see Figs. 13 and 14) and therefore we replace N_a by $J_a(x, z)/V$ where $J_a(x,z)$ is the atom flux density and V is the atom velocity. The fact

that there is a distribution of velocities in the atom flux is taken into account by integrating the scattering probability over this velocity distribution:

$$dP' = \int dP f_A(V)\, dV$$
$$= dz\, J_a(x,z)\, Q \int \frac{1}{V} f_A(V) = C V f_o(V)$$
$$= dz\, J_a(x,z)\, Q \left\langle \frac{1}{V} \right\rangle$$

where $f_A(V)$ is the normalized velocity distribution of the atom beam flux.

If the atom beam is due to diffusion from an ideal slit (see Section VII-B), then the normalized atom beam flux velocity distribution will have the modified Maxwellian form:

$$f_A(V) = \frac{M^2 V^3}{2k^2 T^2} e^{-MV^2/2kT}$$

where k is the Boltzmann constant and T is the temperature of the source in degrees kelvin. With this particular distribution, a standard integration then yields:

$$\left\langle \frac{1}{V} \right\rangle = \left(\frac{M\pi}{8kT} \right)^{\frac{1}{2}}.$$

This, in fact, is the reciprocal of the mean atom velocity in the source as the following argument will show. The beam flux velocity distribution is related to the normalized velocity distribution in the source $f_o(V)$ by:

$$f_A(V) = C V f_o(V)$$

where C is a normalization constant. Since both distributions are normalized, $C = 1/\bar{V}$ where $\bar{V}$ is the mean velocity of the atoms in the source.

Therefore:

$$\left\langle \frac{1}{V} \right\rangle = C \int \frac{1}{V} V f(V)\, dV$$

$$\left\langle \frac{1}{V} \right\rangle = C \int \frac{1}{V} V f_0(V)\, dV$$

$$\left\langle \frac{1}{V} \right\rangle = C = 1/\bar{V}$$

And: $$\bar{V} = \left(\frac{8kT}{M\pi} \right)^{\frac{1}{2}}.$$

The total number of electrons scattered* per second I_s is obtained from

$$I_s = \iiint dx\, dy\, J_e(x,y)\, dP'$$

where J_e (x,y) is the electron beam flux density. Expanding this expression we obtain:

$$I_s = \rho \left\langle \frac{1}{V} \right\rangle \iiint dx\, dy\, dz\, J_e(x,y)\, J_a(x,z).$$

The above triple integral is known as the overlap integral. Since the interacting electron and atom beams

---

*Under the thin target conditions which exist in the interaction region, there are negligible multiple collisions and the number of scattered electrons equals the number of scattered atoms.

are rectangular in cross section, the overlap integral can be easily evaluated with certain assumptions. The geometry of the interaction region differs for each electron gun design, and therefore two evaluations of the overlap integral are necessary. Figures 13 and 14 depict the interaction region geometry for each gun design.

(1) 4-grid gun: in the equipotential region, the height of the electron beam (.150", X-dimension) exceeds that of the atom beam (.101"). The overlap integral is:

$$\int_{-\frac{h}{2}}^{\frac{h}{2}} dx \int_{-\frac{\ell}{2}}^{\frac{\ell}{2}} dy \int_{-\frac{W}{2}}^{\frac{W}{2}} dz \; J_a(x,z)\, J_e(x,y) \; .$$

Assuming that the electron beam flux density is constant over its width in the interaction region (y-dimension) and uniform over the height of the electron beam** leads to:

$$J_e \int_{-\frac{\ell}{2}}^{\frac{\ell}{2}} dy \int_{-\frac{h}{2}}^{\frac{h}{2}} dx \int_{-\frac{W}{2}}^{\frac{W}{2}} dz \; J_a(x,z)$$

$$= \left(\frac{I_e}{\ell H}\right) \ell \, I_a$$

$$= \frac{I_e I_a}{H}$$

** This particular assumption will be discussed further in Section VII.

where I_a is the number of atoms/second through the interaction region

I_e is the number of electrons/second through the interaction region

$I_e = I/e$ with I the measured electron gun current and e the electron charge.

If we take the atom beam flux velocity distribution to be a modified Maxwellian distribution, then the empirical expression for the total cross section in the case of the 4-grid gun will be given by:

$$Q = \left(\frac{I_s}{I_a}\right)\frac{H\bar{V}}{I/e} \quad . \tag{3}$$

(2) 3-grid gun: the equipotential region height of the atom beam (.067") exceeds that of the electron beam (.057").*** For the overlap integral we have:

$$\int_{-\frac{H}{2}}^{\frac{H}{2}} dx \int_{-\frac{l}{2}}^{\frac{l}{2}} dy \int_{-\frac{W}{2}}^{\frac{W}{2}} dz \; J_a(x,z)\, J_e(x,y) \; .$$

Assuming that the atom beam is uniform over its height yields: $J_a(x,z) = I_a(z)/h$

***The effective height of the atom detector is .238" which is more than 3-½ times the height of the atom beam in the interaction region.

and the above becomes:

$$\frac{1}{h}\int_{-\frac{w}{2}}^{\frac{w}{2}} I_a(x)\,dx \int_{-\frac{l}{2}}^{\frac{l}{2}} dy \int_{-\frac{w}{2}}^{\frac{w}{2}} dx\; J_e(x,y)$$
$$= I_a I_e / h.$$

The empirical expression for the total cross section in the case of the 3-grid gun is then given by:

$$Q = \left(\frac{I_s}{I_a}\right)\frac{h\bar{V}}{I/e} \quad . \tag{4}$$

VI. SYSTEM PERFORMANCE CHECKS

To ensure that the electron gun and the detection system were performing properly, the following studies were made:

(a) Scattering-Out Signal vs. Electron Gun Collector Voltage:

With the atom beam intensity maintained constant, data runs (at several different equipotential region voltages for both electron gun designs) were taken to check that the scattering signal was independent of the electron gun collector voltage over a wide range of collector voltages. The results of these runs indicated that there was no significant field penetration of the collector potential into the interaction region and that secondaries from the collector could be neglected. Figure 15 displays two such runs.

(b) Scattering-Out Signal vs. Hot Wire Temperature:

At constant electron gun current and atom beam intensity, the variation of the scattering signal with the temperature of the hot wire was studied for all three alkalies. The detector wire must be hot enough so that its response time is very much less than the time for one modulation cycle (50 milliseconds). If the detector

temperature is not sufficiently high, there will be surface adsorption times large enough to cause an unwanted shift in the phase of the detection signal. Over a wide range of hot wire temperatures, it was found that both the peak signal phase setting of the AC detection system and the magnitude of the scattering signal remained the same. Below this range, due to non-negligible surface adsorption times on the hot wire for the ionized atoms, the peak phase setting was different and the magnitude of the scattering signal smaller. At temperatures above the constant phase range, there is excessive hot wire noise due to emission by the wire itself, and there is also danger of vaporizing the wire.

(c) Scattering-Out Signal vs. Atom Beam Intensity:

At constant electron gun current and for several equipotential region voltages, studies were made of how the scattering signal varied with the atom beam. In Figure 16 are the results of one such run, indicating a maximum percentage deviation of 2% and therefore verifying the proportionality of scattering signal to atom beam. This linearity also verified the existence of thin target conditions in the interaction region.

(d) Scattering-Out Signal vs. Electron Gun Current:

To make certain that the scattering signal was linear with the electron gun current, data runs, at constant atom beam intensity, of scattering signal versus gun current were taken at a number of equipotential region voltages. At all but the lowest voltages, the results indicated linearity to a high degree over a wide current range. For electron energies below .6ev, there was linearity over only the lower portion of the current range. At higher currents, the results were very nonlinear due to excessive space charge in the equipotential region. In normal operation, the electron gun current at each scattering voltage was set to be within the linear range. Figures 17 and 18 display the results of two such runs.

VII. DISCUSSION AND ESTIMATE OF EXPERIMENTAL ERROR

A. Random Error

The overall random error is primarily due to noise in the atom beam, arising from vacuum fluctuations and shot noise in the beam itself. Because of the overall high degree of stability of the experimental system and the accumlation of data for long periods, the statistics of the measured total cross sections have been exceptionally good: in the majority of cases the room mean square deviation was less than 5%.

B. Systematic Error

(1) Discussion

The best starting point for enumerating and estimating the sources of systematic error is through consideration of the empirical expression for the total cross section:

$$Q = \left(\frac{I_s}{I_a}\right)\frac{\bar{v}\,\mathcal{H}}{I/e} \qquad (5)$$

where $\mathcal{H}$ is a geometrical parameter representing the interaction region height of the atom beam for the 3-grid gun and the height of the electron beam for the 4-grid gun. The other quantities have previously been defined.

In using the 4-grid gun, it was assumed that the electron beam was uniform in density over its interaction region height. This assumption was tested through use of the 3-grid design in which the atom beam was taken to be of uniform density over its height in the interaction region. For potassium over the electron energy range 1.5ev - 9ev, the largest percentage difference found in the measured cross sections obtained with both gun designs was about 7%.

The expression for Q will be proportional to the mean velocity of the atoms in the source if the velocity distribution of the atom beam flux is a modified V^3 Maxwelliam distribution. According to Miller and Kusch[24], who performed a series of experiments to determine the velocity distribution of a thermal potassium beam, the beam flux will have this V^3 distribution if certain conditions are met on the oven design, namely:

(1) the oven is made of high thermal conductivity material to avoid significant temperature gradients.

(2) the oven slits approximate an ideal aperture, i.e. the slit width in the direction parallel to the beam propagation is very much less than the mean free paths of the atoms in order to eliminate

scattering in the neighborhood of the slit.

The oven has been designed to conform with these requirements. The mean velocity $\overline{V}$ is related to the absolute temperature of the source (see Section V), and uncertainty in measurement of the source temperature contributes to the overall systematic error. In order to confirm the modified Maxwellian velocity distribution of the atom flux, an independent measurement of the atom velocity using certain properties of the recoil method has been made. This will be fully discussed in section VIII).

In the relation for the total cross section is the ratio I_s/I_a. Because of this, uncertainties in the detection system such as the gain of the electron multiplier and the efficiency of the hot wire detector are removed.

Since the AC output voltage of the electrometer is measured using a lock-in amplifier, it is necessary to accurately determine its gain. This was accomplished using the built-in calibration of the instrument itself. As a check on this calibration, some cross section measurements were taken in which the lock-in amplifier was also used to measure the electron current. In this mode of operation, the gain of the lock-in cancelled out in the ratio of

I_s/I_e as well as any uncertainties with the duty cycle and shape of the modulation pulse. The obtained cross sections agreed with previous values to within 5%. Therefore any error involved in the calibration of the lock-in appeared to be quite small.

Physically, the scattering-out signal corresponds to the difference between the number of atoms per unit time striking the atom detector with the electron beam cut off and the number striking the detector with the electron beam present. This measured difference can to a large degree be incorrectly related to I_s because of the presence of backscattering (see Appendix A) in the electron gun and because of deficiencies in the detection system. With respect to the detection system, we have verified that its AC response was unchanged over a wide range of hot wire temperatures, that the scattering signal remained the same at several different modulation frequencies and was unaffected by the selected input impedance of the electrometer.

(2) Explicit Estimate of the Systematic Error

Consider: $$Q = \left(\frac{I_s}{I_e}\right)\frac{\bar{V}\,\%}{I/e}$$

The scattering signal SS* = $\frac{g_{LI} g_K g_{EM} c I_s}{2.22}$

where g_{LI} = gain of the lock-in amplifier

g_K = gain of the Keithley electrometer

g_{EM} = gain of the electron multiplier

c = efficiency of the hot wire detector

and the divisor 2.22 is present because the signal deflection indicated on the lock-in amplifier corresponds to the rms value of the peak amplitude of the fundamental of the input square wave.

The full atom beam signal DCB** = $g_K g_{EM} c I_a$.

The electron gun current signal $I_g = fZG_R I$,

where G_R = the gain of a differential amplifier

Z = the impedance in the plate circuit of the electron gun

f = the modulation fraction, i.e. the amount of each cycle that the electron gun is not cut off. This was adjusted to equal $\frac{1}{2}$.

---

*The measured scattering signal SS is the output voltage (DC) of the lock-in amplifier.

**The full atom beam signal DCB is the DC output voltage of the electrometer.

The atom velocity $\bar{V} = \left(\frac{8kT}{M\pi}\right)^{\frac{1}{2}}$

$$= \left(\frac{8k}{M\pi}\right)^{\frac{1}{2}} \left(299 + 2500\,\frac{TCR}{G_L}\right)^{\frac{1}{2}}$$

where G_L = gain of a differential amplifier

TCR = a reading or signal derived from a thermocouple mounted on the oven.

All of the above leads to the following operational expression for the total collision cross section:

$$Q = \frac{2.22\left(\frac{SS}{g_{L1}\,g_K\,g_{em}\,C}\right)\mathcal{H}\left(\frac{8k}{M\pi}\right)^{\frac{1}{2}}\left(299+2500\frac{TCR}{G_L}\right)^{\frac{1}{2}}}{\left(\frac{DCB}{g_K\,g_{em}\,C}\right)\left(\frac{I_g}{f\,Z\,G_a\,e}\right)} \qquad (6)$$

$$Q = 2.22e\left(\frac{8k}{M\pi}\right)^{\frac{1}{2}}\frac{f\,Z\,G_a}{g_{L1}}\frac{\mathcal{H}}{I_g}\left(\frac{SS}{DCB}\right)\left(299+2500\frac{TCR}{G_L}\right)^{\frac{1}{2}} \qquad (7)$$

where we have the following:

Parameter	Estimated Uncertainty
$\mathcal{H}$	$\pm$ 1% - 4 grid gun $\pm$ 5% - 3 grid gun
f	$\pm$ 1%
Z	$\pm$ 1%

Parameter	Estimated Uncertainty
g_{LI}	± 1%
G_R	± 1.5%
G_L	± 1.5%
TCR	± 3%
I_g	± 2%
SS	± 3% 3 grid gun
	± 11% 4 grid gun
DCB	± 5%

The most probable error, then, in the measured cross section due to systematic errors is:

δQ = ± 12% 4 grid gun
± 9% 3 grid gun
} SYSTEMATIC ERROR.

C. Absolute Electron Energy Determination

Because of the presence of contact potentials and space charge effects, the absolute energy of the electrons passing through the interaction volume is not equal to the potential applied to the electrodes defining the electron gun's equipotential region. To determine the contact potential and also the spread in the electron energy distribution, the standard technique of applying a retarding

potential between the collector and the cathode (RPD method) was employed. For the electron gun designs described previously, the electrons were retarded in the region between the slit anode and anode electrodes. This reduced space charge effects since only a small fraction of the electron beam was sampled and also prevented retarded electrons from returning to the equipotential region. The potential applied to the slit anode was maintained fixed at 11 volts above ground potential while the potential difference between the anode and the grounded cathode was decreased until no electrons reached the anode. This technique has been previously discussed in great detail in reference 23 and Figure 19 is a schematic of the circuitry.

The electron energy distribution or spread about the central energy at a particular applied equipotential region voltage is determined by tracing a retarding potential curve and measuring the curve's full width at half maximum (FWHM). A typical curve is shown in Figure 20. Since there is extra space charge produced immediately in front of the anode due to the retarding of the electrons, this method tends to give a somewhat larger energy spread than probable. By taking a series of RPD curves at progressively smaller

applied scattering voltages (and consequently smaller current densities), the effects of space charge are reduced to a degree where the point of zero effective kinetic energy of the electrons in the equipotential region, and thus the contact potential, may be determined, but only to $\pm$ .1ev. (See Fig. 21) This undertainty derives from a lack of precision in defining the cutoff point of the electron energy distribution.

Space charge effects in the interaction region require a further correction to the measured electron energies. This correction is made by calculating for a given current density the electrons' energies over that portion of the equipotential region intersected by the atom beam. For both electron gun designs, the calculation is outlined in Appendix B.

We estimate that the obtained absolute electron energies are uncertain by $\pm$ .15ev with an average energy spread (FWHM) of approximately 275 millivolts for the higher electron energies ($\geq$2ev) and $\leq$220 millivolts for the lower electron energies. This determination of the absolute electron energies has been confirmed by an independent method which utilizes properties of the recoil technique

and is discussed in the next section.

VIII. INDEPENDENT MEASUREMENT OF ATOM VELOCITY AND ABSOLUTE ELECTRON ENERGY

This technique required that the atom beam be velocity selected. To accomplish this, a Stern-Gerlach type magnetic velocity filter was employed (see Figure 22 for some details of the magnet design) with the oven laterally offset from the axis of the system. The amount of this offset is directly related to the fractional spread in atom velocity about the selected velocity through the simple relation:

$$\frac{\Delta V}{V_o} = \frac{w}{S}\,\frac{(l_1+l_2+l_3)}{l_3} \qquad (8)$$

where: ΔV is the spread in the atom velocity about the selected velocity

V_o, the selected velocity, is usually the most probable transmitted velocity

w is the width of the slit opening on the oven orifice

S is the amount that the center of the oven opening is offset from the system axis

l_1, l_2, l_3 are system dimensions.

This is depicted schematically in Figure 23. In reference 25, equation 8 is derived, and this mode of velocity selection is described at length. The magnitude of the offset S was such that $\frac{\Delta V}{V_0} \leq .2$.

Complete details of this measurement of atom velocity and absolute electron energy, and the theory behind it, are fully discussed in references 15 and 26. Below, a brief summary is presented.

The method consists of locating a peak in the differential scattering-in signal as the detector is swept horizontally across the atom beam in the direction of the scattering. The peak occurs for two reasons:

(1) the detector collects all atoms raised from the ground to the first excited state by electrons scattered through zero degrees(polar).

(2) the inelastic cross section is peaked in the forward direction.

The basic features of the recoil process are illustrated in Fig. 24. A velocity selected atom beam travelling in the y direction is intersected at right angles by an electron beam travelling in the z direction. θ and ϕ are the polar

and asimuthal angles of the scattered electron while the trajectory of the scattered atom is characterized by the angles Ψ and χ. The detector can be displaced so that the atom scattering signal can be measured as a function of the asimuthal angle Ψ. Also from momentum transfer considerations, the azimuthal angle of recoil of an atom excited by an electron scattered through zero degrees is given by:

$$\Psi = \frac{mv}{MV}\left(1 - \frac{v'}{v}\right) \tag{9}$$

where v is the initial electron velocity, v' is its velocity after the collision and V is the atom velocity. The horizontal displacement of the peak is given by $Z = L\Psi$, where L is the distance between the center of the interaction region and the plane of the detector. In terms of the excitation energy E_x and the initial electron energy E, we obtain:

$$Z = \frac{m}{MV} L \left(\frac{2e}{m}\right)^{\frac{1}{2}} \left\{1 - \left(1 - \frac{E_x}{E}\right)^{\frac{1}{2}}\right\} \tag{10}$$

where both E_x and E are in electron volts. From this relation both the atom velocity and absolute electron energy were determined in the following manner.

Using a cesium atom beam, a large enough voltage (31 volts) was applied to the equipotential region so that the error or uncertainty in the retarding potential determination of the contact potential was a very small fraction (<1%) of the electron energy. Then the excitation peak (for Cs, the transition $6S \rightarrow 6P$, $E_x = 1.45ev$) was located and its displacement Z off the axis of the unscattered atom beam measured. The peak in the differential scattering signal is sharper at higher electron energies (≥20ev) since the spread in the electron energy distribution is at these energies only a very small fraction of the central energy. The atom velocity V followed at once from solution of equation 10. Maintaining the atom velocity constant, smaller voltages (5 volts, 4 volts) were applied to the scattering region and total cross section data runs taken. Substitution of the measured atom velocity into the empirical expression for Q (equation 5) yielded values for the total cross section. These were compared with data obtained without a velocity selected atom beam and with the atom velocity derived from measurements of the source temperature. Within the estimated uncertainties, the two methods of measurement showed excellent agreement (percentage

difference 5%) and consequently lent credence to the assumption of a modified V^3 Maxwellian velocity distribution for the atom beam flux.

The same relation was used to determine absolute electron energies. For different applied scattering voltages, the excitation peak is found at different displacements. Keeping the atom velocity constant throughout, the measurement of each displacement at once yielded the corresponding absolute electron energy.

For both the measurement of the atom velocity and the absolute electron energies, the main sources of error were in the precise location of the excitation peak (uncertainty of $\pm$ .001"), in the spread of the atom velocities about the selected velocity, and in geometrical measurements. These cause the electron energies determined by the recoil technique to be uncertain by $\pm$ .15ev. In Table I are listed the results of three such determinations and the corresponding electron energies obtained from the retarding potential method (RPD) and space charge depression calculation.

Although this technique is applicable only above threshold, the fact that its absolute electron energies

agree with those of the retarding potential method modified by space charge corrections gives confidence that this latter method is valid at energies below threshold.

TABLE I

Comparison of Absolute Electron Energies determined by two methods

Equipotential Region Voltage	Absolute Electron Energy	
	Recoil Method	RPD-Space Charge Calc.
9 volts	$8 \pm .15$ ev	$7.9 \pm .15$ ev
7 volts	$6 \pm .15$ ev	$5.9 \pm .15$ ev
4 volts	$3 \pm .15$ ev	$2.9 \pm .15$ ev

IX. RESOLUTION

In the atom beam recoil method, for total cross section measurements, the detector is normally situated on the axis of the unscattered atom beam, and an electron-atom collision is observed only if the atom has departed enough from its initial trajectory to miss the detector. In this case, the worst minimum angle of resolution of the system is given by: $\Psi_0 = \frac{w}{L}$

where Ψ is the atom azimuthal scattering angle

w is the full width of the atom detector (.010")

L is the distance between the plane of the detector and the center of the interaction region.

Figure 25 depicts the trapezoidal distribution - resulting from the collimation imposed upon the effused atoms - of the atom beam in the plane of the detector. In the umbra region the source is completely unobscured, while in the penumbra regions the atom intensity as "seen" by an infinitely narrow detector varies linearly with displacement since the amount of exposed source varies in this manner. For a detector of finite width, the atom beam's half-width

can be obtained from the calculated geometrical profile by considering the observed beam intensity to be the integral of that portion of the trapezoid that is included within the detector width. This has the effect of rounding off the sharp edges of the trapezoid. Figure 26 displays the results of such a calculation. It is to be noted that the half-width obtained from the system geometry agreed to within 5% with half-widths determined from measured profiles of the atom beam.

Referring to Fig. 25, if the detector is displaced a few mils anti-parallel to the electron beam, the experimental resolution will be improved. This happens because the resolution is affected by two considerations:

(1) the distribution of atom beam within the region of the detector (region B) since this determines the percentage of atoms within B that miss the detector.

(2) the amount of atom beam to the right of the detector (region C) which determines the percentage of scattered atoms that are scattered into the detector.

Thus when the detector is displaced as indicated above, the number of atoms in region C is decreased, and some atoms that previously were collected by the detector

will now miss it with the result that the scattering-out signal increases. The resolution therefore has been improved. The further the detector is displaced to the right, the more improved will be the system resolution. In principle, the minimum resolved atom scattering angle could be reduced to zero corresponding to perfect resolution. However, as the detector is moved off axis, the signal to noise ratio continuously worstens due to a progressive decrease in the level of the atom beam signal. This makes it impossible to experimentally achieve perfect resolution. Therefore, because of the finite resolution of the apparatus, the cross section that is measured, Q_m, will always be less than the cross section Q_T that would be measured with perfect resolution.

If we consider a sliver of atom beam, of width dz, contained within the region of the detector (see Fig. 27), then for this element the relation between the measured total cross section and the perfect resolution total cross section is given by:

$$\Delta Q_T = \Delta Q_m + 2\pi \int_0^{\theta^*} \sigma(\theta) \sin\theta \, d\theta \qquad (12)$$

where the integration is over the unresolved small angle

scattering, with $\sigma(\theta)$ being the differential cross section and θ^* the smallest resolved electron polar scattering angle. This is the electron angle corresponding to the minimum atom angular deflection Ψ^* necessary to miss the detector. θ^* varies over the detector width as does the atom beam. To take into account both of these characteristics we average the expression (12) over the distribution of atom beam within the detector region. This yields:

$$Q_T = Q_m + 2\pi \frac{\int_{x-w_2}^{x+w_1} dx\, I_a(x) \int_0^{\theta^*} \sigma(\theta) \sin\theta\, d\theta}{\int_{x-w_2}^{x+w_1} dx\, I_a(x)} \qquad (13)$$

where $I_a(t)$ represents the atom beam intensity per unit length within the detector region and can be evaluated from the geometrical trapezoidal distribution.

For elastic scattering events*, the atom azimuthal scattering angle Ψ is related to the electron angle θ by the momentum transfer relation:

$$\Psi = \frac{\sqrt{2meE}}{MV} (1-\cos\theta) \qquad (14)$$

---

*We only have to consider elastic scattering because the inelastically scattered atoms suffer deflections that are large compared to the dimensions of the detector.

where E is the electron energy. Assuming that the differential cross section is constant over the small range of angles spanned by the detector width and utilizing eqs. 13 and 14 we obtain:

$$Q_T = Q_m + \frac{2\pi MV}{(2meE)^{\frac{1}{2}}} \frac{\sigma(0)}{L} \frac{\int_{\pi-\alpha/2}^{\pi+\alpha/2} dt\, I_a(t) \int_0^z dz}{\int_{\pi-\alpha/2}^{\pi+\alpha/2} dt\, I_a(t)}$$

where $dz = L\, d\Psi$

$z = L\Psi^*$

$\Psi^* = \frac{(2meE)^{\frac{1}{2}}}{MV}(1-\cos\theta^*)$

and $\sigma(0)$ is the differential cross section at zero degrees.

Referring to Figure 27, $z = \pi+\alpha/2-t$ and this leads to:

$$Q_T = Q_m + \frac{2\pi MV}{(2meE)^{\frac{1}{2}}} \frac{\sigma(0)}{L} \left\{ \frac{\int_{\pi-\alpha/2}^{\pi+\alpha/2} dt\, I_a(t)\left[\pi+\alpha/2-t\right]}{\int_{\pi-\alpha/2}^{\pi+\alpha/2} dt\, I_a(t)} \right\} \quad (15)$$

The term in brackets in the above has the units of length and can be physically interpreted as representing the effective width of the detector. We will designate this quantity by ΔX. It is clear that ΔX decreases as the detector is moved to the right. Equation 15 indicates that Q_m should increase linearly with decreasing ΔX, approaching Q_T as $\Delta X \rightarrow 0$. Thus it should be possible from a plot of

Q_m vs. ΔX to obtain Q_T by extrapolation to $\Delta X = 0$.

For rubidium, Fig. 28, and for cesium, Fig. 29 present some results on the variation of Q_m with ΔX. The behavior appears to be linear but the poor statistics prevent a very good extrapolation. The extrapolated curves for rubidium indicated the following percentage differences between Q_T and Q_m:

5% at electron energy 7 ev

4.8% at electron energy 4 ev

2.4% at electron energy 2 ev

The curve for cesium indicates a percentage difference of 7.4% at an electron energy = 1.9ev.

With the detector displaced .006" off axis, there is no atom beam to its right and $\Delta X = .0026"$. In Table II for each of the alkalies studied, we present values of the effective minimum resolved electron scattering angle θ_{min} at three different electron energies**. It can be seen that θ_{min} increases both with decreasing electron

---

**These values were obtained by solving equation 14 for χ as a function of θ over a range of electron energies. Comparison of the results with $\chi_{min} = \Delta X/L$ then yielded θ_{min} at each electron energy.

energy and with increasing atom mass. However, we cannot at present definitively state that the resolution improves as the electron energy increases. This is because at higher electron energies increases in the small angle scattering could offset the decrease in θ_{min}. This was in fact reflected by the results for rubidium in Fig. 28.

TABLE II

Unresolved small angle scattering for K, Rb and Cs at several electron energies

Alkali	Electron Energy (ev)	Effective Electron Resolution Angle
Potassium	1	7.7°
	3	5.8°
	5	5.1°
Rubidium	1	11.8°
	3	9.9°
	5	8.9°
Cesium	1	15.1°
	3	11.4°
	5	10.1°

X. EXPERIMENTAL RESULTS AND EVALUATION

A. Pre-Data Taking Procedure

Prior to each data run or group of data runs, a series of checks and calibrations were made to ensure that everything was working properly. They are briefly described below:

(1) The digital system was calibrated with a standard cell. This permitted the conversion of each recorded number into an absolute input voltage.

(2) The digitized electron gun current measurement was verified through use of a precision microammeter, and the digitized oven temperature reading was checked with a potentiometer.

(3) The gain of the lock-in amplifier was checked by employing the internal calibration of the instrument.

(4) The output voltage of the electrometer was calibrated against several known inputs.

(5) Using the digital system, a point by point profile of the atom beam half-width was compared with that obtained from the calculated geometrical profile.

(6) The absolute electron energies and electron energy spreads were checked by retarding potential measure-

ments.

(7) For each alkali investigated, the phase of the lock-in amplifier was carefully adjusted.

B. Results

In Figures 30 and 31 are shown total cross section data on rubidium and potassium obtained with both the 3-grid and 4-grid electron gun designs. These cross sections were measured with the atom detector centered on the axis of the unscattered atom beam, and the plotted values demonstrate excellent agreement between the two guns. The fact that there was such good agreement in measured total cross sections derived from two gun designs with significantly different interaction region geometries (see Section V) removes the possibility of any large source of error arising from assumptions made about the electron and atom beams in the interaction volume.

Figure 32 displays two total cross section curves on rubidium taken with the 3-grid electron gun design. There is a quantitative, but not qualitative, difference between the two sets of points. The smaller magnitude values were obtained with the atom detector on axis while the larger values reflect the improved system resolution derived with

the detector displaced .006" off axis.* On the average, the improvement in the system resolution resulted in about an 8% increase in the magnitude of the total cross sections.

The results of our total cross section measurements on potassium, rubidium and cesium are presented in Figures 33 - 35. These cross sections were obtained with the 3-grid electron gun and with the atom detector displaced .006" off axis. At all electron energies, the statistical deviation of the data was less than $\pm$ 6%. Each point represented a total integration time of at least ten minutes taken in intervals of 80 seconds. The most probable systematic error for this data was estimated to be less than $\pm$9%, and the electron energies were considered to be uncertain by $\pm$ .15ev.

C. Comparison With the Results of Others

In Figures 33 - 35 are also shown both the theoretical and experimental results from other sources. From examination of Figure 33, it is quite apparent that the potassium cross sections of the present experiment are in

---

*As indicated in Section IX, at this detector displacement there is no atom beam to the right of the detector and therefore no scattering-in.

excellent agreement with the close coupling calculations of Karule[4] and Karule and Peterkop[5] as well as being very close to the measurements of Collins[10]. Over most of the investigated electron energy range, our potassium values lie above those of Collins. Most of the discrepancy can probably be explained by our improved system resolution since Collins measured total cross sections with his detector centered on the atom beam axis. Below .4ev because of difficulties with his electron gun due to excessive space charge**, Collins did not make any claims concerning the accuracy of his results. Above .4ev, he assigned an uncertainty of $\pm$20%. Below .5ev the cross section varies so rapidly with electron energy that disagreement between our results and the theoretical predictions can most likely be attributed to the uncertainty in our electron energies. For potassium our lack of perfect system resolution was investigated by using Karule's phase shifts to determine the amount of unresolved small angle scattering. At one ev it was found that there should be less than a 5% difference

---

**These difficulties involved non-linearity of the scattering signal with electron gun current.

between our total cross section measurement and Karule's calculation. This is consistent with what is shown in Figure 33.

In Figure 34 our total cross section values for cesium are plotted as well as theoretical predictions by Crown and Russek[6]*** and Karule and Karule and Peterkop. Below 1.5ev it can be seen that the disagreement with the theoretical values is well beyond the estimated uncertainty of our results. With their calculation showing a definite minimum at $\approx$ .6ev, our disagreement with Crown and Russek is qualitative as well as quantitative. This minimum was not found by Karule, and because of the difficulties associated with the adiabatic approximation (discussed in section II) it is felt that this minimum is spurious. Based on the resolution investigation shown in Fig. 29, we feel that the quantitative difference between our results and those of Karule cannot be attributed to our imperfect system resolution. However, it is possible that the wave-functions used by Karule for cesium were in error since,

---

***Crown and Russek employed the adiabatic exchange approximation using a combination of core, monopole and induced electric dipole potentials.

as mentioned in section II, atomic wave functions calculated for cesium using a different potential yielded different total cross section values.

In the case of rubidium, it can be seen from Fig. 35 that the results of the present experiment disagree with the theoretical predictions of Balling [8] at most electron energies by more than our estimated experimental error. Considering the resolution investigations at three different electron energies displayed in Figure 28 and also the outcome of using Balling's phase shifts to calculate the unresolved small angle scattering, we concluded that the discrepancy between our data and Balling's was not due to resolution.

For all three alkalies it is apparent that our measured cross sections are in much closer agreement both quantitatively and qualitatively with existing theoretical and experimental data than are the measurements of Brode. In no case do we obtain the broad maximum which was gotten by Brode for all three elements. This maximum was approximately one volt wide and with our electron energy resolution being less than 300 millivolts (FWHM) it does seem possible for us to have missed it.

D. Conclusion

We have made measurements on low energy electron scattering with potassium, rubidium and cesium. In carrying out these measurements, we have made strenuous efforts to remove and reduce and account for every possible source of error: systematic, statistical and resolutional. For all of our data there is substantial disagreement with the earlier measurements made by Brode but good to excellent agreement with some recent experimental and theoretical results. Therefore we must conclude that Brode's data is in error.

APPENDIX A

Some of the electrons which pass through the interaction region will be intercepted by the mesh of the fourth grid of the electron gun and reflected back. These electrons, travelling at low velocities, have a high probability of collision with the beam atoms. Such collisions are referred to as backscattering and cause a spurious increase in the scattering-out signal.

As a result of being backscattered, an atom recoils directionally opposite to that of normal scattering. Consequently, to check for the presence of backscattering, the atom detector is swept across the atom beam in a direction opposite to that of the electron beam and a profile of the AC signal (output of the lock-in amplifier) versus detector position is taken. (The backscattering signal, if present, is a scattering-in signal, and thus like the differential scattering signal will be 180° out of phase with the scattering-out signal.) Such profiles (traced out by a Varian X-Y recorder) were taken over the range of electron energies studied.

In the case of the 3-grid gun, no backscattering

signal was detected. But for the 4-grid gun, the profiles indicated the presence of backscattering. Fig. 36 is a reproduction of one such profile. The percentage of backscattering was found to be dependent on the electron energy. At the higher electron energies (>4ev), there was little or no backscattering seen and therefore it was neglected here. However, at lower electron energies, a correction procedure was necessary. This correction was made by referring to the traced profile at each considered electron energy and calculating the ratio R of the area under the backscattering curve to that under the differential scattering curve. (Instead of employing the recorder to obtain a profile, the digital system can be used to plot a point by point profile.) The ratio was largest, approximately .1, at the lowest electron energies studied. Consequently, for total cross-sections measured with the 4-grid gun, the corrected values for Q were obtained from the relation:

$$Q = (1-R)\ Q_m$$

where Q_m was the directly obtained cross section. Because of the uncertainties associated with this correction procedure, the scattering-out signal SS for the 4-grid gun was assigned an additional uncertainty of $\pm$ 10%.

APPENDIX B

Space Charge Depression Calculation

The following is an abbreviated presentation, applied to the electron gun designs employed, of the detailed investigations by Haeff[27] of space charge effects in a long magnetically focussed electron beam.

Consider a uniform parallel beam of electrons of current density j amps./cm^2 entering a region which has two dimensions very much greater than the third. (See Figures 37 and 39) In the absence of the electron beam, the region potential is constant and equal to the potential V_b established on the boundaries. The presence of an external axial magnetic field, of strength approximately 1200 gauss, prevents lateral spreading of the beam to any great extent. Then, according to Haeff, Poisson's equation in one dimension is applicable to calculating the effects of the space charge of the electrons along the direction of the small dimension.

Case I: 4-grid design gun

Referring to Figure 37, the potential at any point x within the region is given by:

$$\frac{d^2V(x)}{dx^2} = -4\pi\rho \qquad (1)$$

where ρ is the volume charge density, related to the current density by $j = -\rho(x)\, v(x)$ and $\frac{1}{2} mv^2(x) = eV(x)$.

This leads to the equation

$$\frac{d^2V(x)}{dx^2} = \left(\frac{8\pi^2 m}{e}\right)^{\frac{1}{2}} j\, V(x)^{-\frac{1}{2}} \tag{2}$$

After integration we have:

$$\frac{4}{3}\left(V(x)^{\frac{1}{2}} - V_o^{\frac{1}{2}}\right)^{\frac{1}{2}}\left(V(x)^{\frac{1}{2}} + 2V_o^{\frac{1}{2}}\right) = \pm\left(16\pi j\sqrt{\frac{2m}{2e}}\right)^{\frac{1}{2}} x \tag{3}$$

where V_o is the minimum value of the potential in the region, occurring at its center because of symmetry (see Figure 38). V_o can be obtained by setting x=b in the above equation.

Employing an iteration technique, this equation was solved by computer for V(x) for a series of values of x and j. At any boundary potential V_b, there is a maximum current density, corresponding to $V_o = 0$, which can be passed through the region. In actual practice, the electron gun was operated with currents such that, in the worst case, V_o differed by no more than .1 volts from V_b. Over the width of the atom beam in the interaction volume ($\leq$ .010"),

the variation from V_o was $< .05$ volts, and therefore V_o was taken as the average potential of the electrons traversing the atom beam.

Case II: 3-grid design gun

Referring to Figures 39 and 40, the potential at any point x for which $-a \leq x \leq a$ is given by equation 3. For $a < x \leq b$, $\rho = 0$ and we have:

$$\left.\frac{dV}{dx}\right|_{x=a} = \frac{V_b - V_a}{b-a} . \tag{4}$$

Matching this at x=a with a relation derived from the first integration of Poisson's equation and substitution into equation 3 yields the two expressions:

$$(V_b - V_a)\left[3V_a^{\frac{1}{2}}\gamma^2 - 2(V_b - V_a)^2\right] = \frac{3\gamma^4 a}{4(b-a)} \tag{5}$$

$$V_o^{\frac{1}{2}} - V_a^{\frac{1}{2}} - \frac{(V_b - V_a)^2}{\gamma^2} \tag{6}$$

where $\gamma \equiv (16\pi j)^{\frac{1}{2}}\left(\frac{\pi}{2e}\right)^{\frac{1}{4}}(b-a)$.

The Newton-Raphson iteration method was used to solve the above equations by computer. V_a and V_o were obtained as functions of the boundary potential V_b and the

current through the equipotential region.

As in case I, equation 3 was employed to obtain the potential for various values of x within the confines of the electron beam and over the entire current range. In effect, the variation in electrostatic potential over the atom beam in the interaction region was mapped out. The amount of current passed through the equipotential region was such that the space charge depression correction for the electron energy was at most .1 volt.

REFERENCES

1. L. B. Robinson, Phys. Rev. 127, 2076 (1962).
2. W. R. Garrett and R. A. Mann, Phys, Rev. 130, 658 (1963).
3. W. R. Garrett and R. A. Mann, Phys. Rev. 135, A580 (1964).
4. E. M. Karule in Atomic Collisions III, edited V. Ia. Veldre (Latvian Academy of Sciences, Riga, 1965) translation JILA Info. Center Report No. 3, Univ. of Colorado, Boulder, Colorado (unpublished) pp. 29-48.
5. E. M. Karule and R. A. Peterkop, JILA Info. Center Report No. 3 (see Ref. 4).
6. J. C. Crown and A. Russek, Phys. Rev. 138, A669 (1965).
7. W. R. Garrett, Phys, Rev. 140, A705 (1965).
8. L. C. Balling, Phys. Rev. 179, 78 (1969).
9. "The Scattering of Electrons by Lithium Atoms", P. Burke and J. Taylor, Tech. Paper No. 367, Harwell, England, April 1969.
10. R. E. Collins, B. Bederson, M. Goldstein, submitted to the Physical Review A, August 24, 1970.
11. R. B. Brode, Phys. Rev. 34, 673 (1929).

12. J. Perel, P. Englander, B. Bederson, Phys. Rev. 128, 1148 (1962).

13. B. Bederson in "Comments on Atomic and Molecular "Physics", V. W. Hughes and H. Foley, Coordinators, Issues No. 5 and 6 (1970).

14. R. B. Brode, Proc. Roy. Soc., August (1929).

15. K. Rubin, B. Bederson, M. Goldstein and R. E. Collins, Phys. Rev. 182, 201 (1969).

16. A. Temkin and J. C. Lamkin, Phys. Rev. 121, 788 (1961).

17. M. H. Mittleman and J. L. Peacher, Phys. Rev. 173, 160 (1968).

18. H. S. W. Massey and C. B. Mohr, Proc. Roy. Soc. A136, 289 (1932).

19. P. G. Burke, S. Ormonde and W. Whitaker, Proc. Phys. Soc. 92, 319 (1967).

20. R. Gaspar, Acta. Phys. Acad. Sci., Hungary 2, 151 (1952).

21. P. M. Stone, Phys. Rev. 127, 1151 (1962).

22. G. E. Chamberlain and J. C. Zorn, Phys. Rev. 129, 677 (1963).

23. R. E. Collins, Ph. D. Thesis, New York University, 1968 (unpublished).

24. R. C. Miller and P. Kusch, Phys. Rev. 99, 1314 (1955).

25. B. Bederson and K. Rubin, Technical Report, Atomic Energy Commission, New York University, NYO-10, 117 (February, 1962).

26. J. A. Slevin, Ph. D. Thesis, City College of the City University of New York, 1970 (unpublished).

27. A. V. Haeff, Proc. I.R.E., p. 586, (1939).

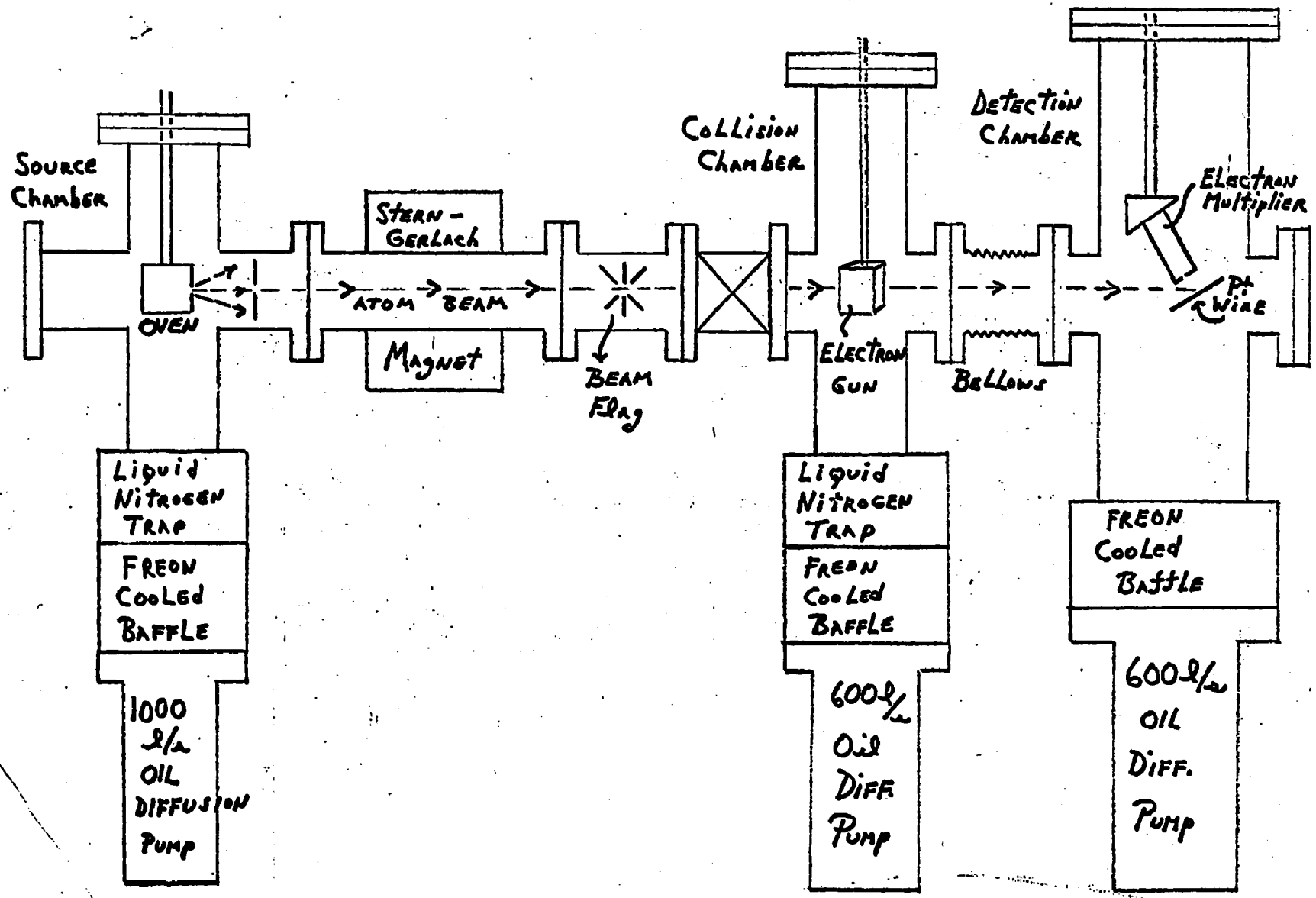

FIGURE 1 - TOTAL CROSS SECTION APPARATUS

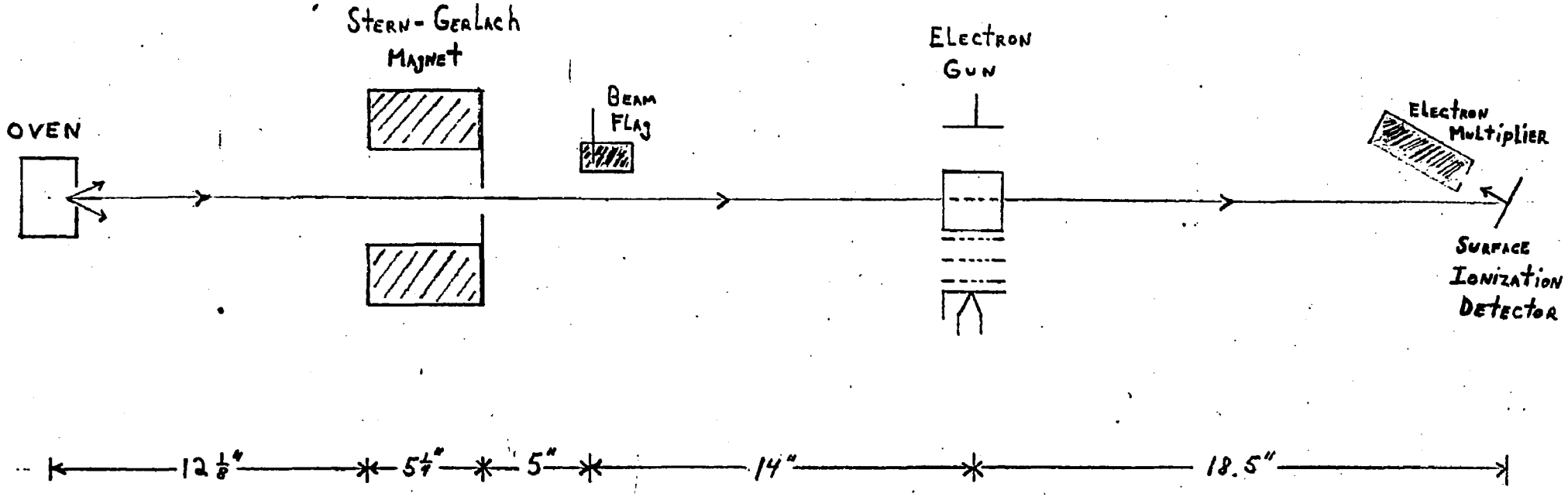
Stern-Gerlach Magnet
Beam Flag
Electron Gun
Oven
Electron Multiplier
Surface Ionization Detector
12 1/8"
5 1/4"
5"
14"
18.5"

Figure 2

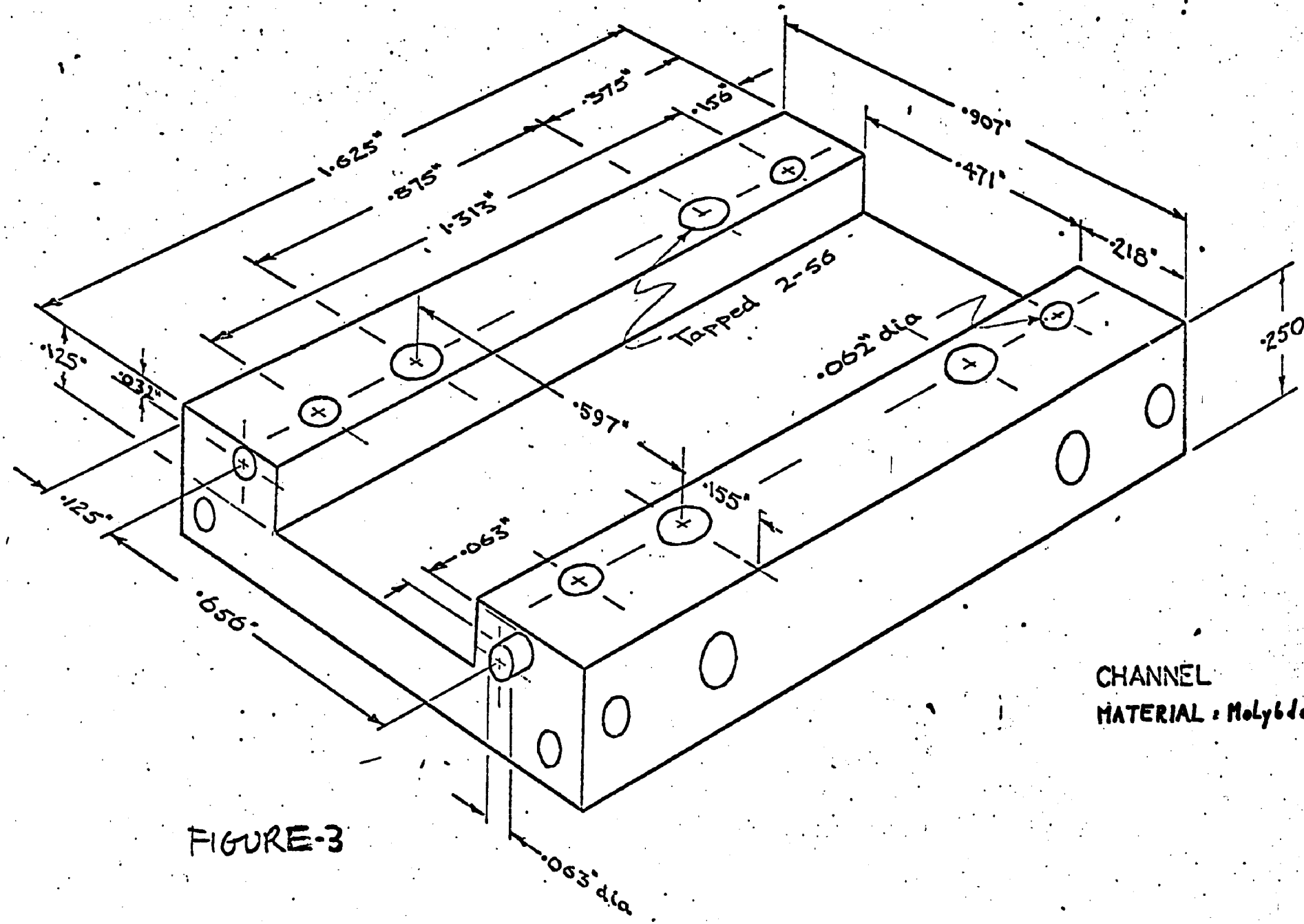

CHANNEL
MATERIAL : Molybdenum

FIGURE-3

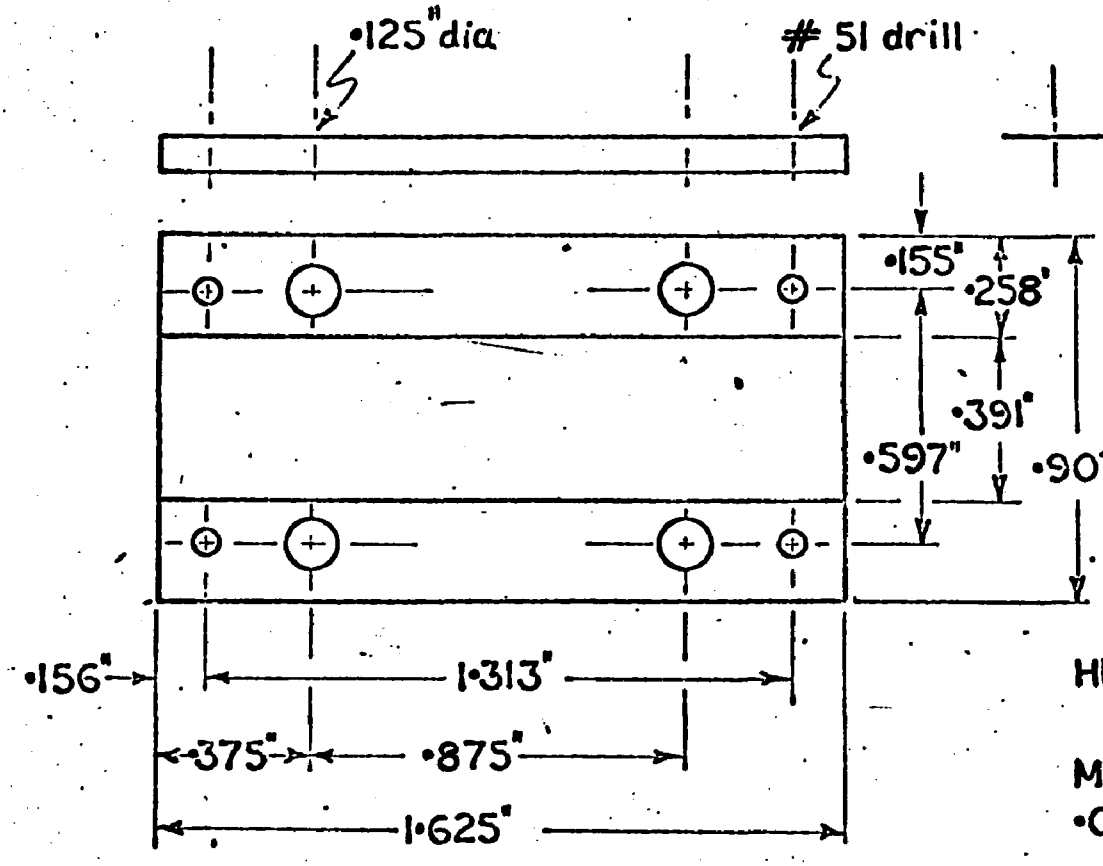

HEAT SHIELD

MATERIAL —
.002" TANTALUM

ALL DIMENSIONS ± .005"

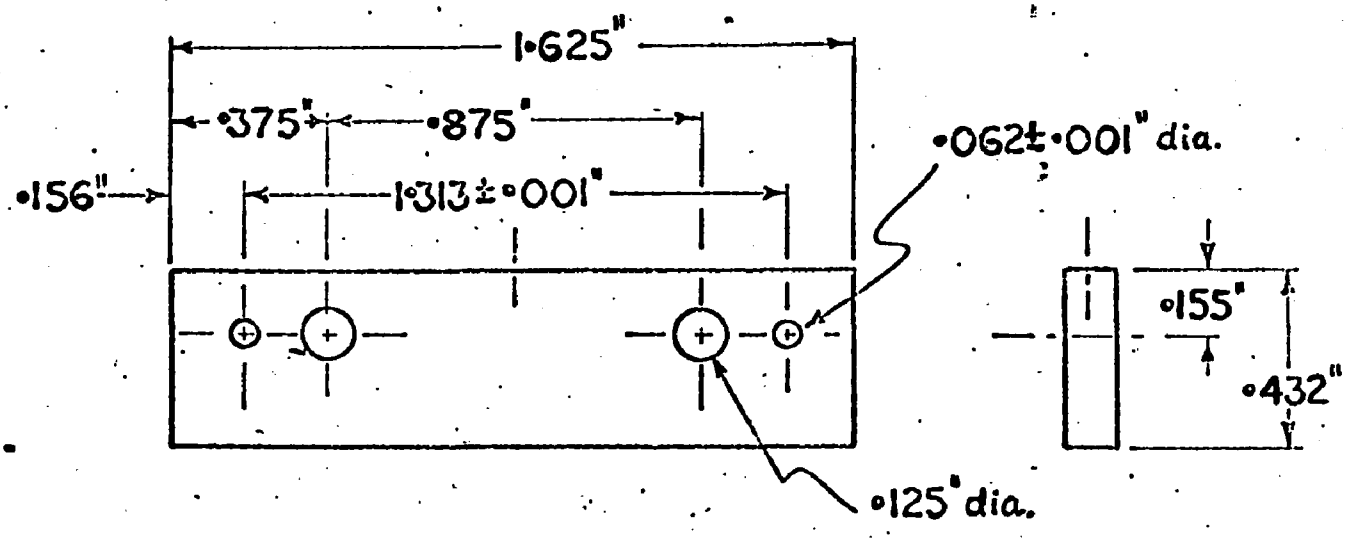

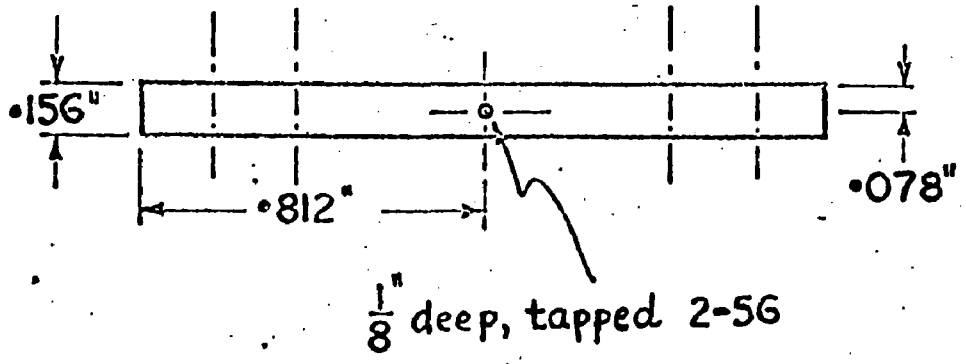

SCATTERING REGION
(TWO REQUIRED)

MATERIAL —
MOLYBDENUM

ALL DIMENSIONS ± .005"
EXCEPT AS NOTED

FIGURE 4.

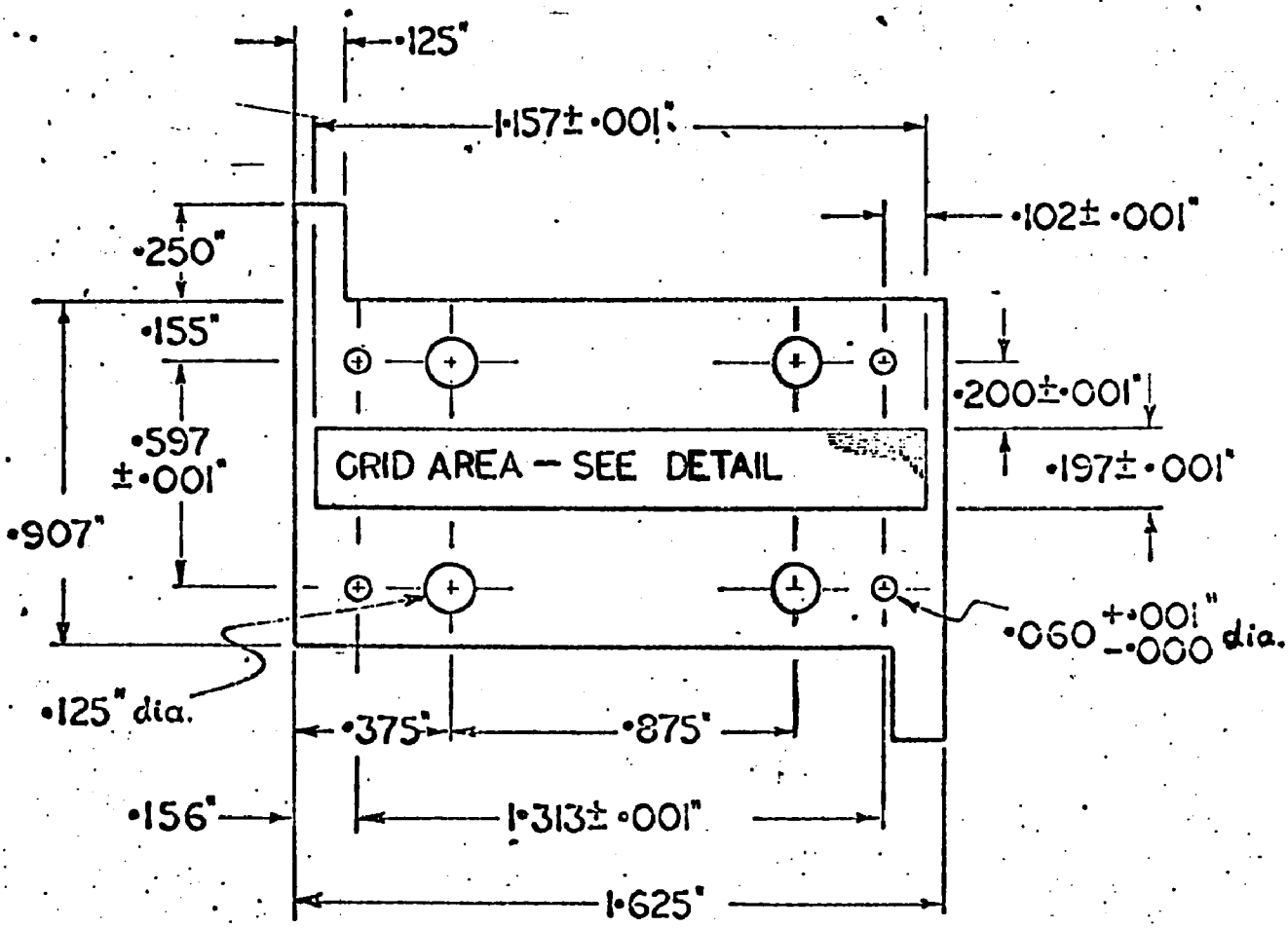

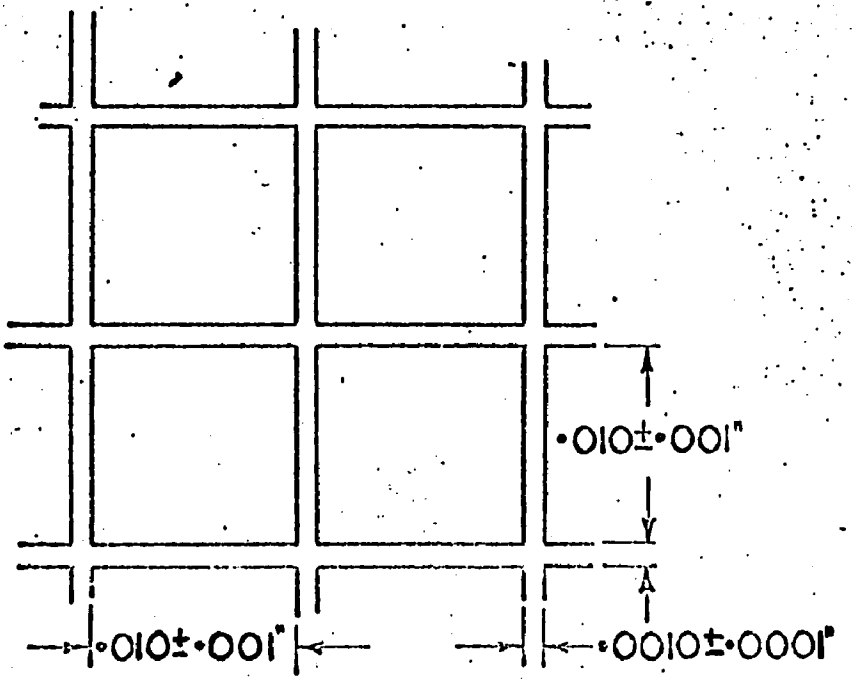

GRID DETAIL

GRID

MATERIAL —
.002" MOLYBDENUM

ALL DIMENSIONS ±.005
EXCEPT AS NOTED

FIGURE 5.

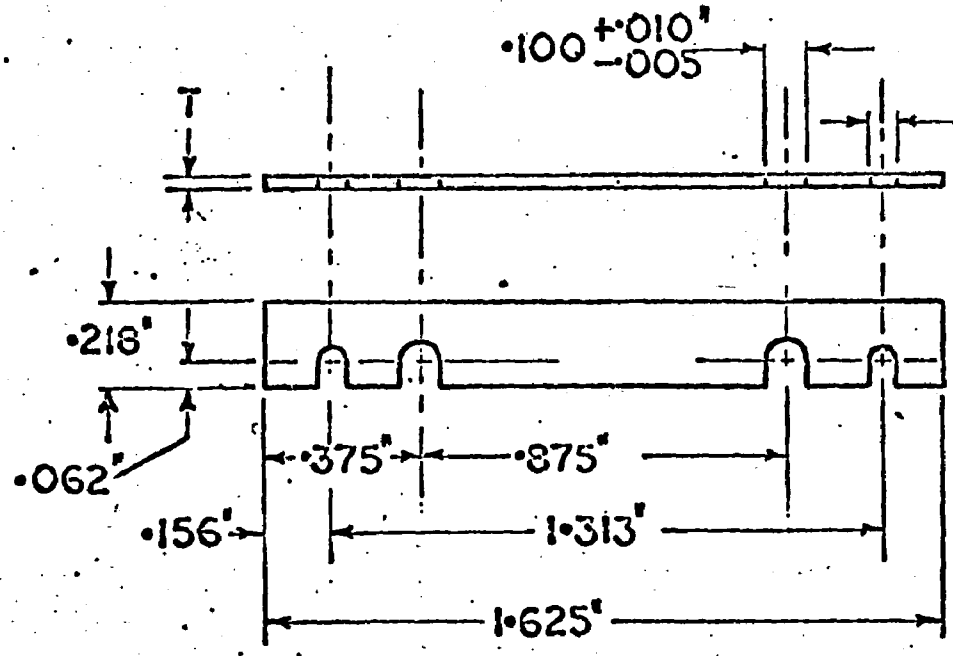

T = .010±.002" / .020±.002"

INSULATOR

MATERIAL — ALUMINUM OXIDE

ALL DIMENSIONS ±.010" EXCEPT AS NOTED

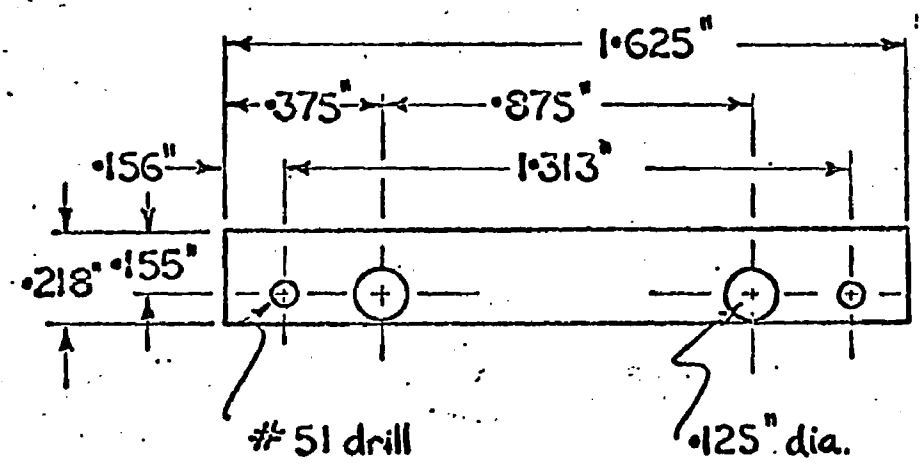

SPACER

MATERIAL —
.005"
.010"
.020"
} MOLYBDENUM

ALL DIMENSIONS ±.005

FIGURE 6

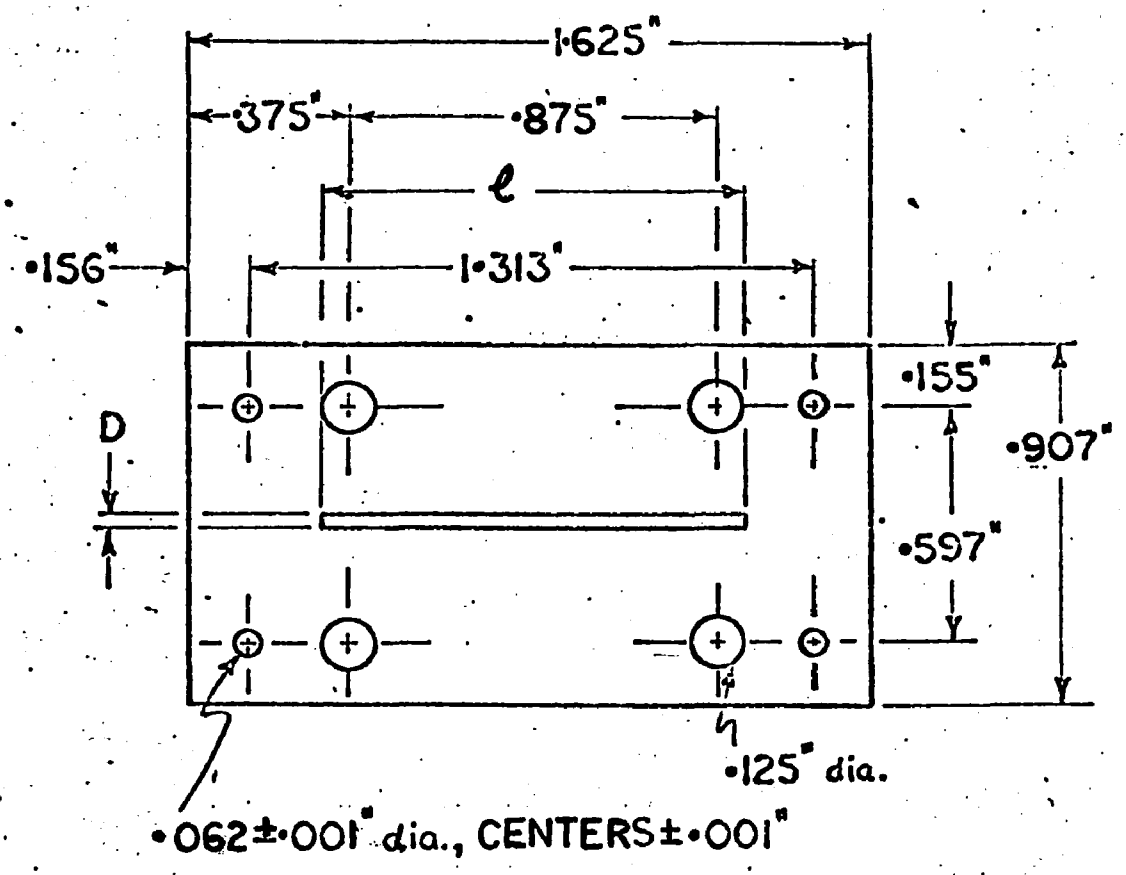

	D	ℓ
MASK	·032±·001"	1·000"
SLIT ANODE	·004±·001"	1·000"
ANODE	—	—

MATERIAL —
·005" MOLYBDENUM

ALL DIMENSIONS ± ·005"
EXCEPT AS NOTED

FIGURE 7.

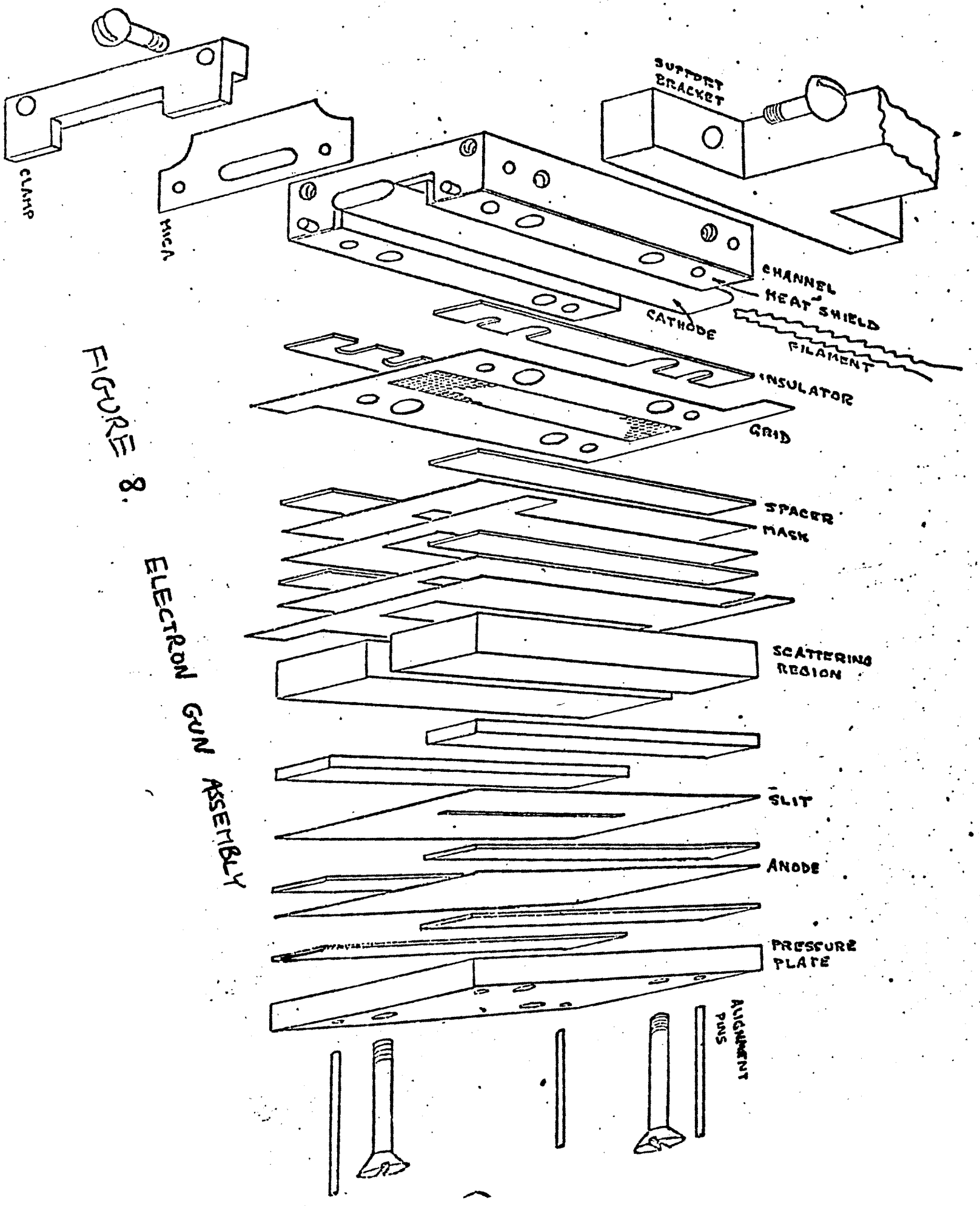

FIGURE 8. ELECTRON GUN ASSEMBLY

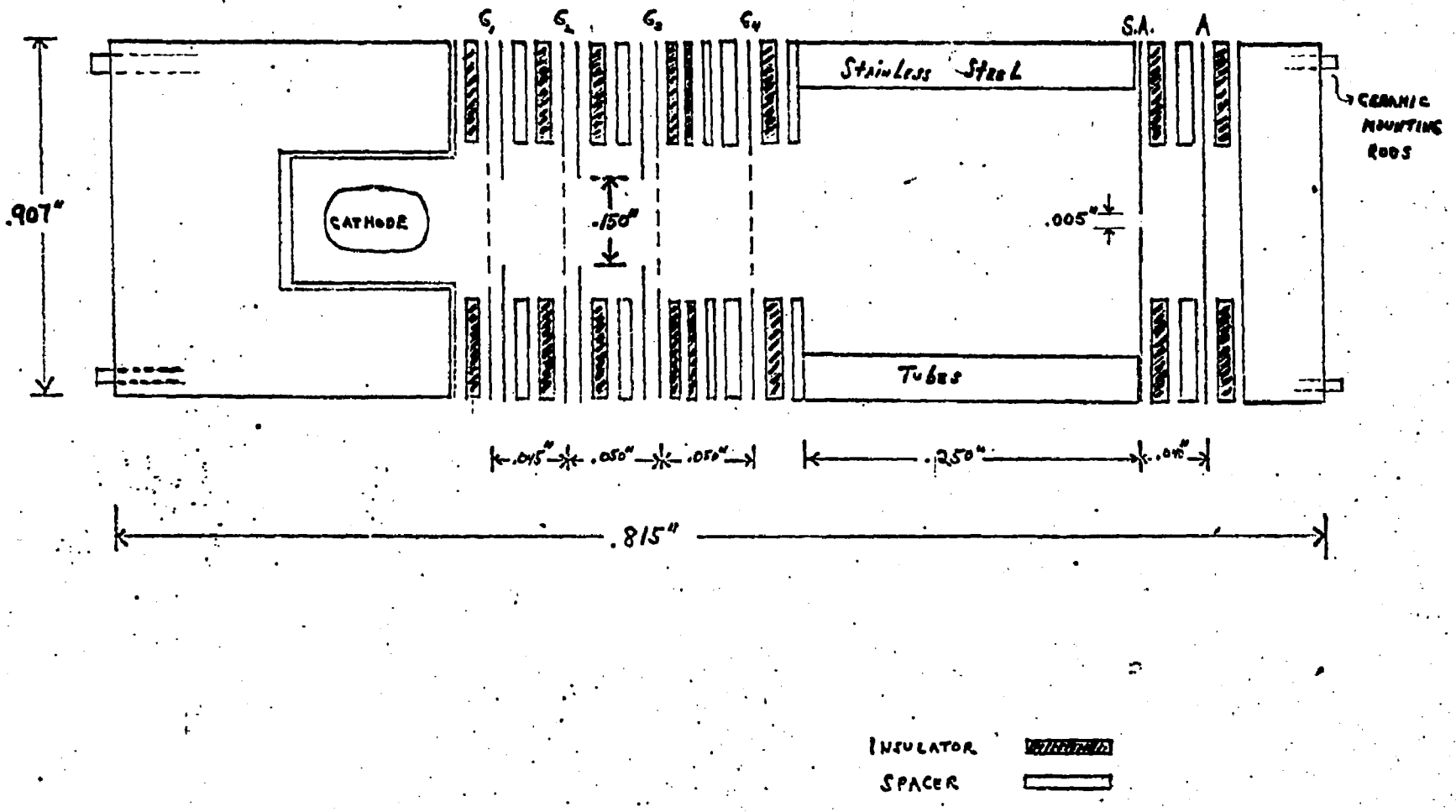

FIGURE 9 FOUR-GRID ELECTRON GUN

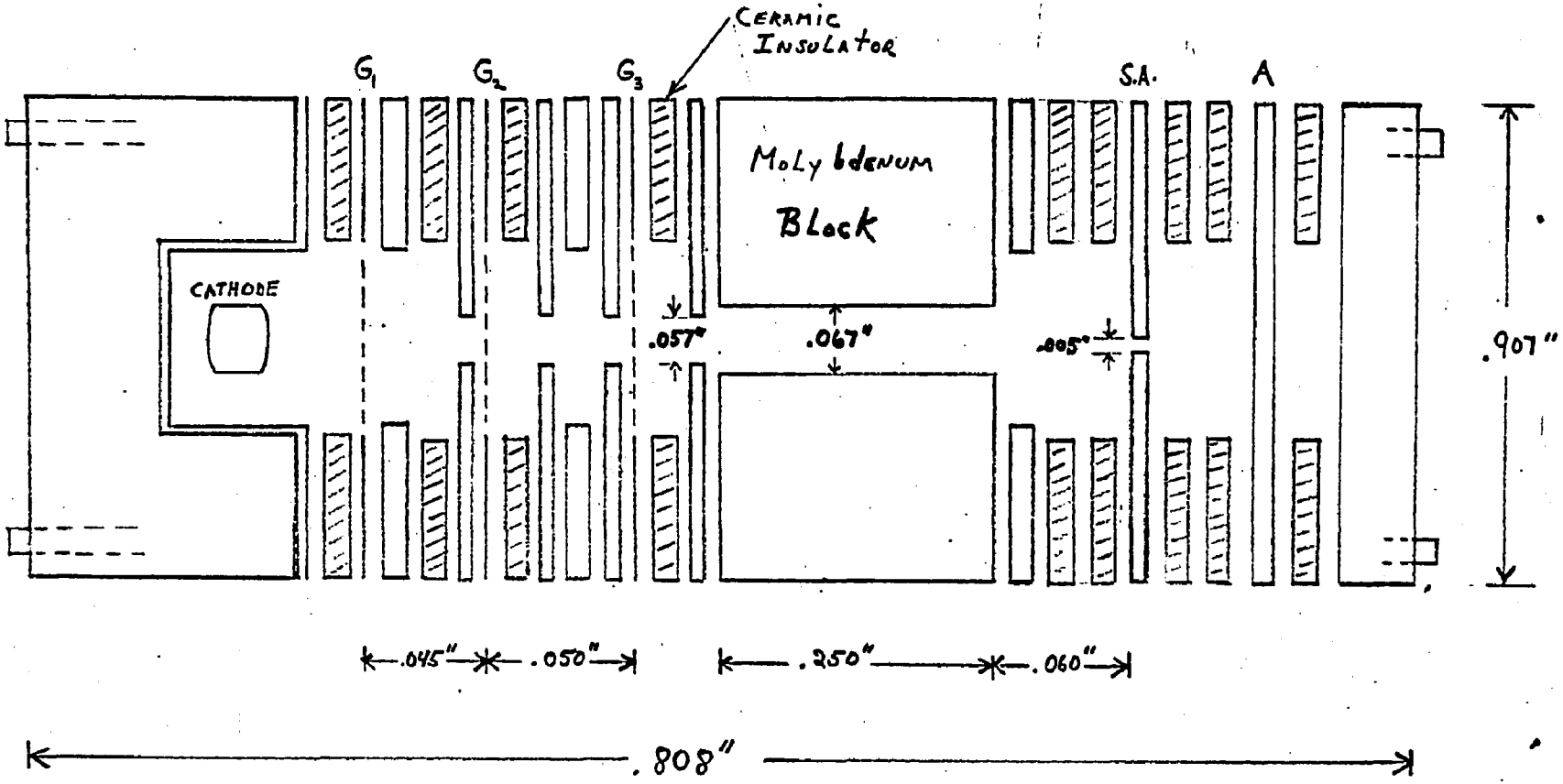

FIGURE 10 3-GRID GUN

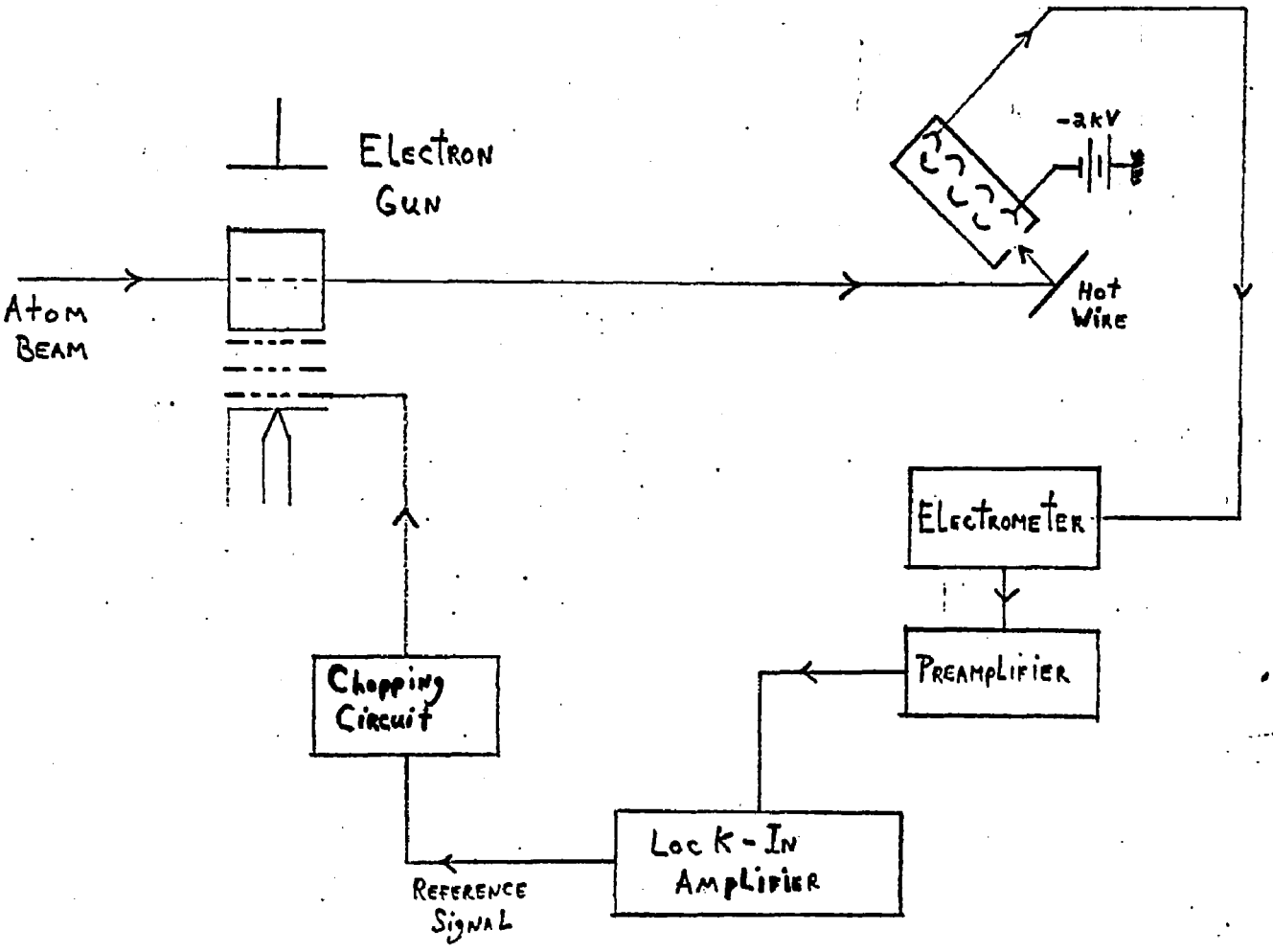

Figure 11 - Detection System

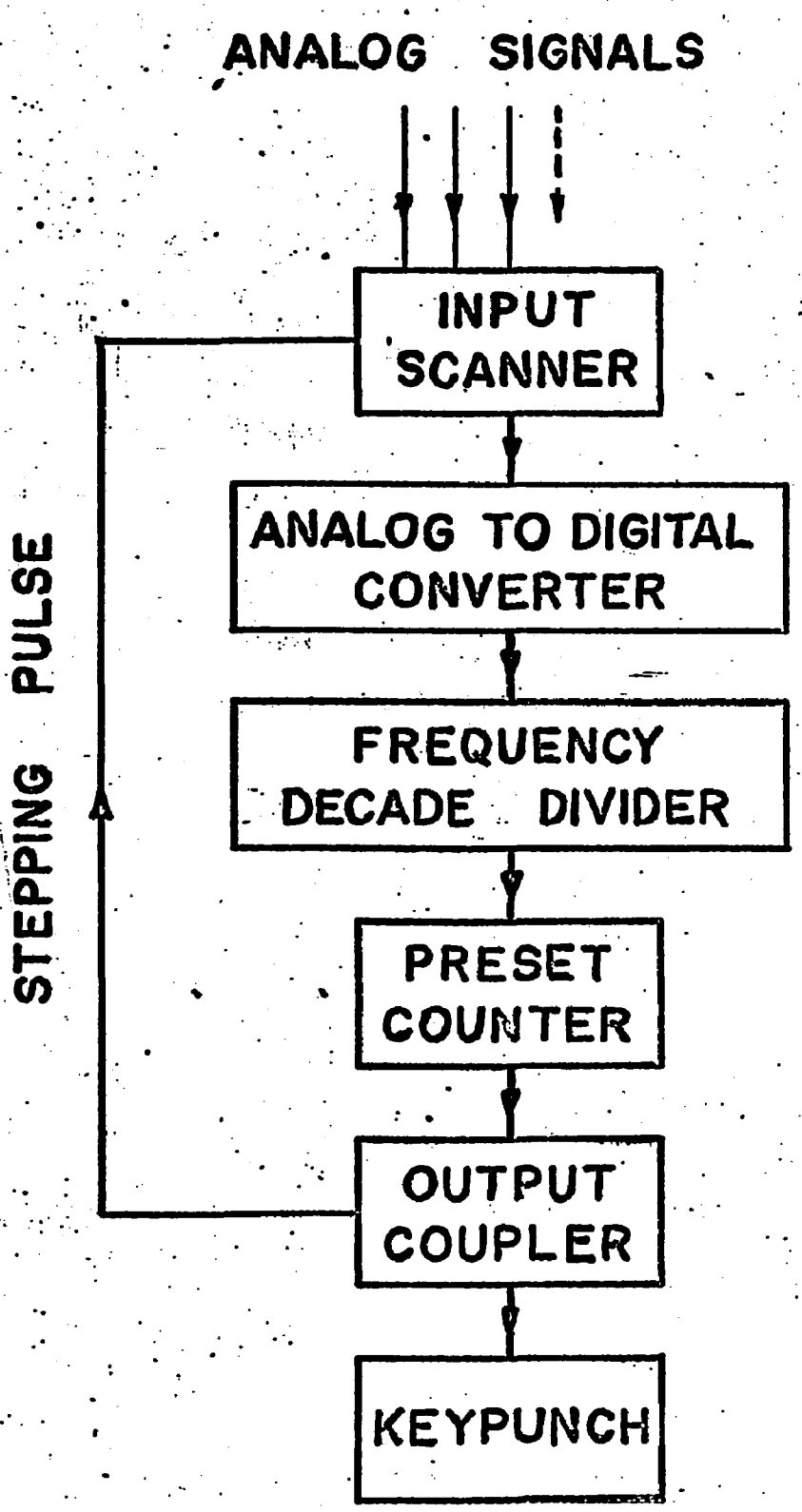
ANALOG SIGNALS
INPUT SCANNER
ANALOG TO DIGITAL CONVERTER
FREQUENCY DECADE DIVIDER
PRESET COUNTER
OUTPUT COUPLER
KEYPUNCH
STEPPING PULSE

Figure 12

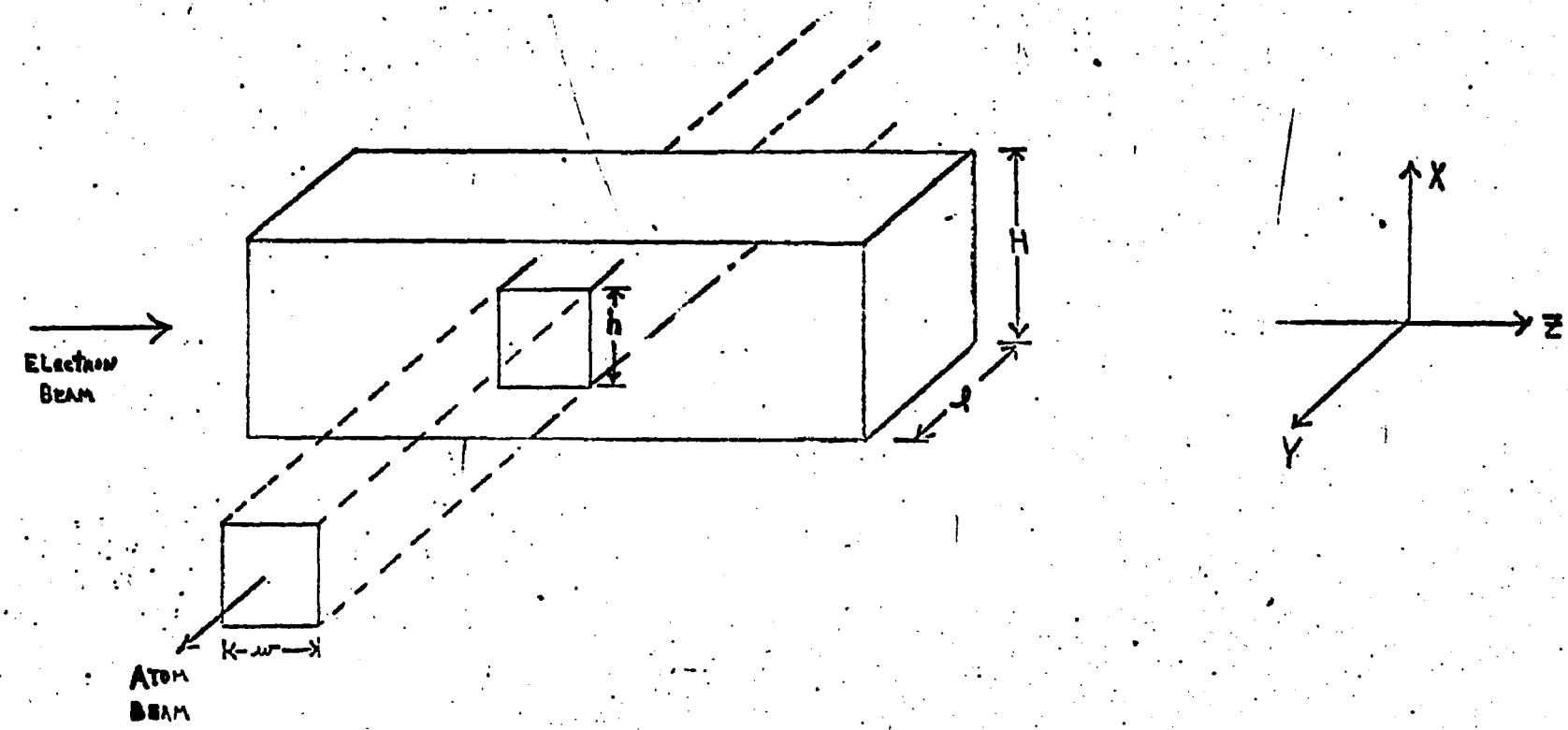

FIGURE 13 - GEOMETRY OF INTERACTION REGION. (4-grid gun)

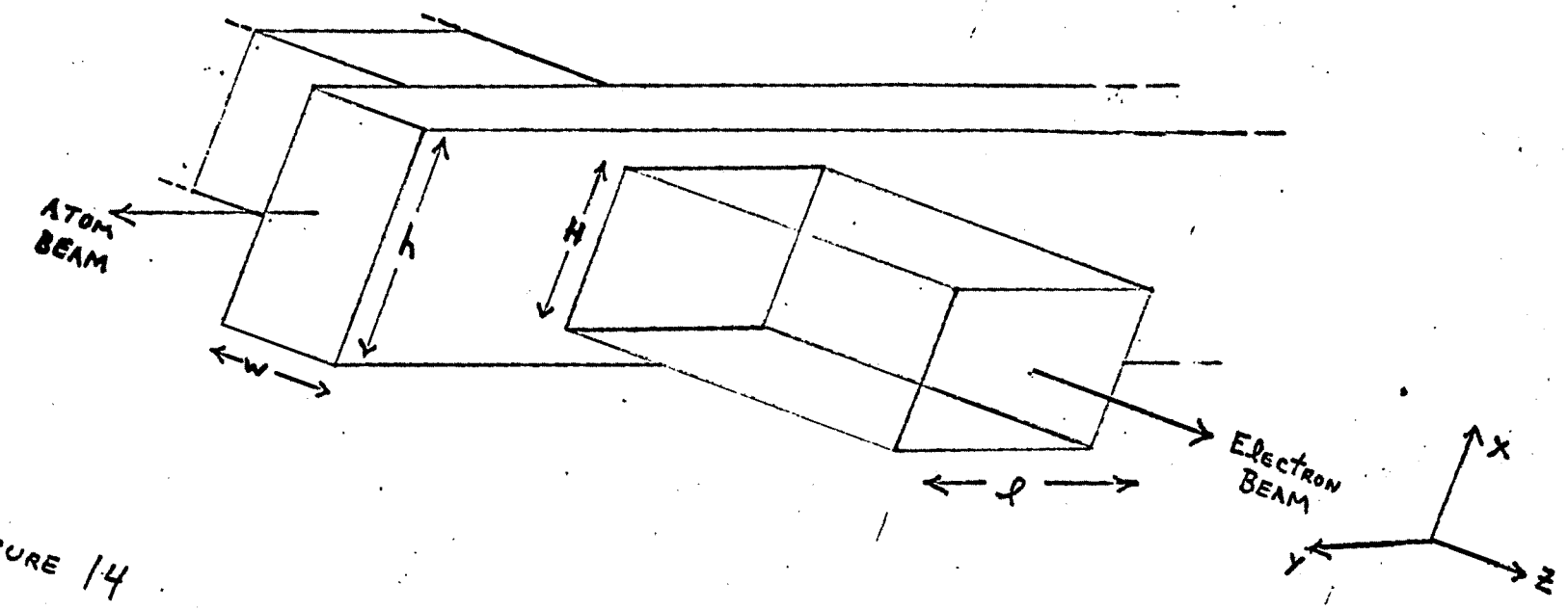

Figure 14

Geometry of Interaction Region (3-grid gun)

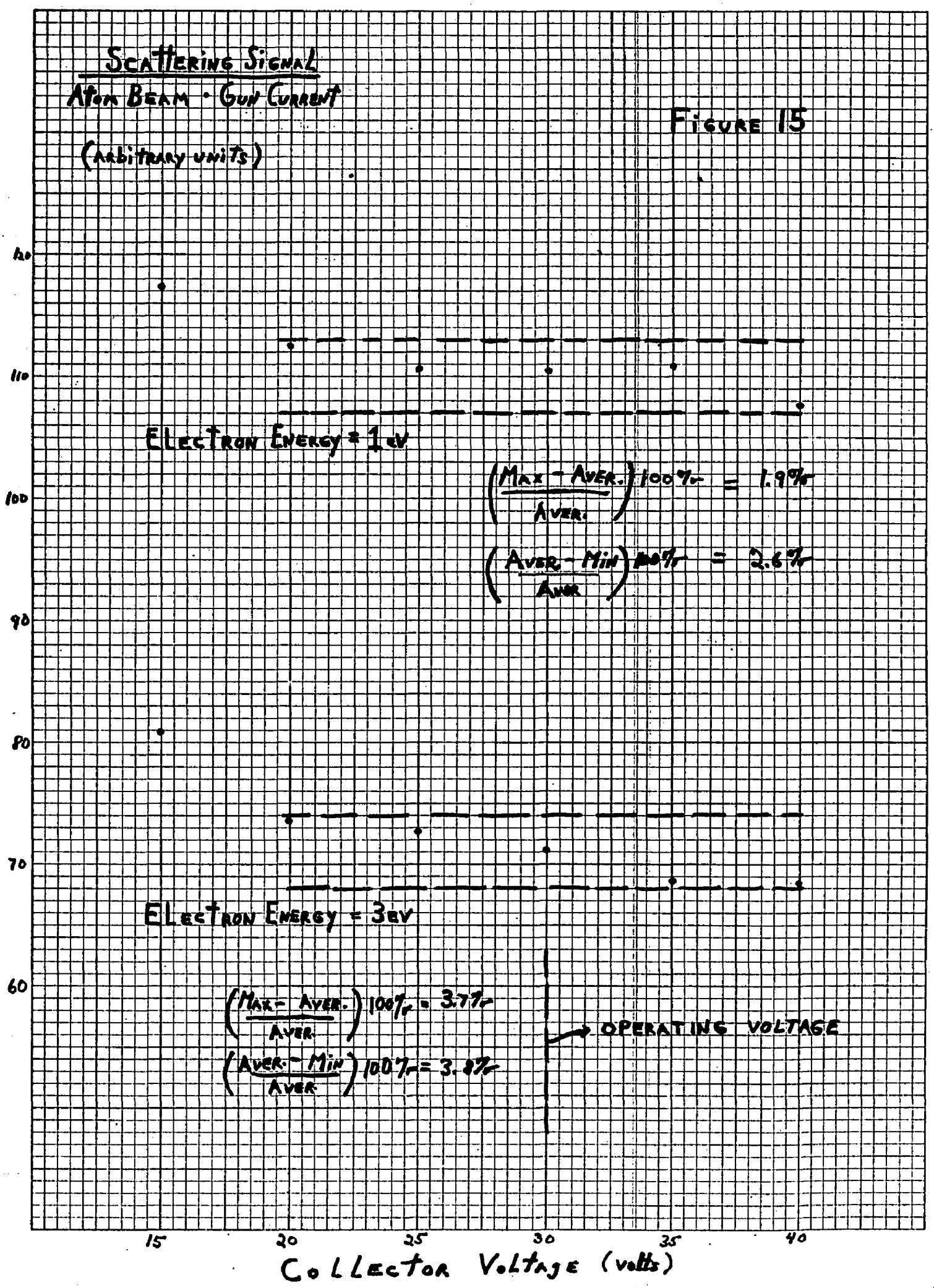
Scattering Signal
Atom Beam · Gun Current
(arbitrary units)
Figure 15
120
110
100
90
80
70
60
Electron Energy = 1 eV
(Max - Aver. / Aver.) 100% = 1.9%
(Aver. - Min / Aver.) 100% = 2.6%
Electron Energy = 3 eV
(Max - Aver. / Aver.) 100% = 3.7%
(Aver. - Min / Aver.) 100% = 3.8%
Operating Voltage
15
20
25
30
35
40
Collector Voltage (volts)

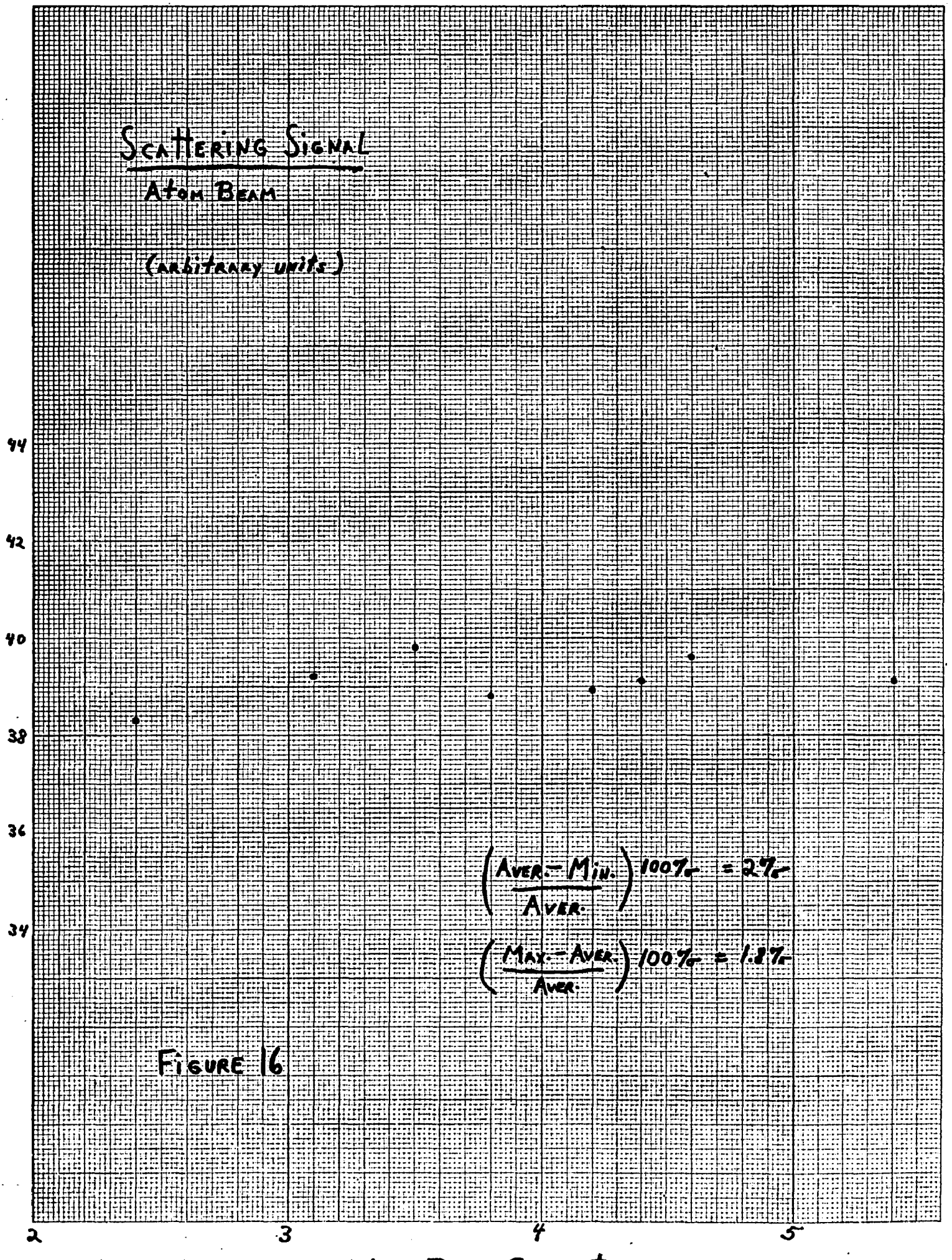
SCATTERING SIGNAL
ATOM BEAM
(ARBITRARY UNITS)
44
42
40
38
36
34
$\left(\frac{\text{AVER.} - \text{MIN.}}{\text{AVER.}}\right) 100\% = 2\%$
$\left(\frac{\text{MAX.} - \text{AVER.}}{\text{AVER.}}\right) 100\% = 1.8\%$
2
3
4
5
ATOM BEAM CURRENT

FIGURE 16

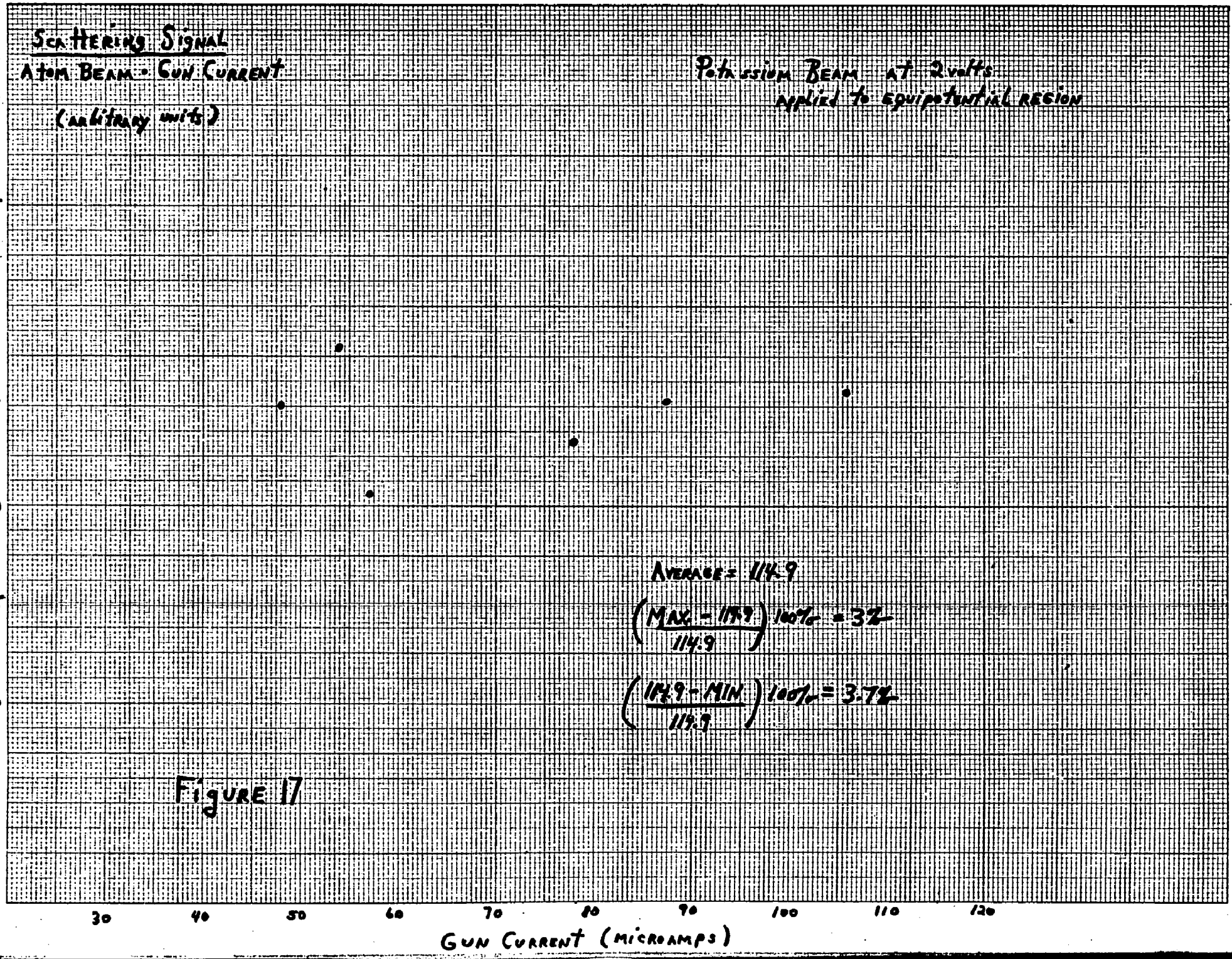
Scattering Signal
Atom Beam - Gun Current
(arbitrary units)
Potassium Beam at 2 volts applied to equipotential region
125
120
115
110
105
100
30
40
50
60
70
80
90
100
110
120
Gun Current (microamps)
Average = 114.9
((MAX. - 114.9)/114.9) 100% = 3%
((114.9 - MIN)/114.9) 100% = 3.7%

Figure 17

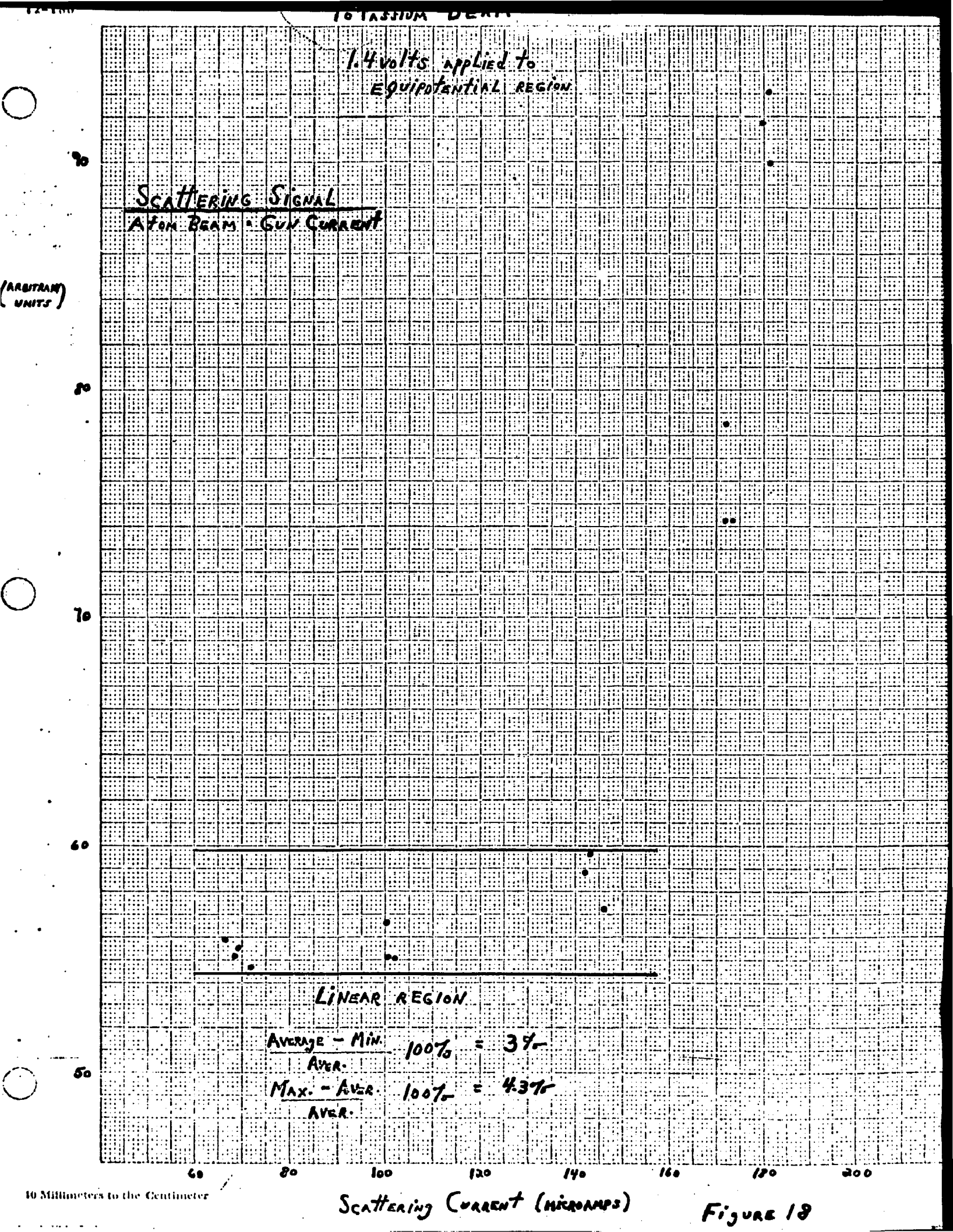

10 Millimeters to the Centimeter

Figure 18

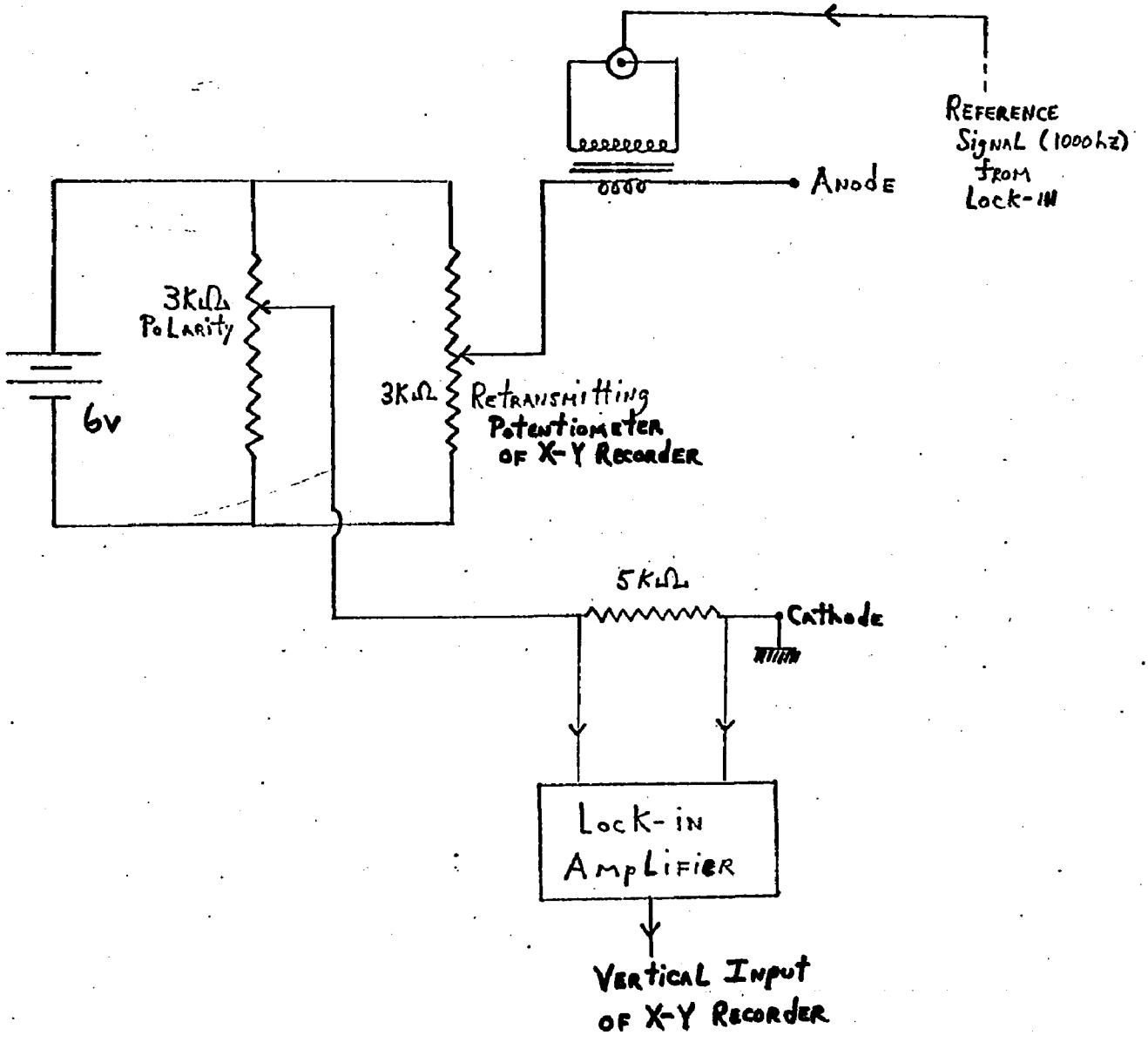
Reference Signal (1000hz) from Lock-in
Anode
3KΩ Polarity
6v
3KΩ
Retransmitting Potentiometer of X-Y Recorder
5KΩ
Cathode
Lock-in Amplifier
Vertical Input of X-Y Recorder

Figure 19

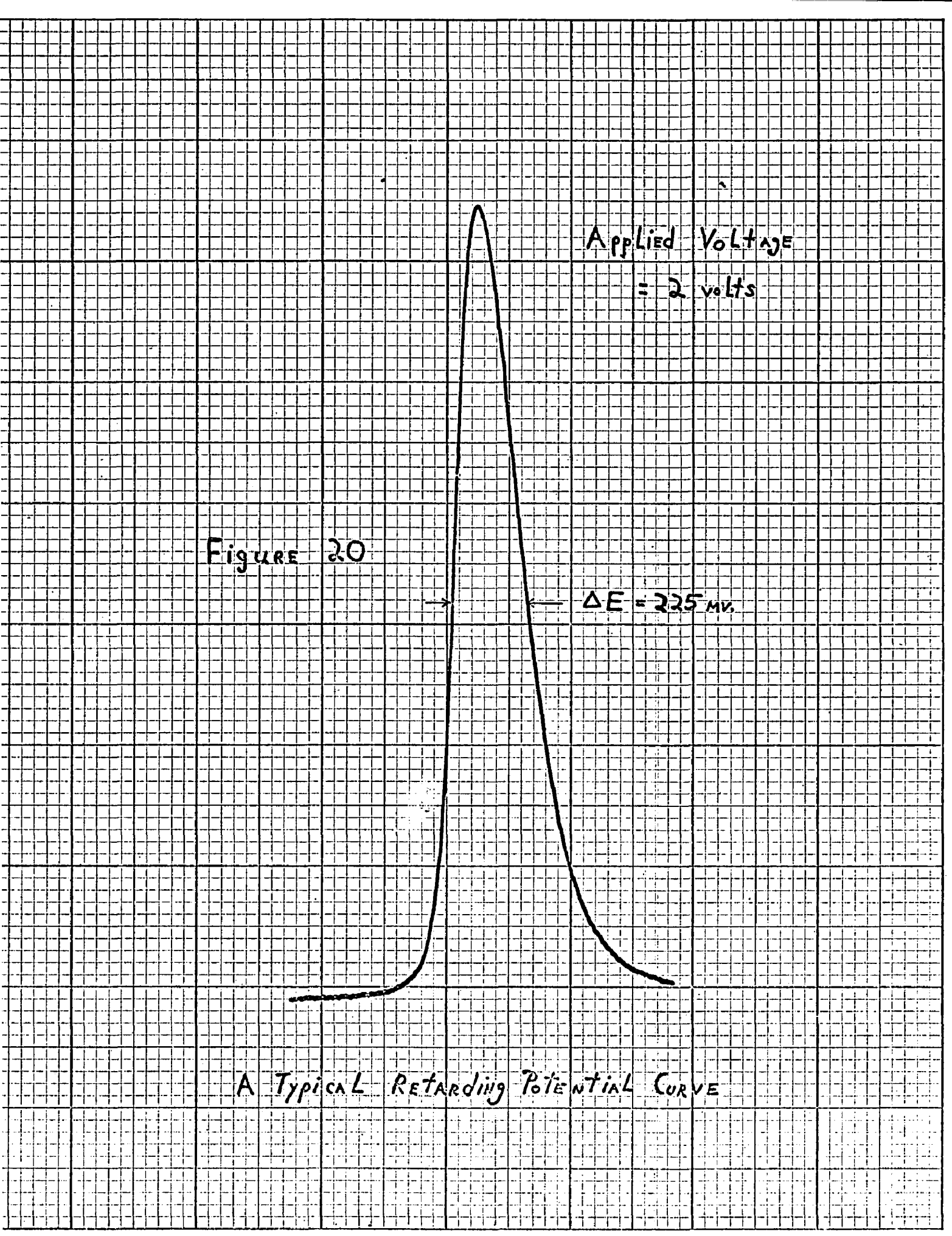

Figure 20

A Typical Retarding Potential Curve

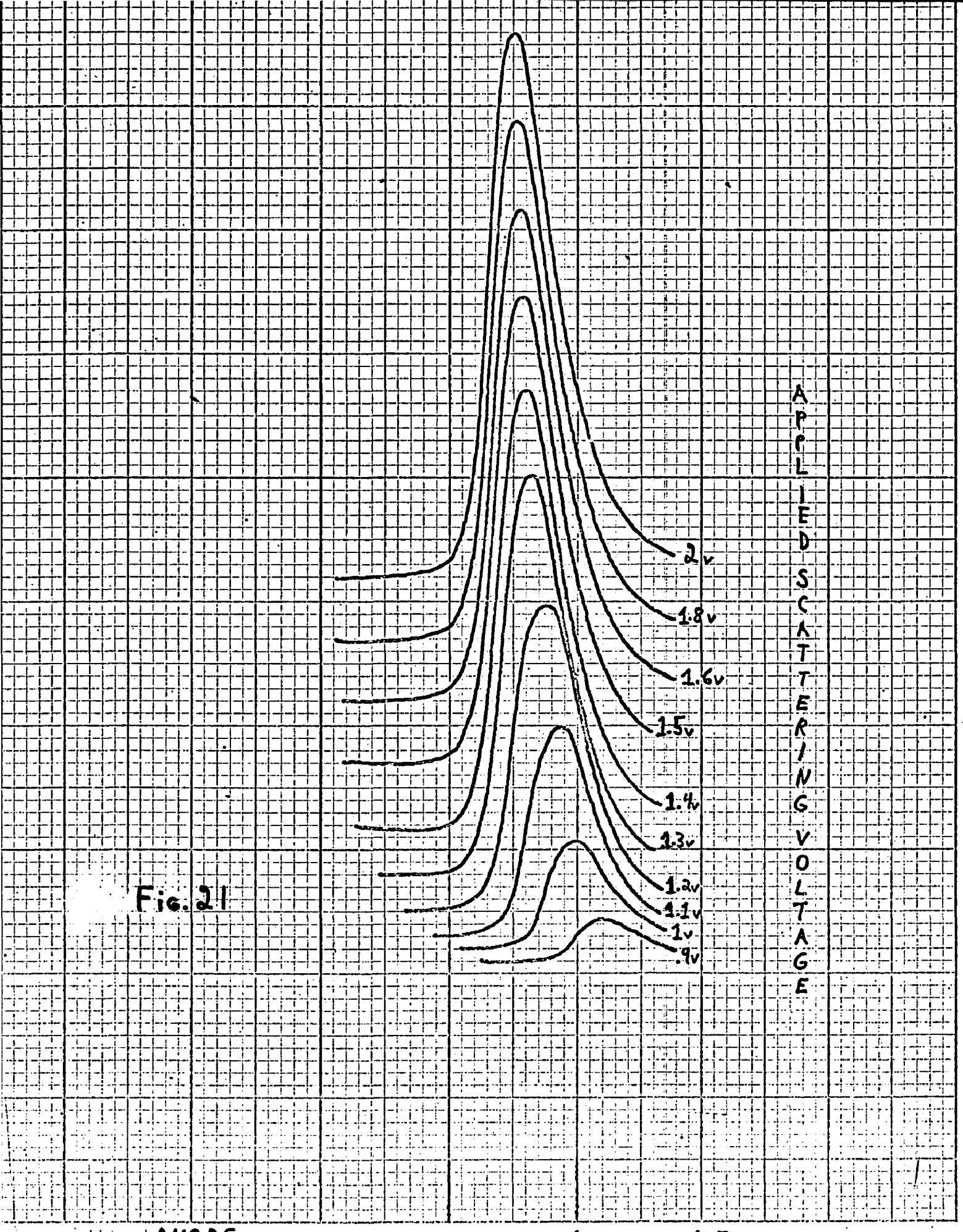
2v
1.8v
1.6v
1.5v
1.4v
1.3v
1.2v
1.1v
1v
.9v
APPLIED SCATTERING VOLTAGE
ANODE VOLTAGE
1.75v
1.375v
1v
.625v

Fig. 21

Pole Pieces of Stern-Gerlach Magnet

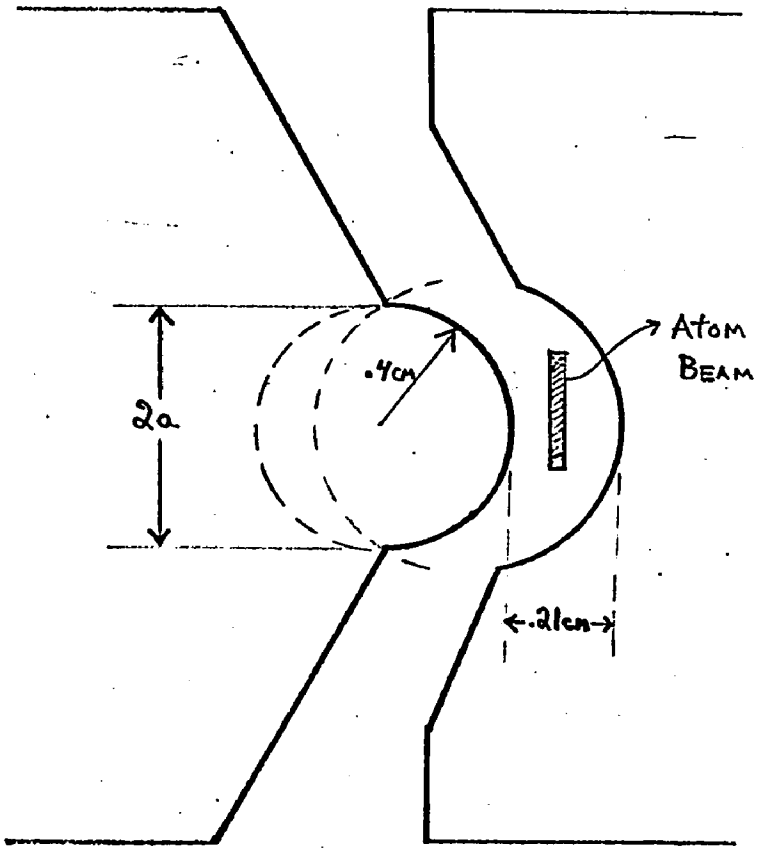

The gap boundaries are the equipotentials corresponding to the field produced by 2 long parallel straight wires carrying equal currents in opposite directions and with a center to center separation of 2a.

Both the field and its gradient are uniform over the atom beam height.

Figure 22

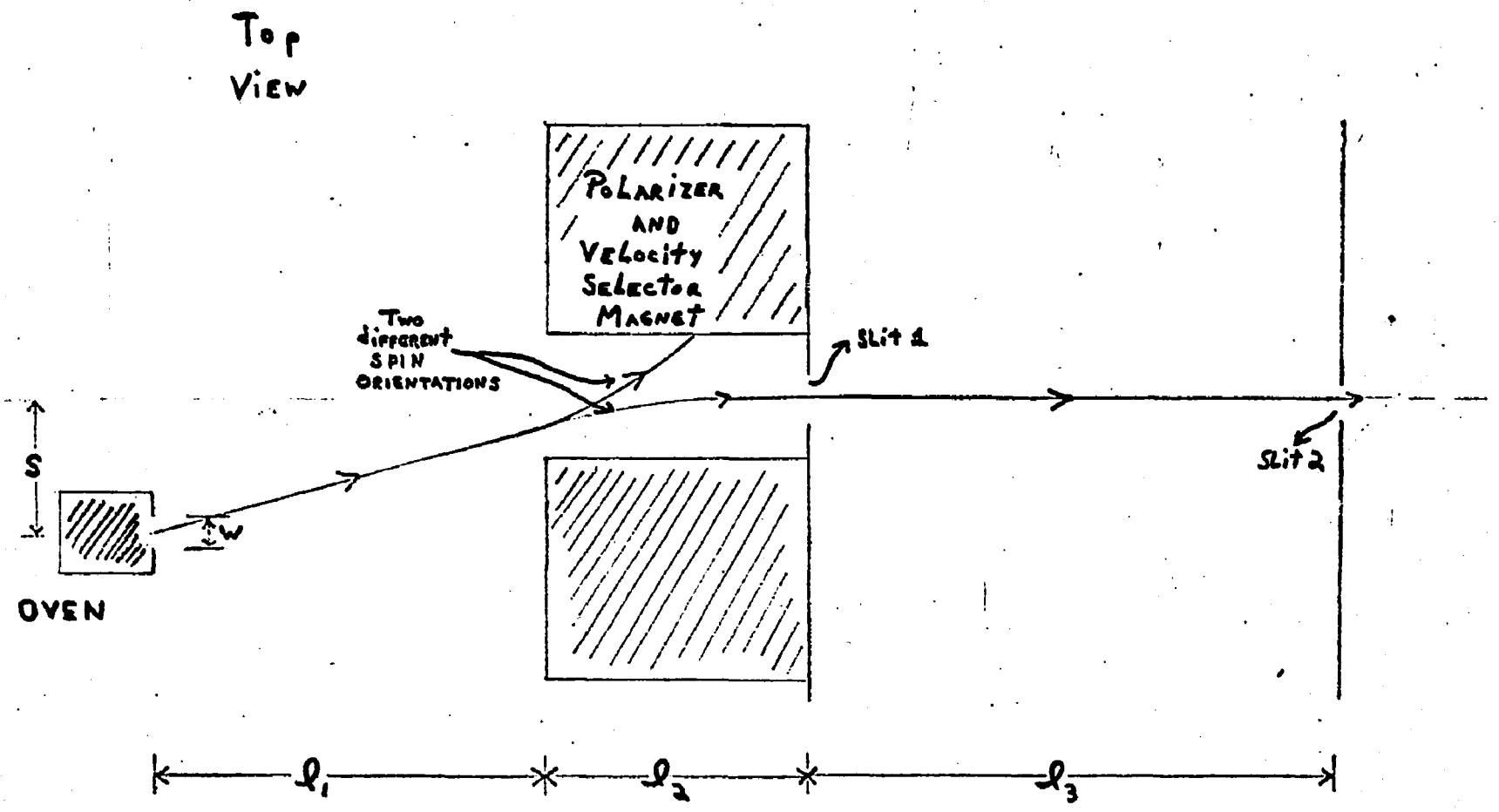
Top
View
Polarizer
and
Velocity
Selector
Magnet
Two
different
SPIN
ORIENTATIONS
Slit 1
Slit 2
S
w
OVEN
ℓ_1
ℓ_2
ℓ_3

FIGURE 23

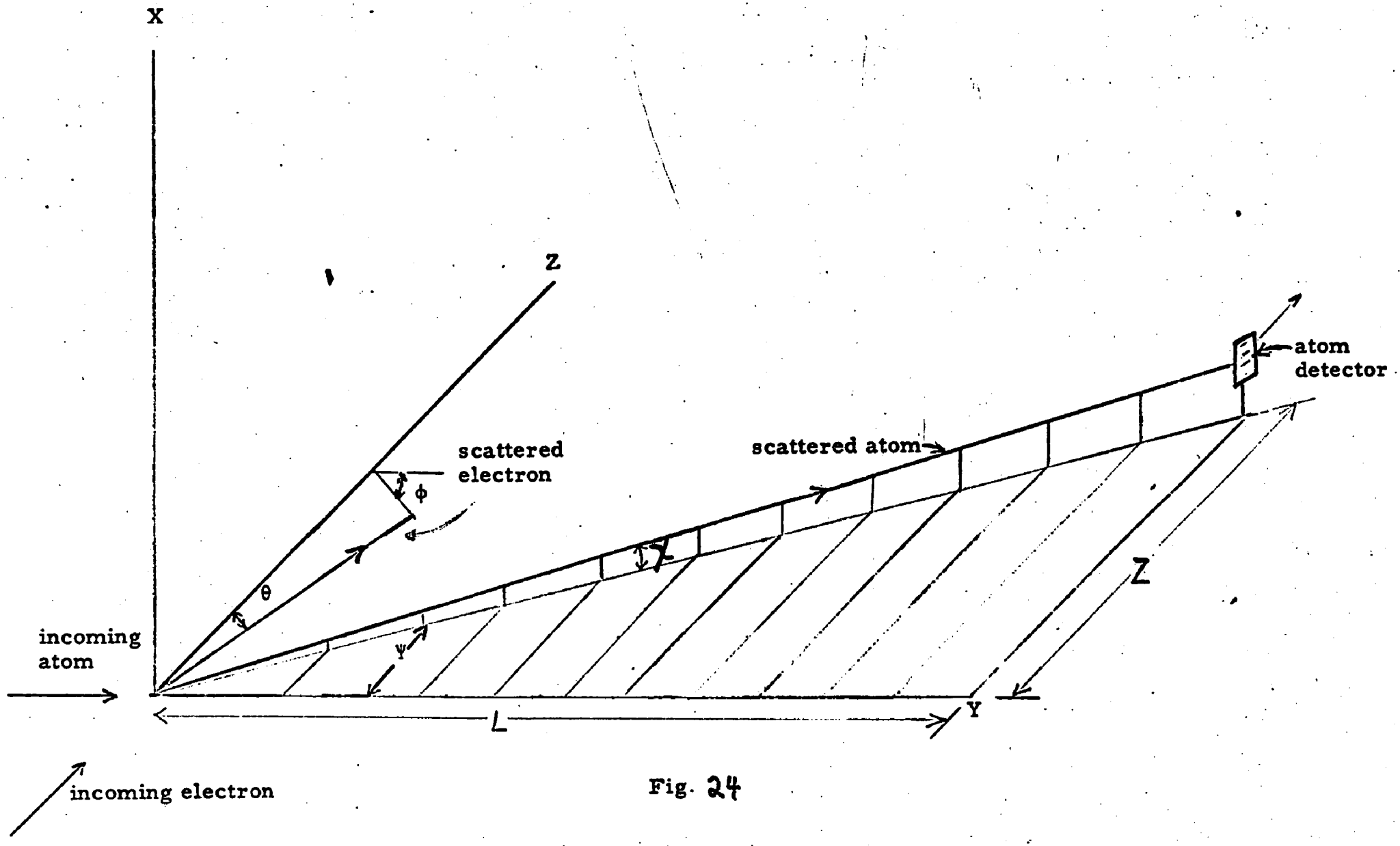
X
Z
scattered
electron
ϕ
scattered atom
atom
detector
θ
incoming
atom
ψ
Z
L
Y
incoming electron

Fig. 24

GEOMETRICAL ATOM BEAM PROFILE

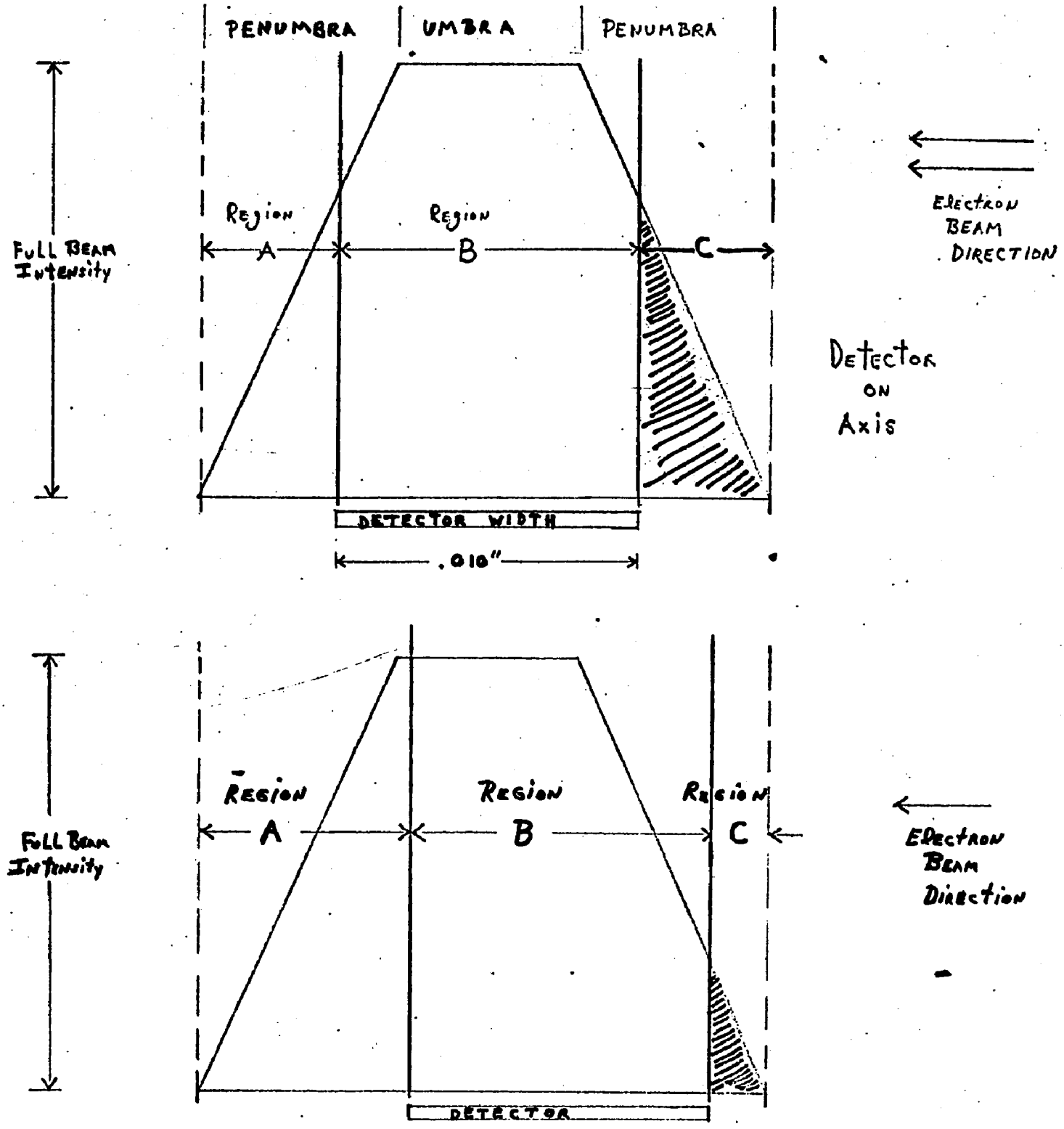

FIGURE 25

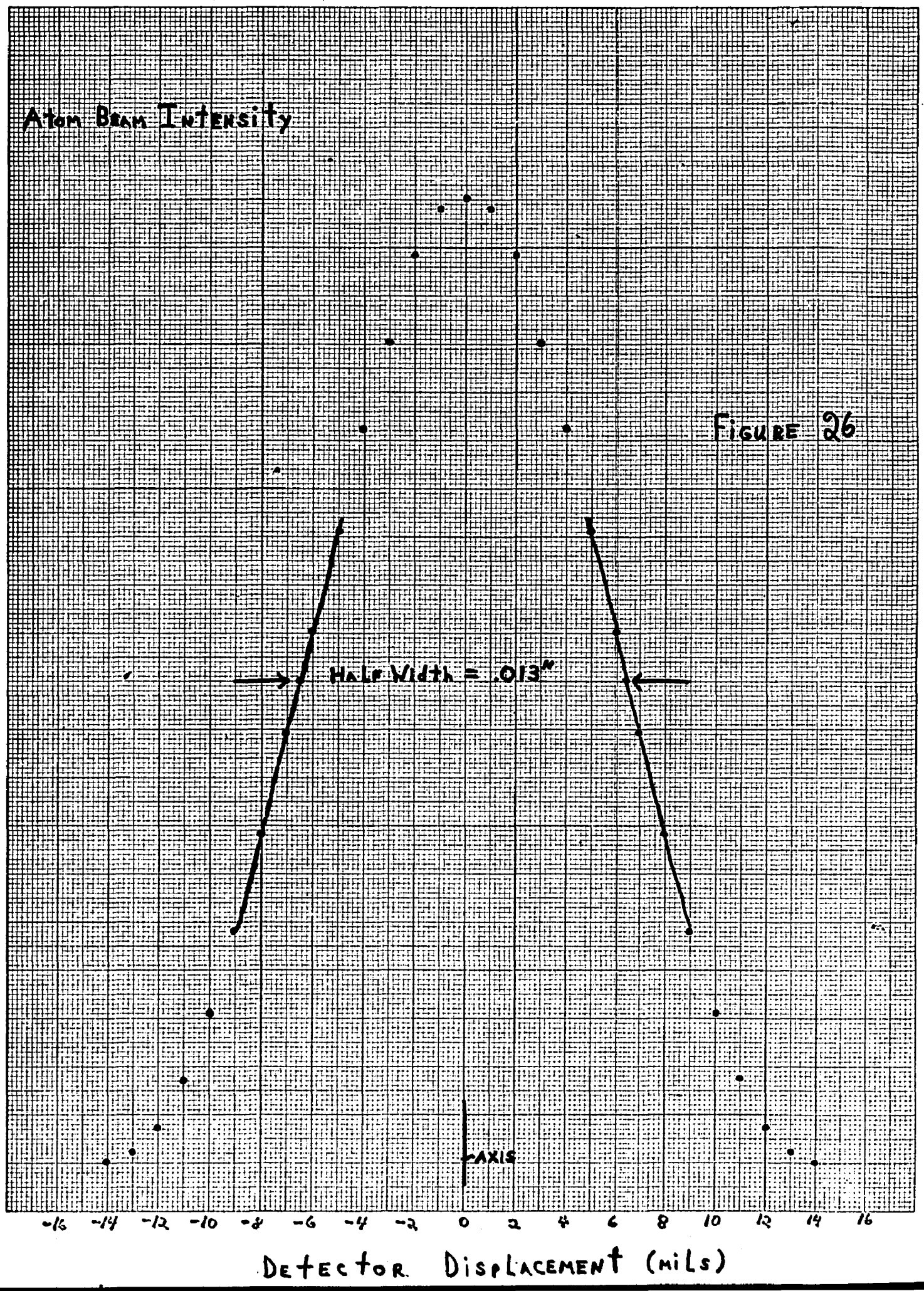
Atom Beam Intensity
1
.9
.8
.7
.6
.5
.4
.3
.2
.1
0
Half Width = .013"
AXIS
-16
-14
-12
-10
-8
-6
-4
-2
0
2
4
6
8
10
12
14
16
Detector Displacement (mils)

Figure 26

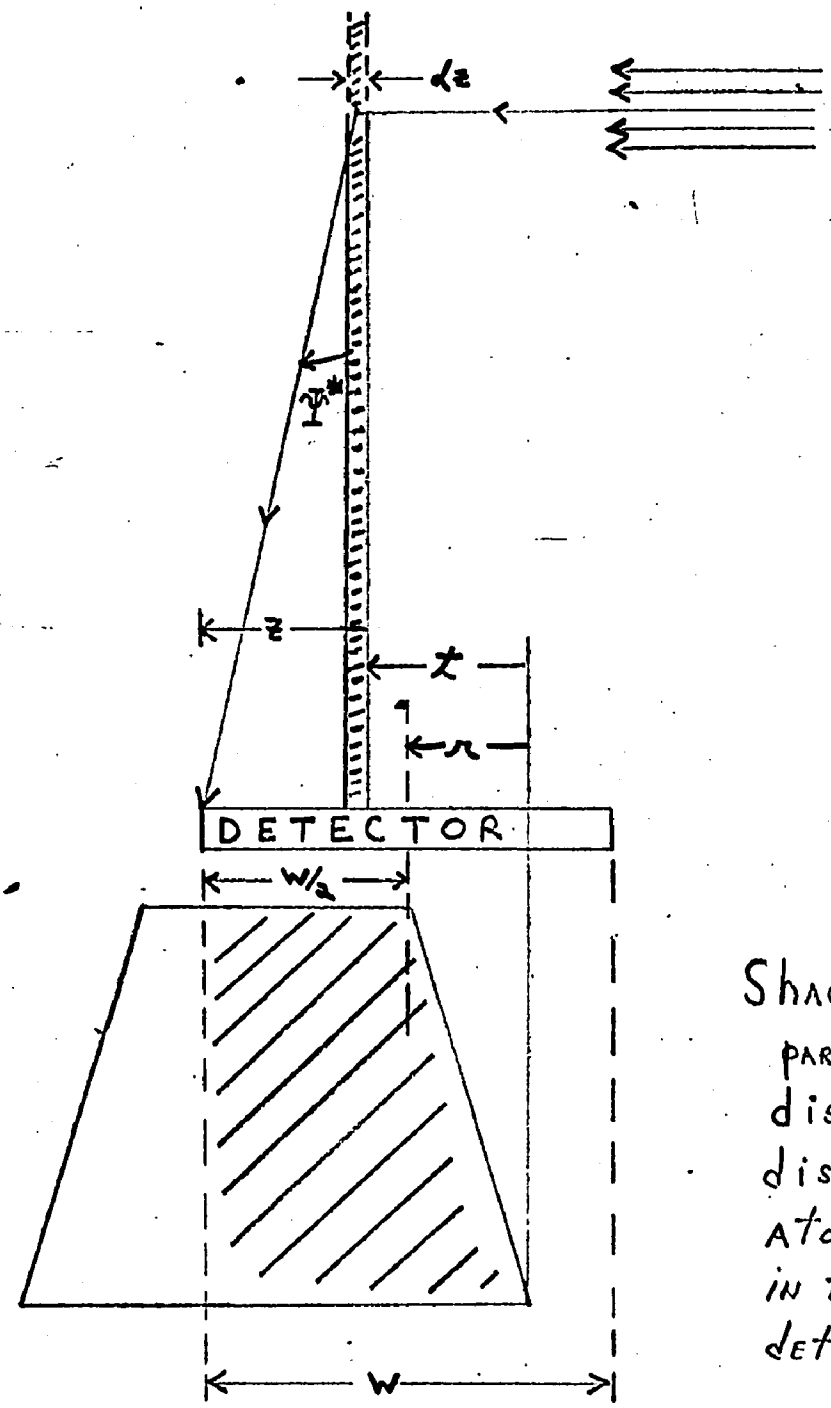

Shaded area: at a particular detector displacement, the distribution of atom beam intensity in the plane of the detector.

Figure 27

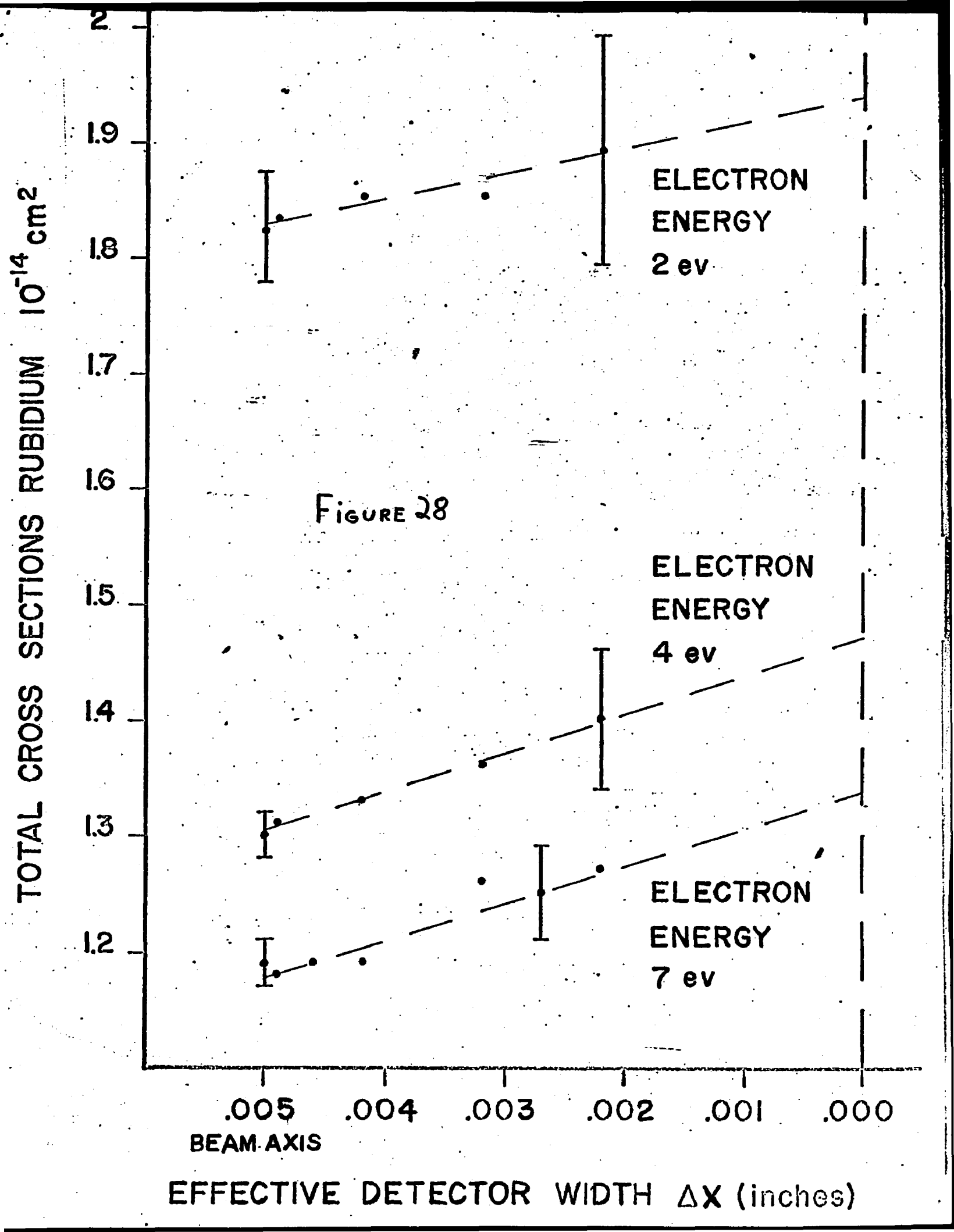
TOTAL CROSS SECTIONS RUBIDIUM 10^{-14} cm^2
2
1.9
1.8
1.7
1.6
1.5
1.4
1.3
1.2
ELECTRON ENERGY 2 ev
ELECTRON ENERGY 4 ev
ELECTRON ENERGY 7 ev
.005
.004
.003
.002
.001
.000
BEAM AXIS
EFFECTIVE DETECTOR WIDTH ΔX (inches)

FIGURE 28

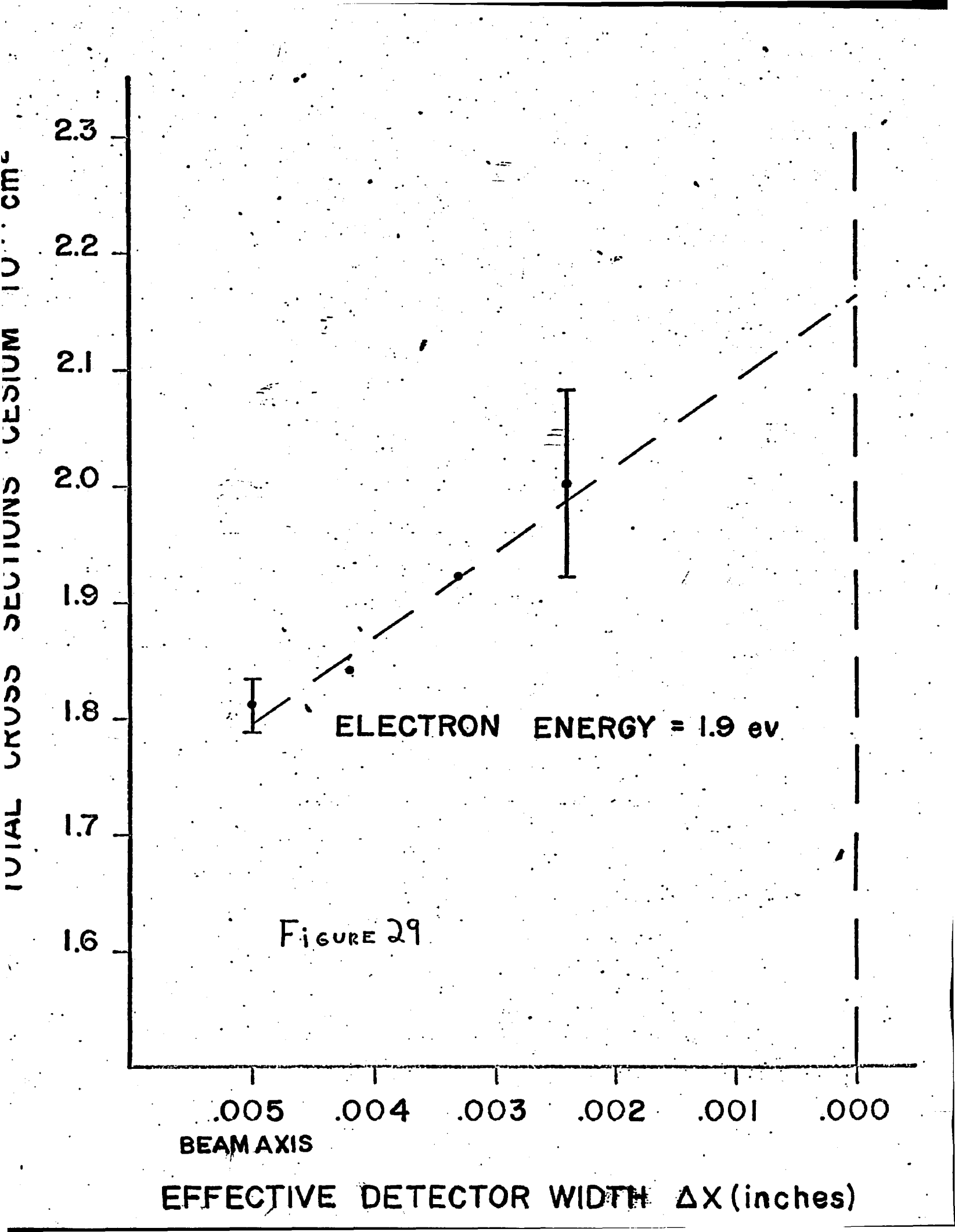
TOTAL CROSS SECTIONS CESIUM 10⁻¹⁶ cm²
2.3
2.2
2.1
2.0
1.9
1.8
1.7
1.6
ELECTRON ENERGY = 1.9 ev
.005
.004
.003
.002
.001
.000
BEAM AXIS
EFFECTIVE DETECTOR WIDTH ΔX (inches)

FIGURE 29

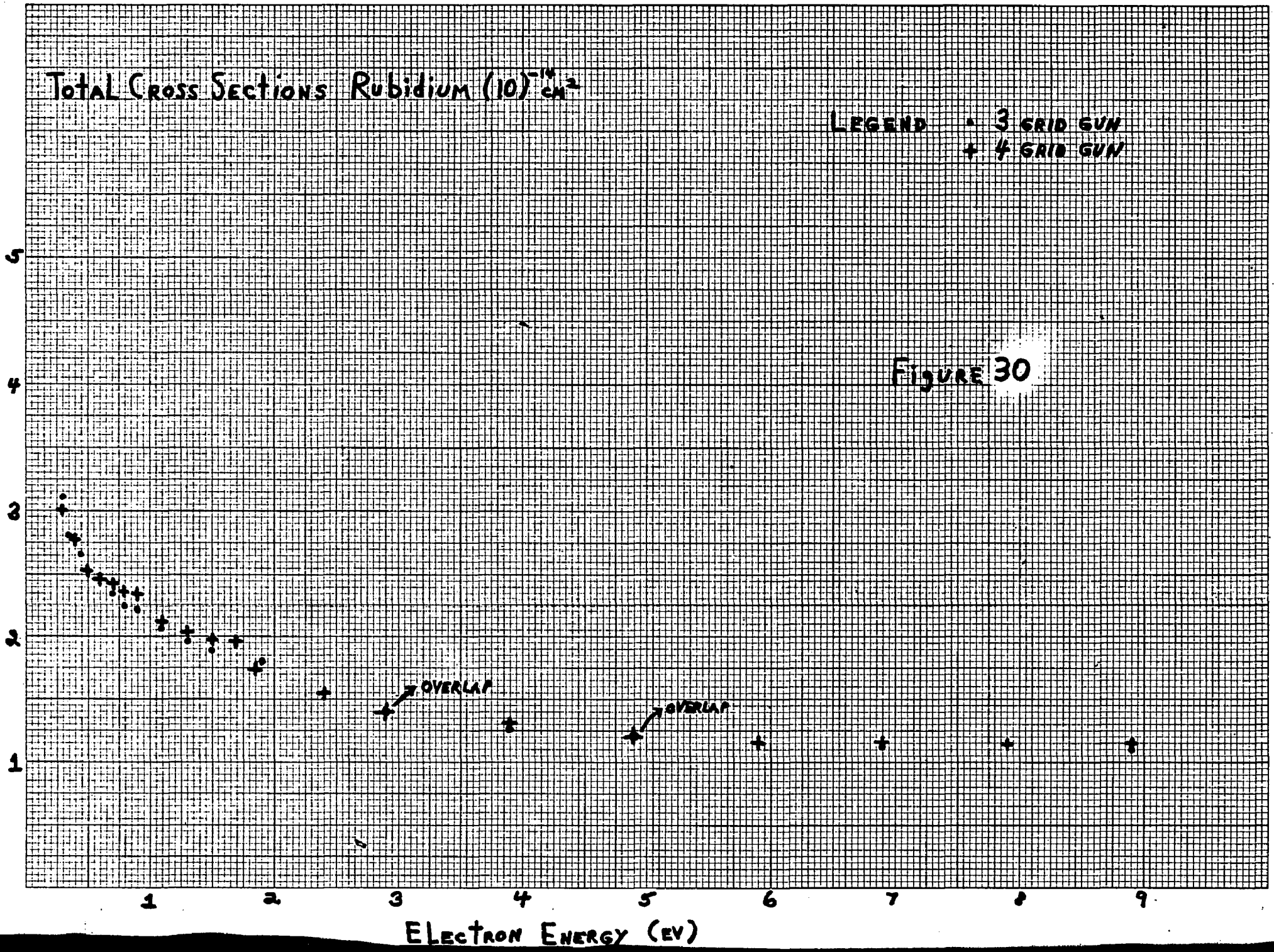
Total Cross Sections Rubidium $(10)^{-16}$ cm^2
Legend • 3 grid gun
+ 4 grid gun
Figure 30
5
4
3
2
1
overlap
overlap
1
2
3
4
5
6
7
8
9
Electron Energy (ev)

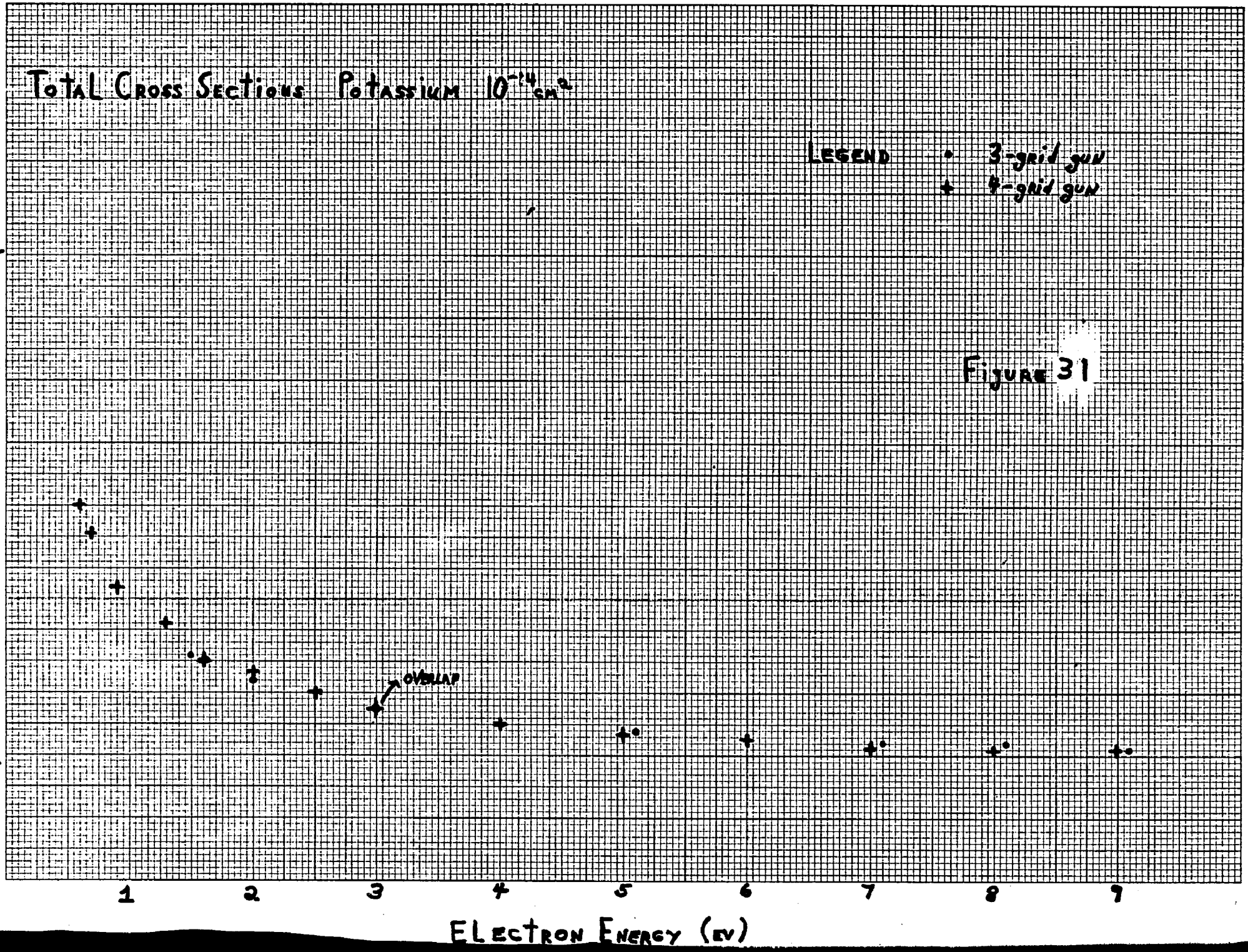
TOTAL CROSS SECTIONS POTASSIUM 10^{-14} cm^2
LEGEND • 3-grid gun
+ 4-grid gun
OVERLAP
5
4
3
2
1
1
2
3
4
5
6
7
8
9
ELECTRON ENERGY (EV)

FIGURE 31

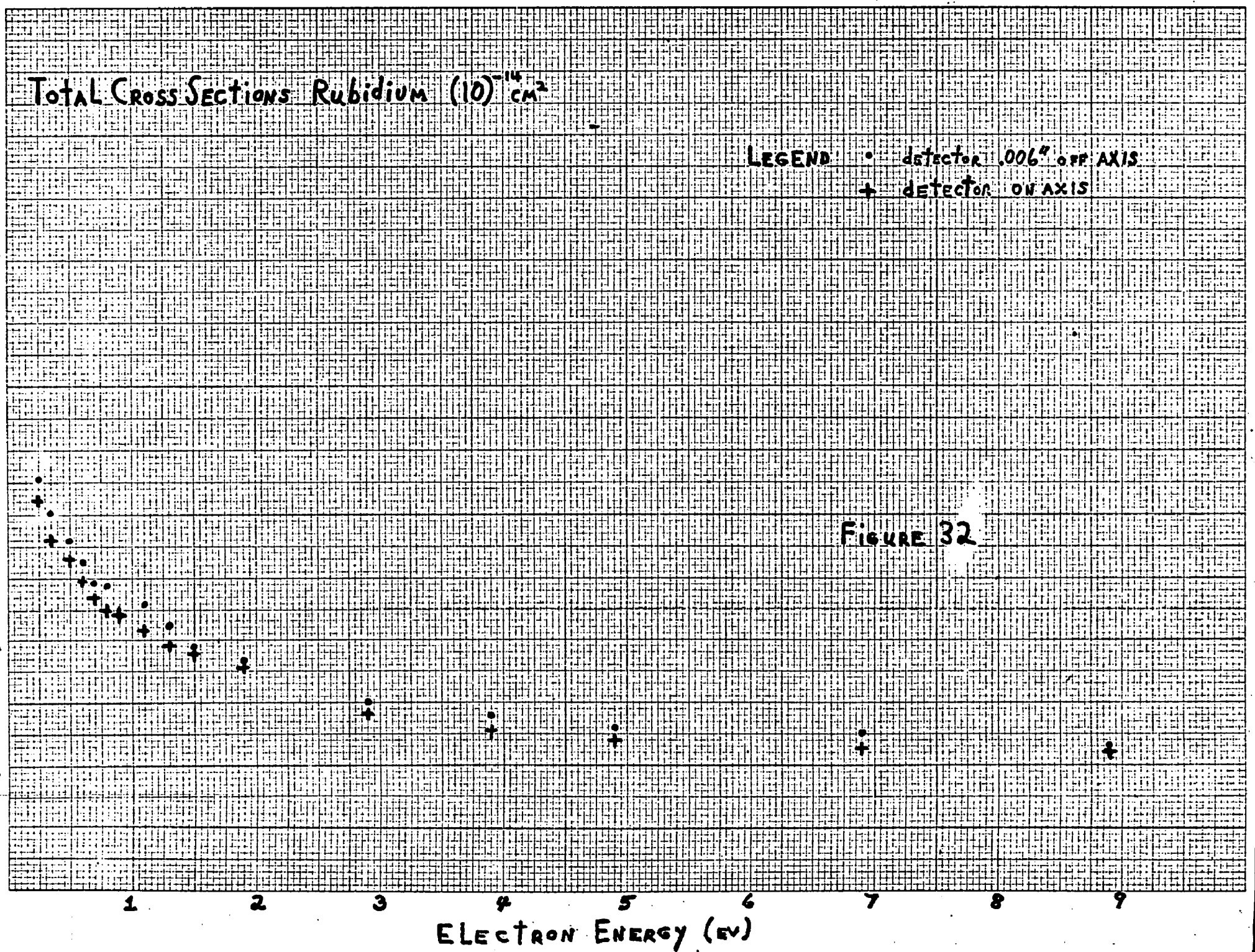
Total Cross Sections Rubidium $(10)^{-14}$ cm^2
LEGEND • detector .006" off axis
+ detector on axis
5
4
3
2
1
1
2
3
4
5
6
7
8
9
Electron Energy (ev)

Figure 32

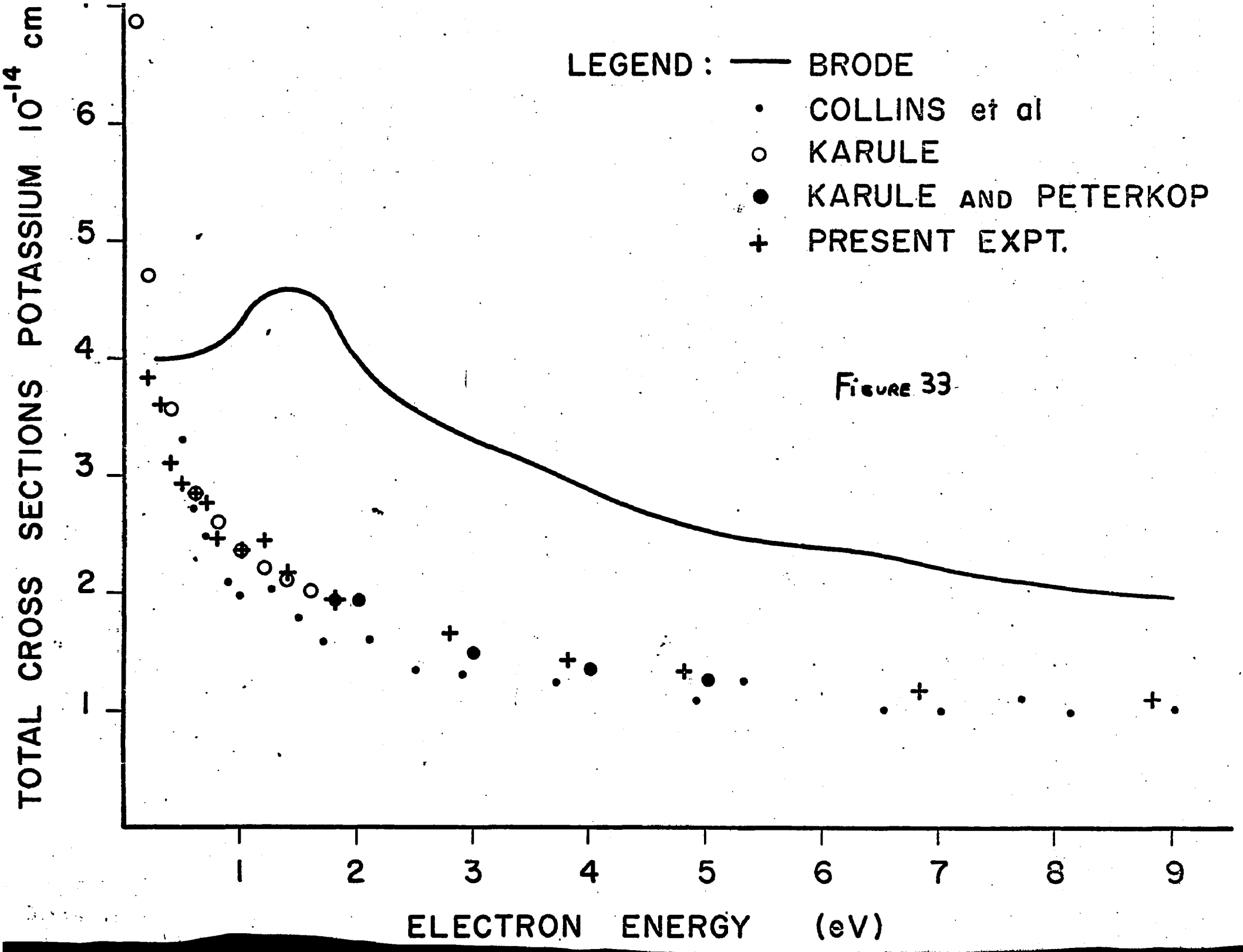
LEGEND : —— BRODE
• COLLINS et al
○ KARULE
● KARULE AND PETERKOP
+ PRESENT EXPT.
TOTAL CROSS SECTIONS POTASSIUM 10^{-14} cm
ELECTRON ENERGY (eV)
1
2
3
4
5
6
7
8
9

Figure 33

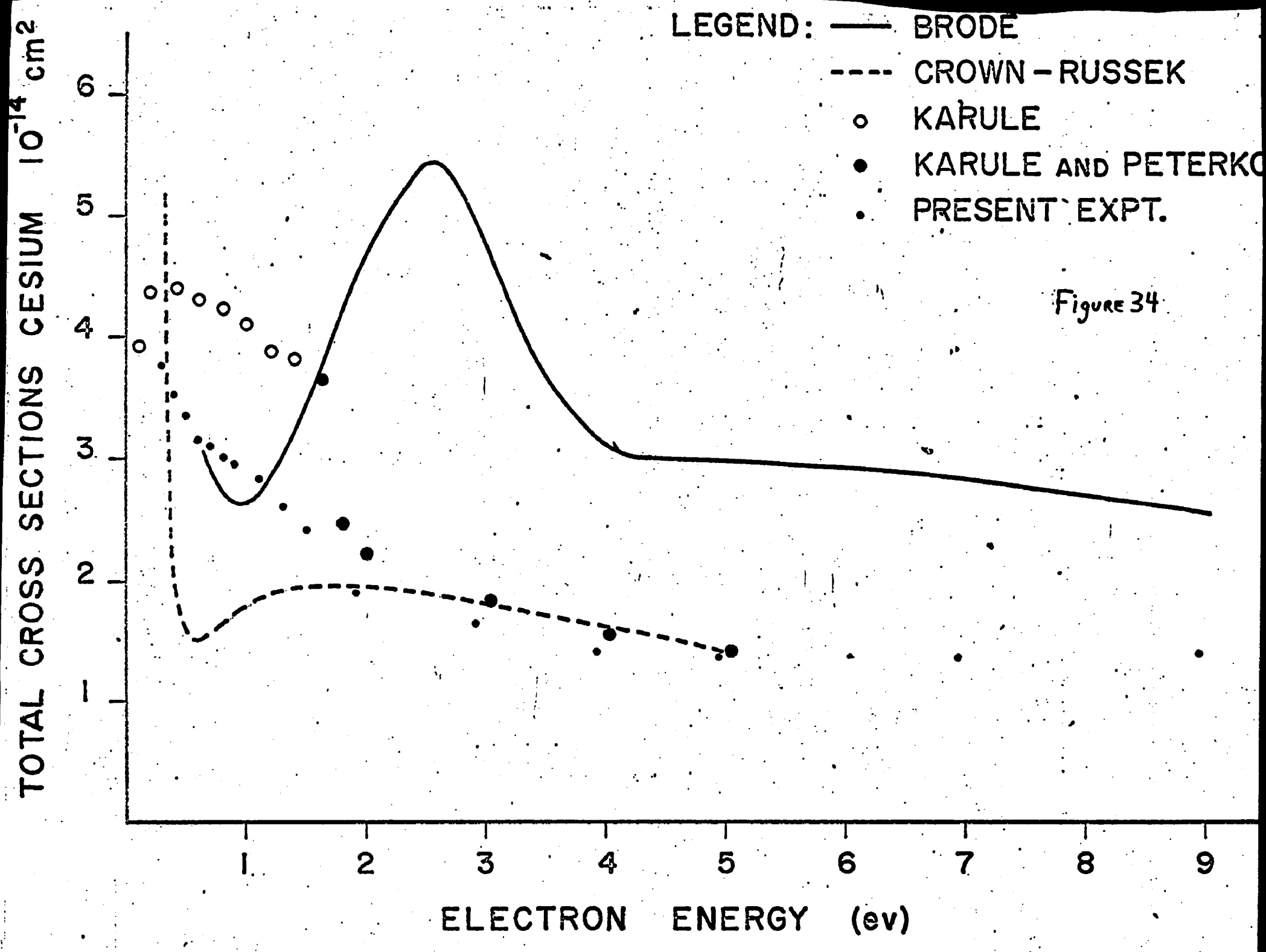
LEGEND:
BRODE
CROWN – RUSSEK
KARULE
KARULE AND PETERKO
PRESENT EXPT.
TOTAL CROSS SECTIONS CESIUM 10^{-14} cm^2
ELECTRON ENERGY (ev)
1
2
3
4
5
6
7
8
9

Figure 34

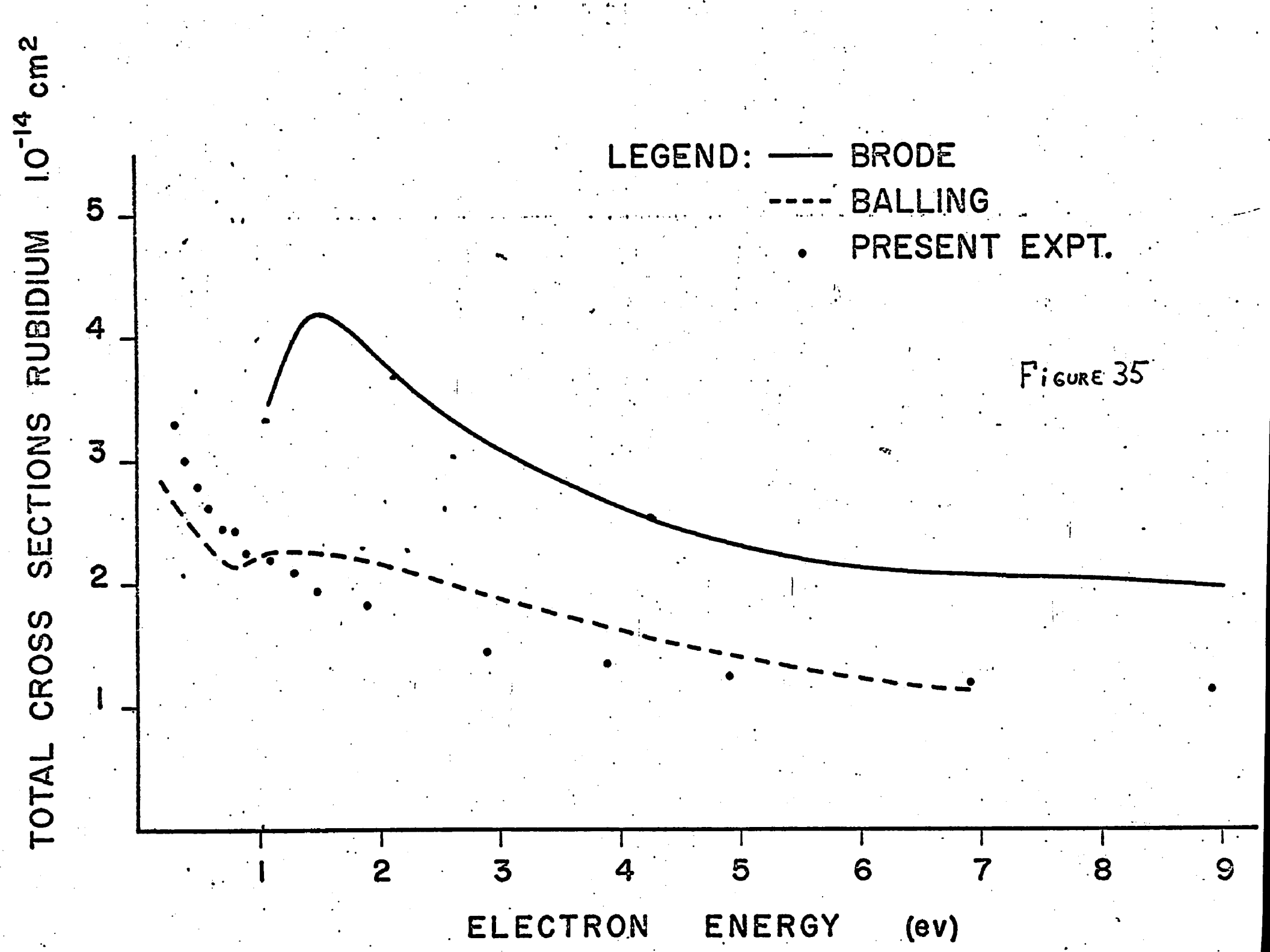
LEGEND: —— BRODE
---- BALLING
• PRESENT EXPT.
TOTAL CROSS SECTIONS RUBIDIUM 10^{-14} cm^2
1
2
3
4
5
1
2
3
4
5
6
7
8
9
ELECTRON ENERGY (ev)

Figure 35

PROFILE OF SCATTERING SIGNAL VS. ATOM DETECTOR POSITION FOR POTASSIUM AT ELECTRON ENERGY = .6 EV

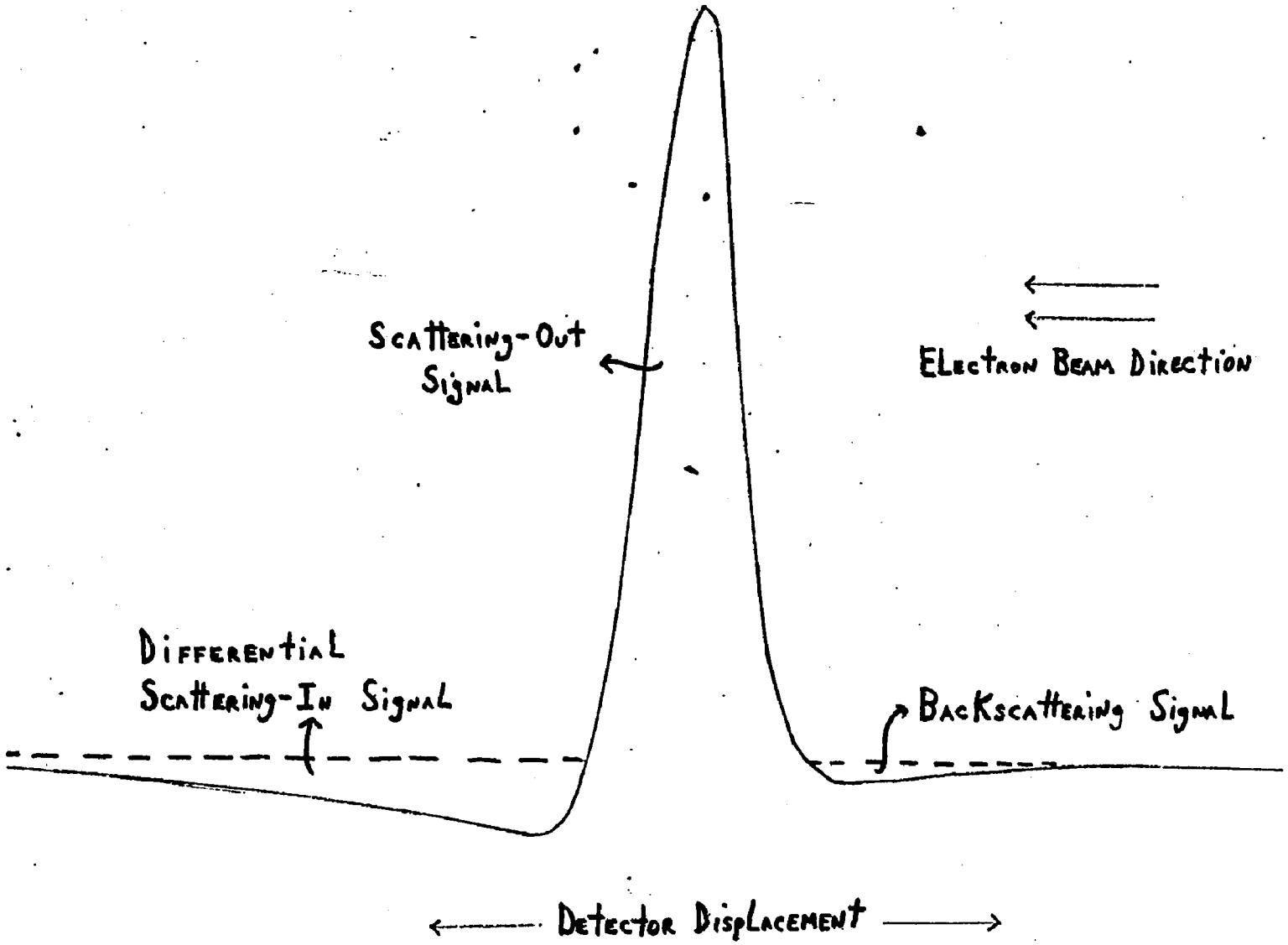

FIGURE 36

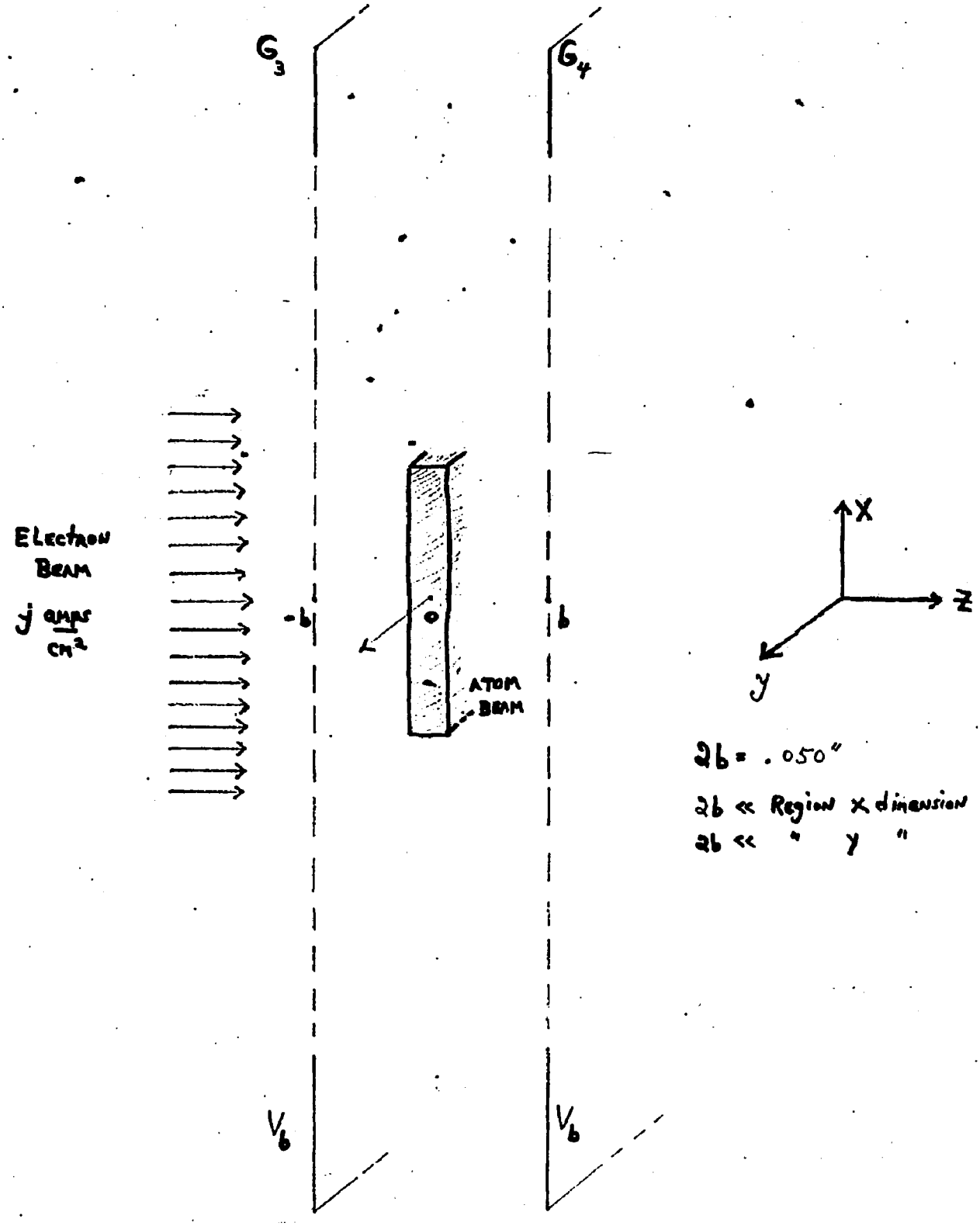

Figure 37 4-grid gun Equipotential Region

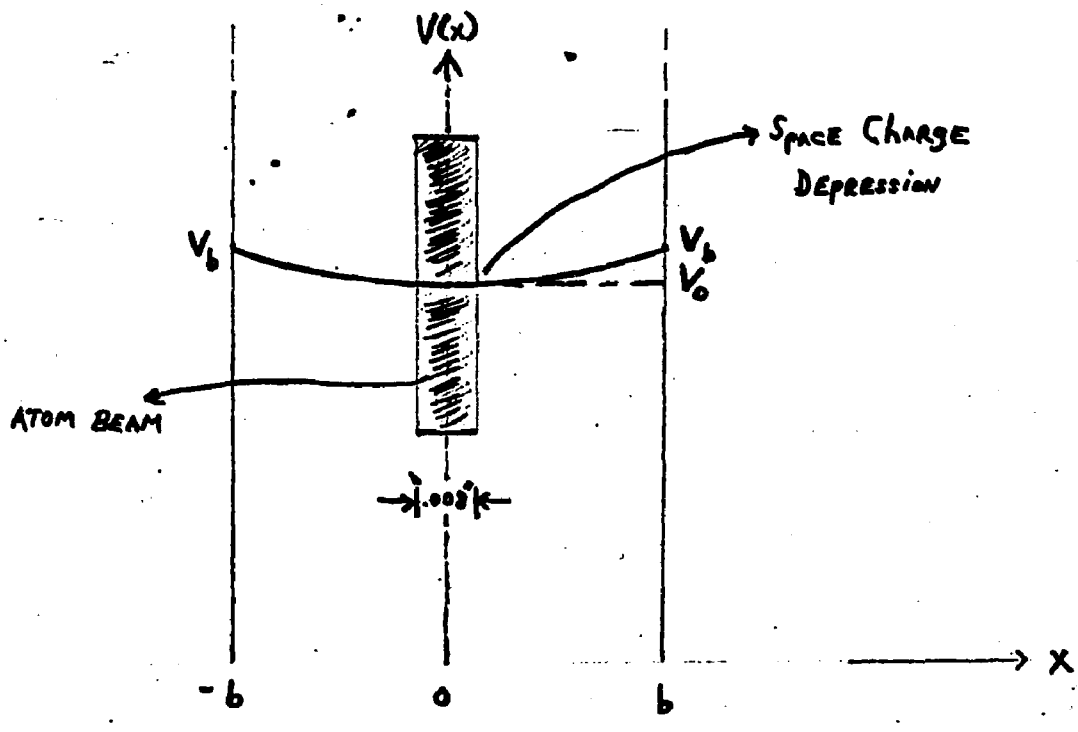

Figure 38 Potential in the Equipotential Region
(4 grid gun)

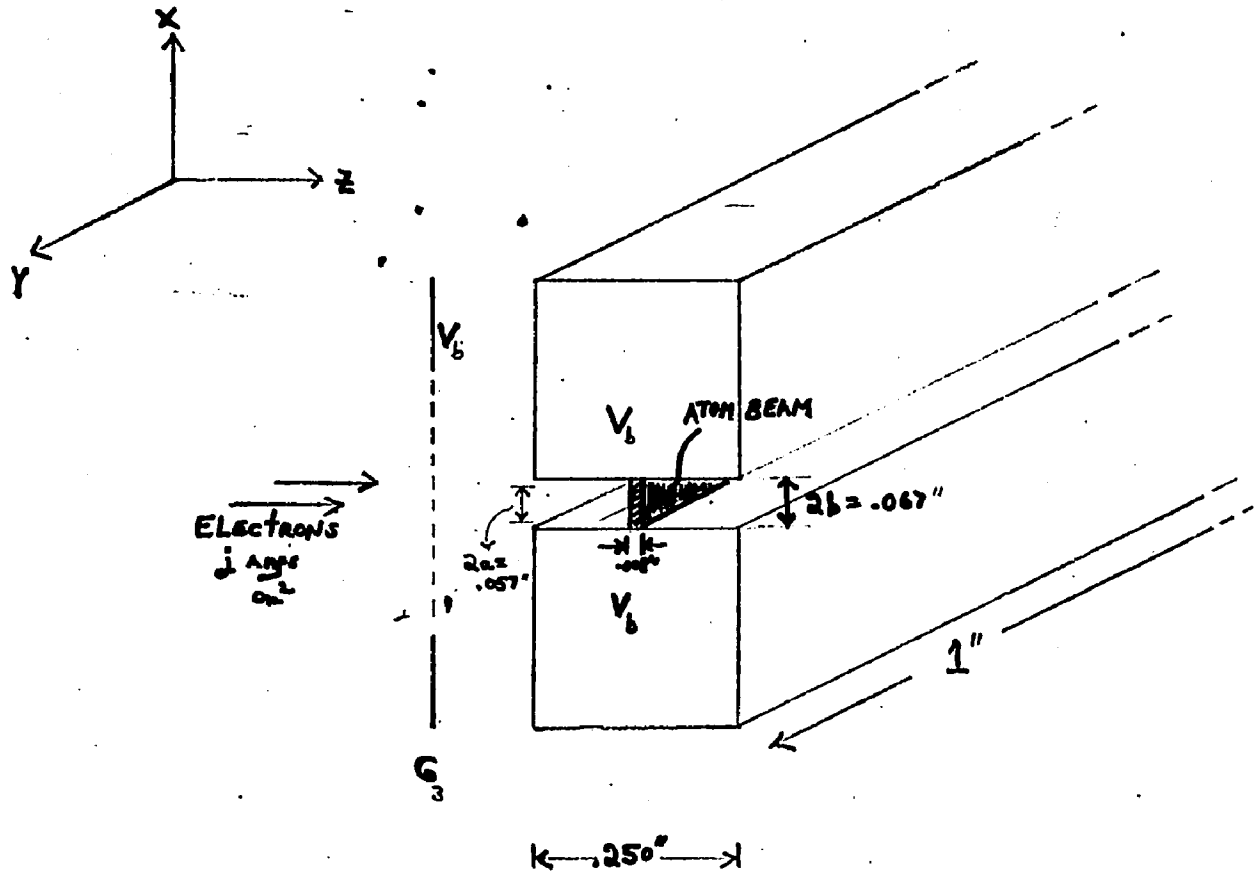

Figure 39 3-grid gun Equipotential Region

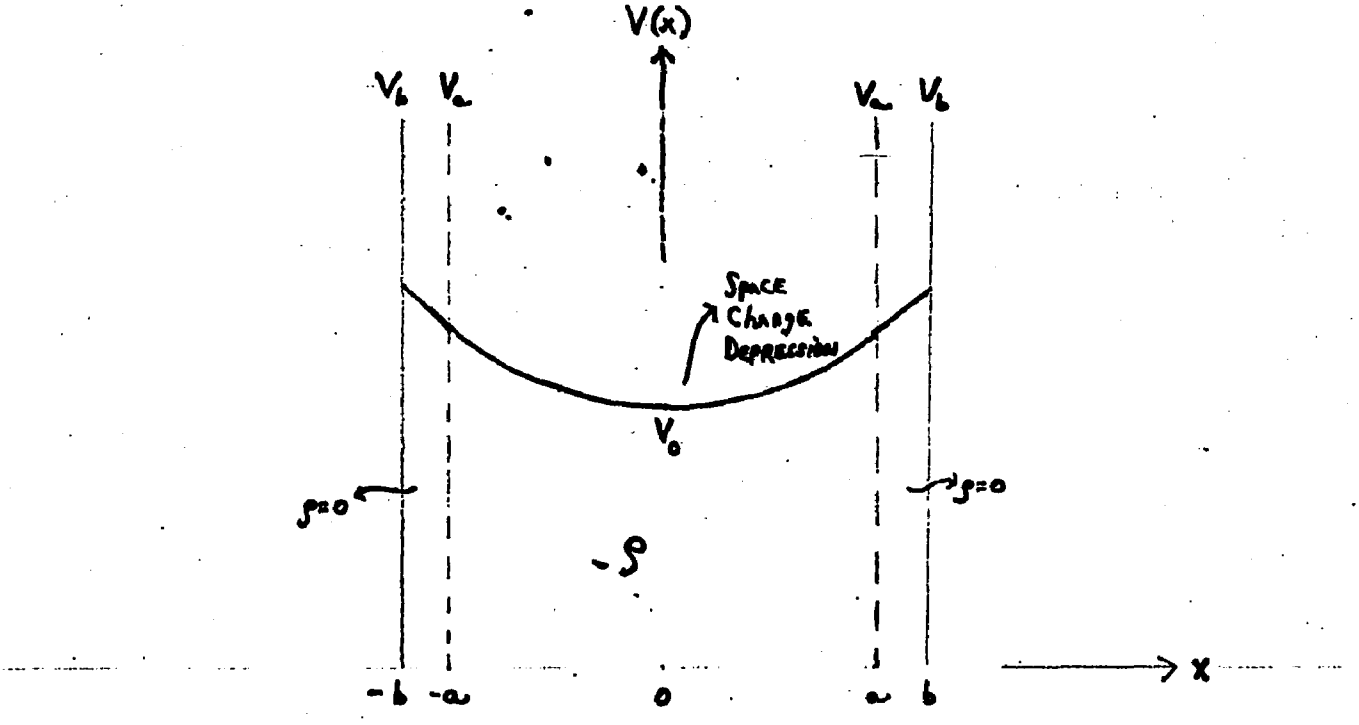

Figure 40 Space Charge Effected Potential Distribution across the height of the Electron Beam (3 grid gun)